ADVANCED OFDM SYSTEMS FOR TERRESTRIAL MULTIMEDIA LINKS

PAR

Renzo POSEGA

dottore in ingegneria elettronica, Università degli Studi di Trieste, Italie
et de nationalité italienne

Acknowledgements

I would like to acknowledge those persons that either directly or indirectly supported me in these years of work. First of all I would like to thank Prof. Daniel Mlynek who gave me the opportunity to join the LTS3 laboratory, and a special thanks to Marco Mattavelli for his guidance and encouragements all over these years. I would also like to thank Prof. Christine Guillemot, Pascal Frossard and Didier Nicoulaz who accepted to be members of the jury, for their suggestions and useful comments to improve the results of this work.

But over all, I would like to thank all my friends that supported me in all this long experience: in random order Graziano, Mauro, Marco, Aizzone, Silvia, Ilaria, Francesca, Franceschina, Tommaso, Luca, Pamela, Elena, Alessia, Arianna, Felicitas, Keiko, Miriam, Scilla and Eric, Tia, the LTS staff, Jeff Csomo and LiveTools crazy guys, Scola, Paolo, Pholo, Zoran, Büri, Cristina, Andrew and Francesca, Berto, Ziscku and all the people that I surely forgot.

This work is dedicated to Takanita, who was always on my side and helped myself maintaining my mental sanity... If you agree on this point. And, last but surely not least, I would like to dedicate this work to my parents that always believed in me well beyond what I deserve from being their son, and always remember me what the word *Home* means.

C'est une grande folie que de vouloir être sage tout seul.
La Rochefoucauld

Abstract

Recently, there has been considerable discussion about new wireless technologies and standards able to achieve high data rates. Due to the recent advances of digital signal processing and Very Large Scale Integration (VLSI) technologies, the initial obstacles encountered for the implementation of Orthogonal Frequency Division Multiplexing (OFDM) modulation schemes, such as massive complex multiplications and high speed memory accesses, do not exist anymore. OFDM offers strong multipath protection due to the insertion of the guard interval; in particular, the OFDM-based DVB-T standard had proved to offer excellent performance for the broadcasting of multimedia streams with bitrates over ten megabits per second in difficult terrestrial propagation channels, for fixed and portable applications. Nevertheless, for mobile scenarios, improving the receiver design is not enough to achieve error-free transmission especially in presence of deep shadow and multipath fading and some modifications of the standard can be envisaged. To address long and medium range applications like live mobile wireless television production, some further modifications are required to adapt the modulated bandwidth and fully exploit channels up to 24MHz wide. For these reasons, an extended OFDM system is proposed that offers variable bandwidth, improved protection to shadow and multipath fading and enhanced robustness thanks to the insertion of deep time-interleaving coupled with a powerful turbo codes concatenated error correction scheme. The system parameters and the receiver architecture have been described in C++ and verified with extensive simulations. In particular, the study of the receiver algorithms was aimed to achieve the optimal tradeoff between performances and complexity. Moreover, the modulation/demodulation chain has been implemented in VHDL and a prototype system has been manufactured. Ongoing field trials are demonstrating the ability of the proposed system to successfully overcome the impairments due to mobile terrestrial channels, like multipath and shadow fading.

For short range applications, Time-Division Multiplexing (TDM) is an efficient way to share the radio resource between multiple terminals. The main modulation parameters for a TDM system are discussed and it is shown that the 802.16a TDM OFDM physical layer fulfills the application requirements; some practical examples are given. A pre-distortion method is proposed that exploit the reciprocity of the radio channel to perform a partial channel inversion achieving improved performances with no modifications of existing receivers.

Version Abrégée

Récemment, on a pu observer un intérêt considérable au sujet de nouvelles technologies et de normes sans fil capables de réaliser des débits élevés. En raison des récentes avancées dans le champ du traitement des signaux numériques et des technologies d'intégration à très grande échelle (VLSI), les obstacles initiaux rencontrés pour la réalisation des systèmes basés sur le multiplexage à division orthogonale de fréquence (OFDM), tels que le grand nombre de multiplications complexes et la nécessité d'avoir des accès mémoire à grande vitesse, n'existent plus. L'OFDM offre une forte protection en cas de chemins multiples comme on en rencontre en transmission hertzienne terrestre grâce, entre autres, à l'insertion d'un intervalle de garde; en particulier, la norme DVB-T, basée sur la technologie OFDM, s'est avérée excellente pour la distribution des flux multimédia avec des débits de plus de vingt millions de bits par seconde, dans des canaux terrestres difficiles, pour des applications fixes et portables. Néanmoins, pour les applications fortement mobiles, l'amélioration de la conception du récepteur n'est pas suffisante pour réaliser une transmission sans erreur, particulièrement en présence d'affaiblissements profonds et de chemins multiples; certaines modifications de la norme DVB-T doivent donc être envisagées. Pour cibler des applications à longue et à moyenne portée comme la production télévisuelle mobile en temps réel, d'autres modifications plus profondes sont nécessaires, par example pour adapter la largeur de bande modulée et pour exploiter entièrement des canaux jusqu'à 24MHz. Pour ces raisons, on propose un système OFDM étendu qui offre à la fois largeur de bande variable, protection améliorée à l'affaiblissement et aux chemins multiples et robustesse augmentée, grâce à un mécanisme d'entrelacement temporel des données couplé à un puissant système de correction d'erreurs enchaîné avec turbo codes. Les paramètres du système et l'architecture du récepteur ont été décrits en C++ et vérifiés avec plusieurs simulations. En particulier, l'étude des algorithmes de réception visait à réaliser le compromis optimal entre performance et complexité. De plus, la chaîne de modulation/démodulation a été réalisée en VHDL et des prototypes ont été fabriqués. Les essais en cours sur le terrain démontrent la capacité du système proposé à surmonter avec succès les problèmes dûs aux canaux terrestres mobiles, comme l'affaiblissement et les chemins multiples.

Pour des applications à courte distance, le partage à division de temps (TDM) est une manière efficace de partager la capacité du canal entre plusieurs terminaux. Les paramètres principaux de la modulation pour un système TDM sont discutés et on montre que la couche physique TDM OFDM du standard 802.16a remplit les exigences de l'application; quelques exemples pratiques sont donnés. On propose ensuite une méthode de pré-déformation qui exploite la réciprocité du canal radio pour exécuter une inversion partielle offrant des performances améliorées sans modifications des récepteurs existants.

Contents

List of Figures

List of Tables

Acronyms

ACI Adjacent Channel Interference

ADC Analog to Digital Converter

AFC Automatic Frequency Control

AGC Automatic Gain Control

ASIC Application-Specific Integrated Circuit

AWGN Additive White Gaussian Noise

BCH Bose - Chaudhuri - Hocquenghem code

BER Bit Error Ratio

BS Base Station

BTC Block Turbo Codes

CCI Co-Channel Interference

CIR Channel Impulse Response

C/N Carrier/Noise Ratio

COFDM Coded-OFDM

COST Co-Operative for Scientific and Technical research

CTC Circular Turbo Codes

DAB Digital Audio Broadcasting

DAC Digital to Analog Converter

DBPSK Differential Binary Phase Shift Keying

DDCE Decision-Directed Channel Estimation

DFT Discrete Fourier Transform

DL DownLink

DSP Digital Signal Processor

DTNG Digital Terrestrial News Gathering

DVB Digital Video Broadcasting

DVB-C DVB-Cable

DVB-S DVB-Satellite

DVB-T DVB-Terrestrial

FDD Frequency-Division Duplexing

FEC Forward Error Correction

FFT Fast Fourier Transform

FIFO First-In, First-Out

FIR Finite Impulse Response

FPGA Field-Programmable Gate Array

FSM Finite State Machine

HDTV High Definition TeleVision

ICI Inter-Carrier Interference

IEEE Institute of Electrical and Electronics Engineers

IF Intermediate Frequency

IFFT Inverse Fast Fourier Transform

IIR Infinite Impulse Response

IP Internet Protocol

ISI Inter-Symbol Interference

LAN Local Area Network

LOS Line of Sight

LSB Less Significant Bit

MAC Medium Access Control (layer)

MAN Metropolitan Area Network

MFN Multi Frequency Network

MOTIVATE Mobile Television and Innovative Receivers

MPEG Moving Picture Experts Group

MSB Most Significant Bit

NAB National Association of Broadcasters

NLOS Non-Line of Sight

OFDM Orthogonal Frequency Division Multiplexing

OFDMA Orthogonal Frequency Division Multiple Access

PAL Phase-Alternating Line

PCCC Parallel-Concatenated Convolutional Code

PHY PHYsical (layer)

PLL Phase-Locked Loop

PMP Point-to-MultiPoint

PRBS Pseudo-Random Binary Sequence

PSAM Pilot Symbol Assisted Modulation

QAM Quadrature Amplitude Modulation

QEF Quasi Error Free

QoS Quality of Service

QPSK Quaternary Phase Shift Keying

RF Radio Frequency

RS Reed-Solomon

RTL Register Transfer Logic

SDRAM Synchronous Dynamic Random Access Memories

SDTV Standard Definition TeleVision

SFN Single Frequency Network

SECAM Systme Sequentiel Couleur A Mmoire

SNR Signal to Noise Ratio

SS Subscriber Station

TDD Time Division Duplexing

TDM Time Division Multiplexing

TDMA Time Division Multiple Access

THD Total Harmonic Distortion

TPS Transmission Parameter Signalling

TS Transport Stream

UL UpLink

VALIDATE Verification And Launch of Integrated Digital Advanced Television in Europe

VHDL Very High level Design Language

VLSI Very Large Scale Integration

WSSUS Wide-Sense Stationary Uncorrelated Scattering

Chapter 1

Introduction

1.1   Wireless modulations

The spectacular growth of video, voice, and data communication over the internet and the equally rapid pervasion of mobile telephony justify great expectations for mobile multimedia.

Recently, there has been considerable discussion about new wireless technologies and standards that support throughput speeds in the tens-of-megabits per second. Such technologies, proponents claim, are fast enough to stream wireless video and robust enough to replace or considerably expand today's wired networks. Among those, Orthogonal Frequency OFDM techniques have demonstrated to be effective and has been widely implemented in high speed digital communications. The concept of using parallel data transmission and frequency division multiplexing was published in the mid 60s, but some early development can be traced back in the 50s. The idea was to use parallel data and frequency division multiplexing (FDM) with overlapping sub-channels to avoid the use of high speed equalization and to combat impulsive noise and multipath distortion, as well as to fully exploit the available bandwidth. The initial interest for this modulation scheme was raised for military applications.

In the telecommunication field the terms of Discrete Multi-Tone (DMT), multichannel modulation and Multi-Carrier Modulation (MCM) are widely used and sometimes they are interchangeable with OFDM. In the 80s, OFDM had been studied for high-speed modems, digital mobile communications and high density recording. In the 90s, OFDM has been exploited for wide-band data communications over mobile radio FM channels, high-bit-rate digital subscriber lines (HDSL), in particular the nowadays popular asymmetric digital subscriber lines (ADSL), digital audio broadcasting (DAB), digital television terrestrial broadcasting (DVB-T).

Due to the recent advances of digital signal processing and Very Large Scale Integration (VLSI) technologies, the initial obstacles of OFDM implementation, such as massive complex multiplications and high speed memory accesses do not exist anymore. Meanwhile, the use of Fast Fourier Transform (FFT) algorithms eliminates arrays of sinusoidal generators and coherent demodulation required in parallel data systems and make the implementation of the technology cost-effective.

Exploiting OFDM modulation scheme, the Digital Audio Broadcasting (DAB) system has been developed to deliver high-quality digital audio programme and data services for mobile, portable and fixed reception from terrestrial or satellite transmitters in the Very High Frequency (VHF)/Ultra High Frequency (UHF) frequency bands as well as for distribution through cable networks [1]. The DAB system is designed to provide spectrum

and power efficient techniques in terrestrial transmitter network planning, known as the Single Frequency Network (SFN).

Since 1992, the Digital Video Broadcasting (DVB) project, which started out as an European activity but has since become global, has developed numerous technical solutions for the coding and transmission of digital television. The three main standard born from this project address different applications: satellite broadcasting (DVB-S), cable distribution (DVB-C) and wireless terrestrial broadcasting (DVB-T). As a result, a common features of the three standards is that they provide quasi-error-free transmission of different types of data within each individual cable, satellite or terrestrial channel. The DVB Project has thus designed systems for data broadcasting. An interesting side effect of the conceptual model is that DVB can very flexibly be used for radio, high-definition television (HDTV), standard definition television (SDTV) and every conceivable mixture of such services as long as the capacity of the data container permits.

The DVB-S standard has been developed for the satellite downlink channel. The characteristics of this channel claim for modulation schemes that mostly offer good protection to gaussian white noise. In fact, the downlink channel power budget is often minimized because the gain of the reception antenna, usually a parabolic-reflector type, is kept to a minimum, thus limiting the dish dimension. The System uses Quaternary Phase Shift Keying (QPSK) modulation and concatenated error protection strategy based on a convolutional code and a shortened Reed-Solomon (RS) code [2]. The constellation order is limited by the non-linearities of satellite spacecraft amplifier. Even if this modulation offers data rates up to 68Mbps over a 54MHz channel, the single-carrier modulation scheme is not intended to offer strong protection in case of multi-path propagation channels.

The DVB-C standard has a similar architecture but employing Quadrature Amplitude Modulation (QAM) with 16, 32, 64, 128 or 256 points in the constellation diagram and achieves capacity up to 50Mbps on a nominal 8MHz channel [3].

For various reasons, but mainly because a considerable market pull first and foremost demanded solutions for satellite, cable and Satellite Master Antenna Television (SMATV), the design of a system for terrestrial transmission of DVB signals was postponed until 1994/1995. In November 1995, the technical module of the European DVB Project was able to finalize what is called the "common 2K/8K specification", otherwise known as DVB-T (terrestrial) [4]. Among the initial specifications for this system, we can cite the need of common similarities with DVB-S and DVB-C architecture, in order to allow the development of multi-standard receivers at low cost. In fact, the three standards share the error-correction scheme, based on a concatenated scheme with convolutional encoder

of mother code rate of 1/2 as inner code and shortened Reed-Solomon encoder as outer code.

A very interesting point of DVB-T is its flexibility, that comes from the possibility to adjust the modulation parameters to implement up to 120 regular modulation modes and up to 1200 hierarchical ones.

Hierarchical modulation constitutes an alternative interpretation (and usage) of the basic 16QAM and 64QAM constellations. Hierarchical modulation can be viewed as a separation of the RF channel in two virtual circuits, each having a specific bitrate capacity, a specific roughness and accordingly, covering two slightly different areas. The characteristics of the two virtual channels follow the constellation and coding rate combinations applied. The first data stream will always use a 4QAM modulation and it is named High Priority stream (HP). The second one, less rugged, either in the 4QAM or 16QAM cases, is named Low Priority stream (LP). The opportunity to split the available bandwidth in two different channels with different performances can be exploited by TV broadcasters in several ways. It can facilitate the deployment of digital transmission in presence of traditional analog ones, can provide different services for fixed and portable receivers and can eventually even improve the aggregate bitrate at the expense of a distortion in the overall coverage area (5dB penalty between HP and LP streams) [5].

Another key features for broadcasters is the possibility to develop Single Frequency Networks (SFN), in which adjacent transmitters emits the same signal on the same frequency for a 100% frequency reuse. The two contributions add constructively at the receiver if the arrival time difference is lower than the guard-interval duration. For this application, the 8k mode offers a clear advantage over 2K mode because symbol period is four times longer and less bitrate capacity is wasted by the guard interval insertion to obtain the same echo protection.

Growing interest is raising for Wireless-Local Area Network (WLAN) systems as a good opportunity for multimedia/data convergence. Anyway, only recently standards with data rate over 10Mbps have been developed.

Among those, two are particularly interesting: 802.11a and 802.16.

The 802.11a WLAN standard [6], developed as an OFDM extension for single-carrier 802.11 modulation in the 5GHz band, can offer up to 54Mbps data bitrate, but due to its relatively short symbol duration of $3.2\mu s$, it supports echo spreads up to $0.8\mu s$, thus limiting the available range to some hundreds of meters.

In April 2002, the IEEE concluded a 2-year-long, open consensus process when it

published the 802.16 standard [8], also known as WirelessMAN (Metropolitan Area Network). The standard addresses fixed wireless data networking over the range of miles or kilometers – a metropolitan area. The 802.16 standard defines a medium access control (MAC) networking layer that supports a number of physical layer specifications. The multiple physical layer specifications are a reflection of the huge bandwidth covered by the standard: 10 to 66 GHz. The MAC supports frequency-division-duplex (FDD) and time-division-duplex (TDD), as well as real-time adaptive modulation and coding. It employs single-carrier modulation, as the high frequencies limit the use to line-of-sight. The initial 802.16 standard was followed by several working groups, some of whom have released their amendments to the standard. Most prominent among the amendments is 802.16a [9], which extends the standard into the spectrum between 2 and 11 GHz. The 802.16a standard also specifies three possible modulations: single carrier, 256-carriers OFDM, and orthogonal frequency division multiple access (OFDMA). The lower frequencies make non-line of sight a possibility, which can also be helped by OFDM's ability to handle multipath signals. Range can be up to 30 miles, with typical cell footprints in the 4 to 6 mile range. Total data rate can be up to 100 Mb/s in each 20MHz channel.

All these systems have been tailored in a different fashion according to the respective system constraints. Especially the time-variance of the transmission channel was treated in different ways. In DAB it was proposed to use differential encoding to mitigate this effect, which obviously limits the use of higher order modulations. On the other side, DVB-T and the WLAN system operating in the lower GHz bands were not supposed to experience a high degree of mobility due to the relatively low speed involved and can thus employ coherent demodulation and higher order modulations.

1.2 Wireless digital television production

In the past years, great interest was raised for applications aimed to wireless digital television productions. The technology evolution made it possible to compress a digital audio/video stream and reduces the required bitrate down to some Megabit-per-second (Mbps). For example, standard-definition, 50-Hz interlaced video generates around 220Mbps of uncompressed digital video stream, and each digital audio channel adds for another 1Mbps. Employing MPEG2 encoding and exploiting both spatial and temporal redundancy, the bitrate can be lowered down to an aggregate 5Mbps (video + 2 audio channels) still preserving a quality adequate for broadcasting. The definition of the DVB-T standard made it possible to implement digital wireless links capable of transporting the compressed multimedia stream over difficult terrestrial propagation channels.

There is a strong demand for such a systems: there are applications where wired systems simply cannot be deployed, as bicycle race, sailing race, marathon just to cite some examples, but even in other scenarios the possibility to use wireless links is greatly appreciated. Wired systems requires specialized and very expensive cables that have to be deployed before and must be collected after the event; the cost in terms of material bill and time spent can be very important. For example, football matches requires a large amount of wiring, in the order of several kilometers, and a couple of days must be accounted for system setup and de-mounting. A wireless system would be easier to setup and would require less time to deploy.

The requirements of these applications can vary over a wide range; the requirements more related to the modulation scheme can be summarized as:

- **long distance** - the wireless links can be as long as 50km. The RF power should be sufficient and the modulation should be robust to gaussian noise in order to overcome the attenuation due to strong propagation loss.

- **high mobility** - the system should withstand a high degree of mobility; transmitter and/or receiver motion can be expected, and the speed can be as high as 300km/h.

- **multipath protection** - in this case of a terrestrial channel, multiple echoes reaches the reception antenna and experience different attenuations and delays. This is the cause of the so-called *multipath fading*. The employed modulation scheme should be able to overcome this effect with less or no performance degradation.

- **shadowing protection** - another impairment deriving from mobility is called *shadow fading*, and is caused by the interposition of obstacles in the line-of-sight between transmission and reception antennas. For power-budget limited wireless links, this translates in short signal loss. The modulation and the error-correction scheme should overcome flawlessly this type of impairment.

- **high bitrate** - the available bitrate should be as high as possible to reduce the compression ratio and allow transmission of high-quality and high-resolution audio/video streams.

- **low latency** - the modulation and error-correction scheme should exhibit a latency as low as possible (typically < 10ms) to allow mixing of wired and wireless system without noticeable delay.

- **backward channel** - a backward channel (broadcasted from the regia to all the cameras) can be used to convey the live feed to each camera along with camera control data.

- **compact size** - the system should be compact and light-weight to allow mounting on the back of a professional camera.

- **low power consumption** - since the system will be mostly powered by batteries, power consumption is still a major issue.

Even without further in-depth discussions, it is clear that some contradictory requirements are given in the above list. For example, long distance calls for high RF power and this directly influences the power consumption and even the physical dimension of the system. Moreover, there is always a tradeoff between bitrate and robustness, and protection to shadow fading cannot be obtained with low latency.

Nevertheless, there are several typical scenarios which can be accounted for; of course, for each one some compromises are needed and some priority are given to the above requirements.

1.2.1 Outdoor events

For outdoor events like bicycle races, marathon and sailing races, multipath and shadowing robustness are the primary requirements. The mobility of the transmitters and eventually of the receiver, often mounted on helicopter or small airplanes, can vary between medium to high. The bitrate can be reduced down to 5Mbps, to obtain the best achievable protection to mobility and noise. Latency is not a major issue, but shadow fading protection is required. A backward channel is not an important feature, but would represent an additional benefit.

1.2.2 Multimedia relay

Relaying the signal by means of helicopter has already been introduced in the previous subsection; anyway, the requirements of the link from the helicopter down to the reception site (usually placed on a high location) are quite different. The main problem is constituted by the long distances that must be covered, that calls for high RF power; anyway, the equipment can be powered by the helicopter, thus power consumption and size is not the major issue. The bitrate would be limited by the power budget, while the latency can be high and the backward channel is not required.

1.2.3 Studio production

For studio productions, some wireless cameras are mixed with wired ones; the latency of the wireless system must be kept to a minimum to avoid noticeable delays when switching between the two different systems. High bitrate allows improved audio/video quality and a backward channel would be an important advantage to implement centralized camera control and the live feed. On the other side, wireless cameras will not experience high mobility, distance and power are usually limited and shadow fading is not expected. Anyway, a strong multipath scenario with high-energy echoes can be expected.

1.3 Motivation of the work

In the last years, several solutions have been presented for wireless digital television production application. In the year 2001, Livetools Technology (formerly Broadcast Services) presented at NAB of Las Vegas the first integrated encoder/modulator ready to be mounted on the back of professional cameras. It received the most prestigious technical award of Broadcast Engineering NAB 2001 "Pick Hit Award". The product was born from the collaboration of Livetools with the Ecole Polytechnique Federale de Lausanne (EPFL) in the scope of a industrial-collaboration project, in which we were personally involved.

Since then, several others products from competing companies were born. Even if they differentiate in terms of audio/video compression schemes, they share the same digital modulation scheme: the 2K mode of DVB-T standard. This choice can be justified by three main reasons:

- The development of a transmission system with comparable performances requires a lot of research effort, due to its complexity, both in terms of economical and engineering resources.

- DVB-T has proven to withstand portable reception and offers a wide range of tradeoff between bitrate and robustness.

- The most difficult part of the transmission chain, the demodulator, can be found as a relatively inexpensive and low-power stand-alone integrated circuit. At the same time, the modulator can be bought as an Intellectual Property (IP) ready to be embedded in programmable components as Field Programmable Gate Array (FPGA).

Even if the DVB-T standard was not originally developed with mobility in mind, it was felt later that such a feature offers a wide range of new and interesting applications, like for trains, cars or even airplanes. European project as VALIDATE and MOTIVATE demonstrates that this standard can be applied to allow the transmission of low bit rate multiplexes (up to 10Mbps) over difficult media [7]. Anyway, to achieve successful mobile OFDM reception there are a number of problems to overcome, that must be accounted for during the receiver design.

- The channel estimation has to track the channel variations in time and frequency. This is not exactly the scope of most of commercial DVB-T receivers, which are intended to withstand fixed reception.

- The receiver has to withstand the noise-like distortion called FFT leakage, created by the time variant channel during the time T_s of a symbol. In this case, the subcarriers are no longer pure sine waves and the orthogonality requirement is no longer fulfilled. Every demodulated carrier will be partly affected by all the other carriers in a symbol, generating Inter-Carrier Interference (ICI), so that the demodulated amplitude and phase values are distorted.

- The received field strength, and consequent C/N, has to be sufficiently high in all locations to permit a reliable mobile service. The field strength is varying from place to place due to two effects: shadow fading (slow fading) and multipath fading (fast fading). The effects of fast fading depend strongly on the system parameters. For a OFDM system with a sufficiently deep time interleaving (in relation to the wavelength and the speed) and strong coding, the fast fading does not play any important role, since the average power during the interleaving depth is high enough. For DAB (at sufficiently high speeds) this condition holds and the system becomes essentially insensitive (from a field strength point of view) to fast fading. DVB-T on the other hand does not have any time interleaving, so the received field strength must be large enough for every received symbol to avoid bit errors.

- Time and frequency synchronization must be acquired and maintained for mobile channels. When the impulse response and the Doppler spectrum of the channel is quasi stationary, or changing only gradually, maintaining synchronization can be an easy task. Problems however arise when there are sudden changes. These changes will either be permanent, then the best behaviour would be to react as quickly as possible, or they might be only temporary, so that the original situation is re-established soon again (in which case it would have been best not to change

anything). Since the receiver does not know what the future will be, a tradeoff between fast and slow receiver adaptation to a changing environment has to be found.

Even if the DVB-T standard had proven to be a good choice as modulation scheme for developing digital wireless television production systems, it doesn't perfectly fulfill all the different requirements for the different scenarios presented before. The DVB-T standard was born for unidirectional broadcasting, and effectively targets only applications where the backward channel is not required. Moreover, some other problems can be identified; in particular, the main concerns are the limited bandwidth (the standard calls for 8MHz channels, with provision for 7 and 6MHz channels) and the lack of explicit support for mobile reception [10]. The initial bandwidth figure of 8MHz was given by the need of progressively replacing existing analog television broadcasting channels. In fact, the DVB-T standard has been developed with particular attention to the possibility of analog and digital co-existence, thus avoiding mutual interference with legacy PAL/NTSC transmissions. The consequence of the lack of protection to shadow fading is that even short shadowing events cause unrecoverable transmission errors. Some different solutions must be studied especially to address this kind of problems, that generates annoying punctual system failures.

Additionally, for short range applications, the increased bandwidth could be exploited to multiplex multiple terminals over the same radio resource; this advantage could be further improved by the possibility to re-allocate in real time the bitrate between multiple cameras to adapt the audio/video quality. A completely different system should be developed to exploit this capacity.

1.4   Main contributions

As part of the preliminary work that has been done, a C/C++ simulator have been implemented and constitutes the primary tool to evaluate the choices of the system modulation parameters and the performances of receiver's algorithms.

The requirements of the applications addressed by this work are very different, and **two different systems have to be developed in order to fulfill the whole range of possible scenarios**.

The first system covers the applications requiring long and medium range links that doesn't require the presence of the backward channel. This is an unidirectional system that can overcome even long shadow fading events thanks to the insertion of deep time

interleaving, at the expense of additional latency. This system have been extensively studied, the modulation specifications have been given and a receiver architecture has been proposed. The complete modulation–demodulation chain has been implemented in VHDL to validate the software simulations with on field trials.

The second system is tailored to short and medium range applications, like studio productions, for which time-division duplexing represents a viable option to share the radio resource and implement a backward channel. The main modulation parameters of this system have been identified and some application examples are given. Anyway, the study of the receiver architecture and the physical implementation of such a system will be the object of future work.

1.4.1 Enhanced-mobility COFDM system

A COFDM system aimed to offer improved performances for mobile applications, derived from the experience on DVB-T standard, is proposed. This system is tailored to satisfy the requirements of **unidirectional medium to long range applications**, and differs from DVB-T by several aspect, while retaining backward compatibility if the advanced features are disabled. Three key points have been identified that can greatly improve the performances and the usability of this system to address the applications in mobile scenarios.

- Deep time-interleaving has been added to achieve protection to multipath fading and especially to shadow fading.

- The modulated bandwidth can be varied to fully exploit the allocated bandwidth.

- Turbo codes have been added to further improve error correction capabilities.

Moreover, this system has been designed to maintain backward-compatibility toward existing DVB-T 2K systems. Since the available *reserved* bits inside Transmission Parameter Signalling (TPS) stream are not enough to house the additional parameters, the TPS format has been carefully modified to preserve the backward compatibility when the advanced features are disabled.

1.4.2 Receiver architecture and system validation

A demodulator architecture has been studied for the enhanced-mobility COFDM system, and extensive software simulations have been performed to find the best balance between performances and computational load. In particular it must be noted that, to

fully exploit the capabilities of the additional features of the enhanced-mobility OFDM
system, the front-end must be able to withstand temporary loss of signal, up to half
the time interleaver depth. The variable modulated bandwidth requires smart channel
estimation techniques to be able to obtain the best performances for both mobile and
quasi-stationary channels. Moreover, turbo codes potentially allow the demodulation of
the OFDM signal even for very low C/N ratios; to effectively exploit these capabilities,
however, we must identify and study the other critical tasks of a receiver. For this reason,
improved robustness time and frequency synchronization algorithms have been developed
and optimized.

In the recent past, the evolution of semiconductor technology and in particular of
Field Programmable Gate Arrays (FPGA) allowed the implementation of complex OFDM
transmission schemes. A prototype hardware platform has been designed to implement
a complete wireless link in order to evaluate the performances of the proposed solutions
by means of on-field trials, exploiting the processing power and reconfigurability of Xilinx
Virtex2/Virtex2Pro FPGAs.

The RTL design required carefully tweaking the C/C++ algorithms. The floating
point arithmetic used by the software simulator must be phased out for a more RTL-
efficient fixed point arithmetic. Several aspects must be addressed in this process, going
from adequate data scaling to avoid numerical overflow and data width selection to opti-
mize the balance between quantization noise and design resources.

The receiver algorithms have been studied with the objective of physical implementa-
tion and some particular design choices aimed to reduce hardware complexity have been
discussed.

1.4.3   TDM OFDM system

The requirements of an **OFDM system tailored to short- and medium-range** multi-
media wireless applications have been analyzed. The limited transmission distances makes
Time-Division-Multiplexing a viable option to efficiently share the RF channel between
multiple terminals without incurring in excessive latency. The main parameters of such a
TDM OFDM system have been studied and the 802.16a standard [9] has been identified
as a good starting point for the definition of a specialized system. The main parameters
of the physical layer have been analyzed and some application examples have been pre-
sented. Moreover, for a reduced-mobility scenario, a mechanism of adaptive pre-distortion
is analyzed that improves the performances for multipath environment.

1.5 Structure of this thesis

This thesis is structured as follows. Chapter 2 introduces some fundamental concepts of OFDM modulation and the mathematical notation that will be subsequently used. The literature review of the OFDM critical receiver tasks as synchronization, channel estimation and diversity techniques is then presented. Finally, a brief resume of the physical layers of DVB-T and 802.16 standards is provided.

Chapter 3 introduces the simulation environment developed to test and evaluate the proposed systems and in particular several implemented channel models are discussed. Among those, a novel sparse shadowing model is introduced.

In chapter 4, the enhanced-mobility COFDM system is proposed, that extends DVB-T capabilities by means of deep time interleaving, variable bandwidth and improved error correction capabilities thanks to PCCC turbo codes.

In chapter 5, the receiver architecture is presented, and the main demodulator tasks are analyzed. In particular, automatic gain control, time and frequency synchronization, channel estimation and analysis, two-branch receiver diversity are discussed. Moreover, the particular problems that arise from the use of the deep time interleaving are addressed. Some hardware optimizations are also presented.

Chapter 6 collects the main simulation results and discusses the performances of the main receiver algorithms. Some simulations of the complete system to evaluate the global performances are also provided.

In chapter 7, the requirements of a TDM OFDM system tailored for short to medium range applications are analyzed. A pre-distortion method based on partial channel inversion is presented.

Finally, chapter 8 contains the conclusion and future work.

Chapter 2

OFDM introduction and state of the art

2.1   Chapter introduction

In this chapter, the principal concepts related to OFDM modulation are presented. The OFDM formulation employing FFT gives rise to the possibility of efficient implementation of the filter banks required for both transmitter and receiver. Bandwidth efficiency is then analyzed, and the insertion of a guard interval is identified as a method to overcome inter-symbol interference due to multipath propagation. Coding is then introduced as an efficient way to overcome errors due to selective frequency fading, and Turbo codes state-of-the-art is presented.

Time and frequency synchronization is one of the most compelling task for an OFDM receiver. The problem of synchronization can be divided in two steps: acquisition and tracking. Some existing methods are analyzed. Coherent modulation requires channel amplitude and phase estimation; three main class of estimators are reviewed. Diversity and adaptive modulation are then presented as efficient ways to overcome the problems of frequency-selective and mobile channels.

Finally, two wireless standards that are very interesting for the development of our applications are reviewed in detail: DVB-T and 802.16.

2.2   OFDM principles

In a conventional serial data system, the symbols are transmitted sequentially, with the frequency spectrum of each data symbol allowed to occupy the entire available bandwidth.

A parallel data transmission system offers possibilities for alleviating many of the problems encountered with serial systems. A parallel system is one in which several sequential streams of data are transmitted simultaneously, so that at any instant many data elements are being transmitted. In such a system, the spectrum of an individual data element normally occupies only a small part of the available bandwidth.

In the OFDM scheme of figure 2.1 the serial data stream of a traffic channel is passed through a serial-to-parallel convertor which splits the data into a number of parallel channels. The data in each channel is applied to a modulator, such that for N channels there are N modulators whose carrier frequencies are $f_0, f_1, ..., f_{N-1}$. The difference between adjacent channels is Δf and the overall bandwidth W of the N modulated carriers is $N\Delta f$.

In the more conventional serial transmission approach, the traffic data is applied directly to the modulator, transmitting at a carrier frequency positioned at the center of the transmission band and the modulated signal occupies the entire bandwidth W. By
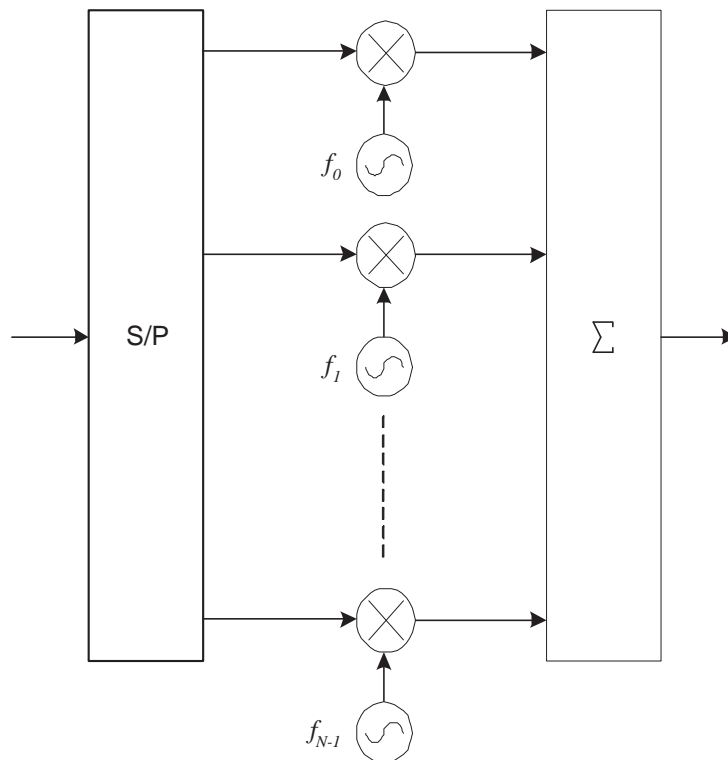
Figure 2.1: OFDM modulation block diagram.

contrast, during a N-symbol period of the conventional system, each of the N OFDM subchannel modulators carries only one symbol, each of which has an N time longer duration.

The principal advantage of OFDM is that because the symbol period has been increased, the channel's delay spread becomes a significantly shorter fraction of a symbol period than in the serial system, potentially rendering the system less sensitive to channel-induced dispersion than the conventional serial design.

The drawback of OFDM systems is their complexity, because of the need of N modulators, receiver filters and demodulators. This is particularly relevant since, in order to achieve high resilience against fades in the channel, the block size N must be in the order of 100, requiring a large amount of subchannel modems.

2.2.1 OFDM employing FFT

Substantial hardware simplifications can be made with OFDM transmissions if the bank of subchannel modulators/demodulators is implemented using the computationally efficient pair of Inverse Fast Fourier Transform (IFFT) and Fast Fourier Transform (FFT) [11].

In fact, for the l-th rectangular-shaped signalling interval of length T_s we can express the k-th subchannel as:

$$c_{l,k} = (a_{l,k} + j \ b_{l,k}) \ rect\Big(\frac{t - lT_s}{T_s}\Big) \tag{2.1}$$

where $a_{l,k}$ and $b_{l,k}$ are real numbers that depends on the input data and on chosen constellation. The modulated signal corresponding to the l-th signalling interval can thus be written as

$$m_l(t) = \Re\{\sum_{k=0}^{N-1} c_{l,k} \ e^{j2\pi f_k t} \} \tag{2.2}$$

If we write $f_k = f_0 + k\Delta f$ and $t = nT_s$, with the orthogonality condition

$$\Delta f = 1/T_s, \tag{2.3}$$

the above equation becomes

$$m_l(nT_s) = \Re\{e^{j2\pi f_0 nT_s} \sum_{k=0}^{N-1} c_{l,k} \ e^{j2\pi kn} \} \tag{2.4}$$

in which we can recall the formula of DFT (inverse) transformation. The parameter N of OFDM systems is always a power of two, thus the more computationally efficient IFFT algorithm can be employed.

With the orthogonality condition 2.3 and employing rectangular pulse shaping, the spectrum of every subcarrier is a $sin(x)/x$ function, whose zeros correspond to the center of the other subcarriers, thus giving no Inter-Carrier Interference (ICI). The overall spectrum is flat over the used bandwidth; in figure 2.2 the frequency-domain transform of every individual subcarrier and the composite spectrum of the transmitted signal, with 12 modulated subcarriers, are shown.

2.2.2   Bandwidth efficiency

One important consideration about OFDM is related to bandwidth efficiency. Using a serial system with one carrier, the minimum bandwidth required is $f_B = 1/T$ and the bandwidth efficiency is $\eta = 1Bd/Hz$ because the spectrum of this pulse is represented by the sync function whose first zero is at $f_B = 1/T$. The approximate bandwidth of a $(2M + 1)$-carriers system using an impulse as well as M sine and cosine carriers of length $(2M + 1)T$ becomes

$$B = \frac{M + 1}{2M + 1}\frac{1}{T} \tag{2.5}$$
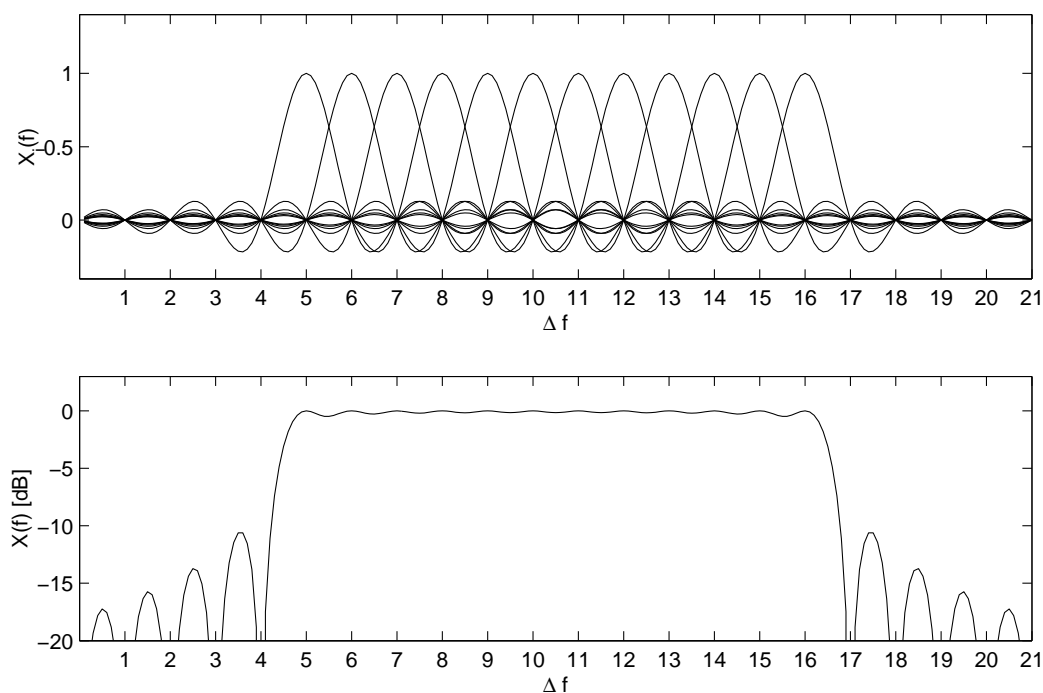
Figure 2.2: Spectrum for an OFDM system with 16 subcarriers.

yielding a bandwidth efficiency of

$$\eta = \frac{2M+1}{M+1} Bd/Hz. \tag{2.6}$$

For large M, the efficiency tends to $2Bd/Hz$. For a value of $M = 512$, the bandwidth efficiency $\eta = 1.998Bd/Hz$.

2.2.3 Modulation

In an OFDM link, the data bits are modulated on the subcarriers by some form of phase shift keying (PSK) or quadrature amplitude modulation (QAM). To estimate the bits at the receiver, knowledge is required about the reference phase and amplitude of the constellation on each subcarrier. In general, the constellation of each subcarrier shows a random phase shift and amplitude change, caused by carrier frequency offset, timing offset and frequency-selective fading. To cope with these unknown phase and amplitude variations, two different approaches exist. The first one is coherent detection, which requires estimates of the reference amplitudes and phases to determine the best possible decision boundaries for the constellation of each subcarrier. The main issue with coherent detection is how to find the reference values without introducing too much training overhead. To achieve this, several channel estimation techniques exist that will be described

in the next sections. The second approach is differential detection, which does not use absolute reference values, but only looks at the phase and/or amplitude differences between two QAM values. Differential detection can be done both in the time domain or in the frequency domain; in the first case, each subcarrier is compared with the subcarrier of the previous OFDM symbol. In the case of differential detection in the frequency domain, each subcarrier is compared with the adjacent subcarrier within the same OFDM symbol.

2.2.4   Guard interval

One of the most important reasons to employ OFDM modulation is the efficient way it deals with multipath delay spread. By dividing the input data stream in N subcarriers, the symbol duration is made N time longer, which reduces the relative multipath delay spread, relative to the symbol time, by the same factor. To eliminate Inter-Symbol Interference (ISI) almost completely, a guard time is introduced for each OFDM symbol. The guard interval is chosen larger than the expected delay spread, such that multipath components from one symbol cannot interfere with the next symbol. The method is best explained with reference to figure 2.3. Every block of N samples as obtained by IFFT is quasi-periodically extended by a length N_g simply repeating N_g samples of the useful information block.
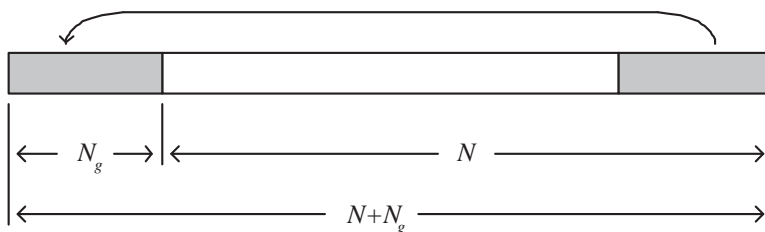
Figure 2.3: Guard interval by cyclic extension.

The total sequence length becomes $N + N_g$ samples, corresponding to a duration of $T_s + T_g$. Trailing and leading samples of this extended block are corrupted by the channel transient response, hence the receiver should demodulate only the central N number of samples, essentially unaffected by the channel's transient response. It must be appreciated that cyclic extension actually wastes channel capacity as well as transmitted power; however, if the useful information blocks are long, the extension length can be kept low relative to the useful information block length. Thus the efficiency in terms of

bitrate capacity can be expressed as:

$$\eta_g = \frac{N}{N + N_g} \tag{2.7}$$

and can be kept as high as 97% [4].

Echo spread longer than the guard interval duration generates ISI. Poole [12] studied the effects of an echo longer than the guard interval duration and gives an expression for the Equivalent Noise Floor (ENF) introduced; the results are extended to the case of multiple echoes. Benedetto *et al.* [13] studied the advantages of using waveform shaping in OFDM system to decrease the side lobes of the transmitted signal and to improve the performances in terms of E_b/N_0.

2.3 Coded OFDM (COFDM)

OFDM avoids the problem of inter-symbol interference by transmitting a number of narrow-band subcarriers together with using a guard time. This gives rise to another problem, however, which is the fact that in a multipath fading channel, all subcarriers will arrive at the receiver with different amplitudes. In fact, some subcarriers may be completely lost because of deep fades. Hence, even though most subcarriers may be detected without errors, the overall bit-error ratio (BER) will be largely dominated by a few subcarriers with the smallest amplitude, for which the bit-error probability is close to 0.5. To avoid this domination by the weakest subcarriers, forward-error correction coding is essential. By using coding across the subcarriers, error of weak ones can be corrected up to a certain limit that depends on the code and the channel. A powerful coding means that the performance of an OFDM link is determined by the average received power, rather than by the power of the weakest subcarriers.

2.3.1 Block codes

A *block code* encodes a block of k input symbols into n coded symbols, with n being larger than k. The purpose of adding the redundant $n - k$ symbols is to increase the *minimum Hamming distance*, which is the minimum number of different symbols between any pair of code words. For a minimum Hamming distance of d_{min}, the code can correct t errors where t is given by

$$t \leq floor\left(\frac{d_{min} - 1}{2}\right) \tag{2.8}$$

where $floor(x)$ denotes the function that rounds x down to the closest integer value. The minimum Hamming distance is upperbound by the number of redundant symbols $n - k$

as

$$d_{min} \leq n - k + 1 \tag{2.9}$$

For binary codes, only repetition codes and single-parity check odes reach this upper-bound. A class of non-binary codes that does reach the above bound are the *Reed-Solomon codes*. Because of their good distance properties and the availability of efficient coding and decoding algorithms [14] [15], Reed-Solomon codes are the most popular block codes. Reed-Solomon codes are defined for blocks of symbols with m bits per symbol, where the code length n is related to m by

$$n = 2^m - 1 \tag{2.10}$$

The number of input symbols k is related to m and the required minimum Hamming distance d_{min} as

$$k = 2^m - d_{min} \tag{2.11}$$

There appears to be little flexibility in the available code lengths as indicated by 2.10. However, a Reed-Solomon code can easily be shortened to any arbitrary length by setting a number of input bits to zero and deleting the same amount of output bits.

According to 2.8 and 2.9, a Reed-Solomon code can correct up to $floor((n - k)/2)$ erroneous symbols. Each symbol contains m bits, so a maximum amount of $m \cdot floor((n - k)/2)$ erroneous bits may be corrected. The latter is true if all bit errors occur within the maximum amount of correctable symbol errors. So, if a Reed-Solomon code is designed to correct up to two symbol errors containing 8 bits per symbol, it cannot correct an arbitrary combination of three bit errors, as these errors may occur in three different symbols. This characteristic makes Reed-Solomon codes particularly useful for correcting bursty channels. One example of such a channel is an OFDM link in the presence of multipath fading, which causes the errors to be concentrated in a few subcarriers that are hit by deep fades.

2.3.2   Convolutional codes

A convolutional code maps each k bit of a continuous input stream on n output bits, where the mapping is performed by convolving the input bits with a binary impulse response. The convolutional encoding can be implemented by a simple shift register and modulo-2 adders. As an example, figure 2.4 shows the encoder for a rate 1/2 code which is actually one of the most frequently applied convolutional codes. This encoder has a single data input and two outputs G_1 and G_2.
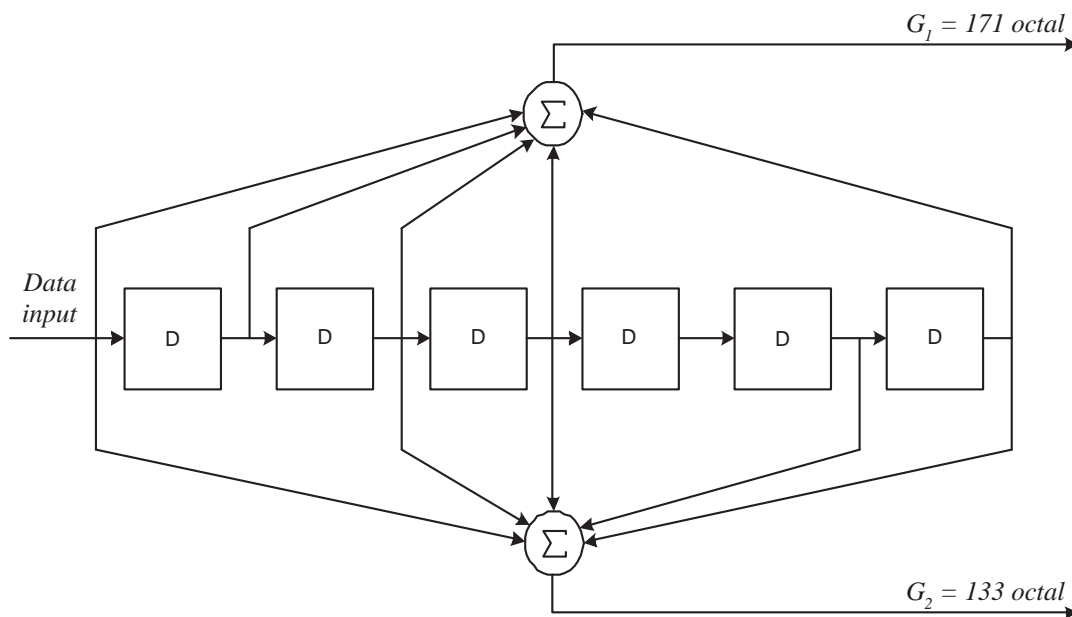
Figure 2.4: DVB-T convolutional inner coder.

Each pair of output bits $\{G_1 G_2\}$ depends on seven input bits, being the current input bit plus six previous input bits that are stored in the length-6 shift register. The value of 7 – or in general the shift register length plus 1 – is called the *constraint length*. The shift register taps are often specified by the corresponding polynomials or generator vectors. For the example of figure 2.4, the generator vectors are $\{1111001, 1011011\}$ or equivalently $\{171, 133\}$ in octal format.

Decoding of convolutional codes is most often performed by *soft-decision Viterbi decoding*, which is an efficient way to obtain the optimal maximum likelihood estimate of the encoded sequence. A description of this decoding technique can be found in [16]. The complexity of Viterbi decoding grows exponentially with the constraint length. Hence, practical implementations do not go further than a constraint length of about 10. Decoding of convolutional codes with larger constraint length is possible by using suboptimal decoding techniques like sequential decoding [16].

Because convolutional codes do not have a fixed length, it is more difficult to specify their performance in terms of Hamming distance and a number of correctable errors. One measure that is used is the *free distance*, which is the minimum Hamming distance between arbitrarily long different ode sequences that begin and end with the same state of the encoder, where the state is defined by the contents of the shift register of the encoder. For example, the previously shown code has a free distance of 10. When hard decision

decoding is used, this code can correct up to $floor((10-1)/2) = 4$ bit errors within each group of encoded bits with a length of about 3 to 5 times the constraint length. When soft decision decoding is used, however, the number of correctable errors does not really give a useful measure anymore. A better performance measure is the *coding gain*, which is defined as the gain in the bit energy-to-noise density ratio E_b/N_0 relative to an uncoded system to achieve a certain bit error ratio. The E_b/N_0 gain is equivalent to the gain in input signal-to-noise ratio (SNR) minus the rate loss in dB because of the redundant bits.

2.3.3 Turbo codes

Parallel concatenated coding schemes known as "Turbo Codes" have been shown to yield remarkable coding gains close to the theoretical limits [17] when compared to classical FEC coding schemes. Such results are achieved by employing iterative decoding techniques. In these coding schemes the core of the iterative decoding structure can be a Soft-Input Soft-Output (SISO) approach to perform a-posteriori probability (APP) estimation. Depending on the constituent encoder polynomials, the block length and the interleaver, the decoder convergence can vary and also the complexity grows proportionally. It has demonstrated in [18] that architecture complexity and decoding latency grow linearly with block length N. An asymptotic analysis of iterative decoding can be based on the method of density evolution [19]. This method allows to analyze the probability density function and to determine the convergence of the decoding process. The extrinsic information transfer chart is another method also used to evaluate the behavior of the iterative decoding [20]. The correct understanding of the behavior of these codes opens new scenarios to the coding theory especially for applications at high bit rates in concatenated mixture codes. These mixtures of outer and inner encoders allow designing better performing forward error correction schemes with more strength and less weaknesses than individual component coder. For Turbo Codes the prediction of cliffs in bit error rate probability depending on the number of iterations is a powerful instrument to evaluate the expected system performances in serial concatenation of interleaved codes [21]. The evolution of this new family of correction codes is now represented by the non-binary turbo-codes introduced by [22] which yield better performances than the classical binary turbo-codes especially at very low BER and high coding rates. These codes, build from a parallel concatenation of Recursive Convolutional Codes (RSC) offers a better convergence than iterative decoding, and a larger minimum distance [23]. Moreover, the lower sensitivity to puncturing pattern and the reduced latency is a very attractive feature for real time applications at high bit rates. The two parallel turbo codes scheme has been

adopted for the European standardization of the return channel for satellite networks [24] but only with an 8-state code which limits the achievable coding gain whereas keeping a reasonable complexity. For this non-binary codes the implementation complexity for high number of states still remain the main unresolved problem for the design of high throughput, low latency systems.

2.4 Synchronization

Synchronization is a critical task of every OFDM receiver. The symbols boundaries must be recovered to avoid Inter-Symbol Interference (ISI), and fine frequency correction has to be provided to avoid Inter-Carrier Interference (ICI). The global process of time and frequency synchronization can be divided into two different phases: initial *acquisition* and subsequent *tracking*.

2.4.1 Acquisition

The time and frequency acquisition processes are often closely interrelated. They must be performed as soon the receiver detects the RF signal. In this case, two scenario are possible:

- the receiver is tuning on a continuous OFDM transmission and tries to acquire time and frequency synchronization onto OFDM symbol boundaries;

- the receiver must acquire the synchronization of a burst-transmission OFDM system (e.g. TDM systems).

In the first case, the receiver can just exploit the cyclic prefix presence; often no additional aiding signals are added into the continuous stream. This topic has been analyzed by Van de Beek *et al.* [25], who exploit the redundancy inserted by the guard interval for time and frequency acquisition, and also for subsequent tracking.

In the second case, time and frequency acquisition must be performed at the very beginning of each TDM burst; the presence of one or more training symbols is essential for these systems, where time, frequency and channel estimations must be performed as soon as possible.

Several studies of optimal training symbol structures are available. Among those, an important early contribution comes from Schmidl and Cox [26], who employ a training symbol of length N composed by two identical repetitions of length $N/2$. The auto-correlation of the received signal allows to extract an approximate OFDM symbol start

time and frequency offset to restore FFT orthogonality. Minn and Bhargava [27] proposed an enhancement over the Schmidl and Cox method that enlarges the frequency offset acquisition range at the expense of reduced channel estimation capability. Gertou *et al.* [28] proposed a complete preamble structure and two algorithms for symbol timing and frequency offset detection in the scope of a fixed broadband wireless access system. Larsson *et al.* [29] proposed a joint synchronization and channel estimation algorithm for the IEEE 802.11a Wireless-LAN standard. Sari [30] proposed the use of a pilot tone embedded into the data symbol, surrounded by zero-valued virtual subcarriers, so that the frequency-shifted pilot can be located easily by the receiver.

2.4.2   Tracking

Fine time-tracking algorithms are generally based on correlation operations either in the time or in the frequency domain. Warner [31] employed the correlation in the frequency domain of the received synchronization pilot tones with known synchronization sequences, while de Couasnon [32] utilized the redundancy of the cyclic prefix by integrating over the magnitude of the difference between the data and the cyclic extension samples. Sandell [33] proposed exploiting the auto-correlation properties of the received time domain samples imposed by the cyclic extension for fine tracking in the time domain.

Frequency tracking generally relies on an already-established coarse frequency estimation having a residual frequency error of less than half the subcarrier spacing. Moose [34] suggested the use of the phase difference between subcarriers of repeated OFDM symbols in order to estimate frequency deviations of up to one-half of the subcarrier spacing, while Claßen [35] employed frequency domain synchronization subcarriers embedded into the data symbols, for which the phase shift between consecutive OFDM symbols can be measured. Daffara [36] and Sandell [33] used the phase of the received signal's autocorrelation function, which represents a phase-shift between the received data samples and their repeated copies in the cyclic extension of the OFDM symbol.

2.5   Channel estimation

In recent years numerous research contributions have appeared on the topic of channel transfer function estimation. Several techniques have been studied, designed for employment in single-user, single transmit antenna OFDM scenarios, since the availability of an accurate channel transfer function estimate in one of the prerequisites for coherent symbol

demodulation within an OFDM receiver. Channel estimation schemes for mobile OFDM systems, in contrast to stationary channels, where solely the frequency selectivity has to be estimated, also have to estimate the time variance of the mobile channel. Furthermore, in mobile OFDM systems inter-carrier interference will occur, resulting in an error floor that increases with Doppler frequency [37]. The techniques proposed in the literature can be classified as *pilot assisted*, *decision directed* and *blind* channel estimation methods.

2.5.1 Pilot-assisted channel estimation

In the context of pilot-assisted channel transfer function estimation a subset of the available subcarriers is dedicated to the transmission of specific pilot symbols known to the receiver, which are used for sampling the desired channel transfer function. This comes at the cost of a reduction in the number of subcarriers available for data transmission. This concept is demonstrated in figure 2.5, which shows a pilot insertion scheme for a 16-subcarriers OFDM system, with frequency pilot spacing $N_k = 3$ and time pilot spacing $N_l = 4$.
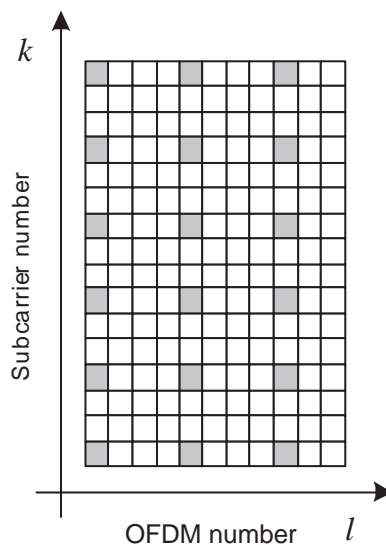
Figure 2.5: Pilot insertion scheme with $N_l = 4$ and $N_k = 3$.

To be able to interpolate the channel estimates both in time and frequency from the available pilots, their spacing has to fulfill the Nyquist sampling theorem, which states that the sampling interval must be smaller than the inverse of the double-sided bandwidth of the sampled signal. For the case of OFDM, this means that there exist both a minimum subcarrier spacing and a minimum symbol spacing between pilots. To determine these

quantities, we need to find the bandwidth of the channel variation in time and frequency. These bandwidths are functions of the Doppler spread B_d in the time domain and of the maximum delay spread τ_{max} in the frequency domain [38]. Hence, the requirements for the pilot spacing in time and frequency are:

$$N_l < \frac{1}{B_d} \tag{2.12}$$

$$N_k < \frac{1}{\tau_{max}} \tag{2.13}$$

Based on these samples of the frequency domain transfer function, an interpolation process must be performed to generate a transfer function estimate for all data subcarriers.

The pilot insertion scheme plays an important role for system performances [39]. For example, figure 2.6 shows an alternative pilot disposition for a 16-subcarrier OFDM system.
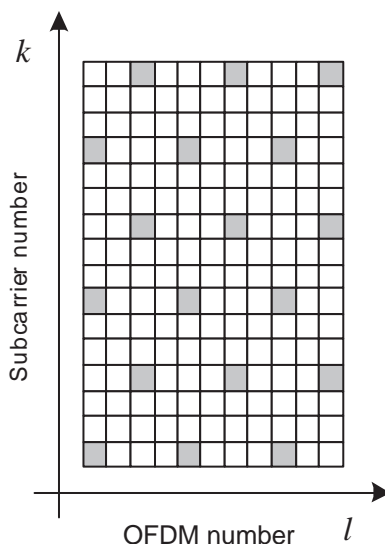
Figure 2.6: Alternative pilot insertion scheme.

Assuming knowledge on channel statistics and SNR, the optimal 2-D interpolation matrix can be computed [40] from the pilot auto-covariance matrix R_{pp}.

Instead of directly calculating the two-dimensional solution, it is also possible to separate the 2-D interpolation process into two 1-D interpolations [41]; depending on channel characteristics, time- or frequency- interpolation can be performed first. In the example of figure 2.6, the choice of performing time interpolation first, and then frequency interpolation leads to $N_l = 4, N'_k = 3$, while the inverse process leads to $N'_l = 2, N_k = 6$.

The family of *pilot-assisted* channel estimation techniques was investigated for example

by Sanzi and Speidel [42], who propose to adapt the bandwidth of the second frequency-interpolator filter depending on the channel time-response.

For the design of the time-interpolation filter, Hutter *et al.* [43] justify the use of simple linear-phase filter instead of a more complex linear minimum mean square error (LMMSE) estimator.

A further improvement of the mean-square error (MSE) versus complexity tradeoff offered by the approach of cascaded 1-D FIR filters was achieved by Edfors *et al.* [44] with the aid of Singular Value Decomposition (SVD) based low-rank approximation techniques. A fundamental characteristic of this type of estimator is that its associated complexity linearly depends on the number of transform coefficients retained.

As demonstrated by Van de Beek *et al.* [45], a further potential complexity reduction can be achieved by substituting the unitary linear transformation employed in the frequency direction filter, related to SVD-based low-rank approximation, by the computationally less complex DFT.

All the above methods rely on the insertion of known pilots directly in the frequency domain. An alternative approach to channel estimation in OFDM transmission systems is to estimate the channel directly from the time domain received signal. Analogous to wideband estimation in serial modems, a training sequence in the transmitted data stream can be employed in order to perform a correlation-based impulse response estimation. The corresponding frequency domain channel transfer function can be computed by FFT from this impulse response [46].

2.5.2 Decision-directed channel estimation (DDCE)

By contrast, in the context of decision-directed channel estimation, all the sliced and remodulated subcarrier data symbols are considered as pilots. In the absence of symbol errors and also depending on the rate of channel fluctuation, it was found that accurate channel transfer function estimates can be obtained, which often are of better quality, in terms of the channel transfer function estimator's mean-square error (MSE), than the estimates offered by pilot-assisted schemes. This is because the latter arrangements usually invoke relatively sparse pilot patterns.

Decision-directed channel estimation can be effectively used to maintain and refine channel estimation after a preliminary channel response acquisition by mean of dedicated training symbols.

Duel-Hallen *et al.* [47] proposed a frequency domain prediction filter assisted DDCE. Furthermore, the contribution of Tufvesson *et al.* [48], [49] must be mentioned, where a

prediction filter assisted frequency domain pre-equalization scheme was discussed in the context of an OFDM system. In a further contribution by Al-Susa and Ormondroyd [50], adaptive prediction filter assisted DDCE designed for OFDM has been proposed upon invoking techniques known from speech coding, such as the Levinson-Durbin algorithm or the Burg algorithm in order to determine the predictor coefficients.

2.5.3   Blind channel estimation

Furthermore, the family of *blind* channel estimation techniques was studied by Petropulu, Lin et al. [51], that employ linear block precoding to efficiently identify the channel up to a complex scalar ambiguity. The method is based upon a cross-correlation operations applied to successive received signal blocks. The proposed approach not only maintains the transmission power, but also provides multipath diversity and bandwidth efficiency.

Many existing blind OFDM channel estimation methods are statistical in nature and usually require large number of data blocks. For example, in [52], [53], and [54], statistical subspace approaches were proposed for blind channel identification that utilize cyclostationarity inherent in the OFDM systems with cyclic prefix. Clearly, these methods require that the channel be constant for a large number of blocks and, thus, have limited applicability in wireless channels involving high mobility when the channel may vary from block to block.

Wang et al. [55] proposed a blind channel estimation algorithm exploiting the cyclic prefix that exploits two-branch diversity and guarantees perfect channel retrieval in the absence of noise. In the presence of noise, the method has the desired property of being data efficient: only a single OFDM block is needed to achieve good estimation performance for a wide range of SNR values. The algorithm is also robust to input symbols as it does not have any restriction on the input symbols with regard to their constellation or their statistical properties.

2.6   Diversity

By deriving a generalized Shannon capacity formula for multiple-input, multiple-output (MIMO) Rayleigh fading channels, and by suggesting a layered space-time architecture concept that attains a tight lower bound on the capacity achievable, Foschini [56] has shown an enormous potential increase in the information capacity of a wireless system employing multiple-element antenna arrays at both the transmitter and receiver. Unfortunately, multiplying the RF parts implies increased cost and power consumption; more-

over, the computational complexity of this approach is quite high, thus leading again to increased hardware complexity and cost. Moreover, all the well-established methods used by current TDM-OFDM systems to perform signal detection, acquire synchronization, estimate channel response and perform error correction have to be revised and redesigned to be adapted to MIMO environments. Signal detection and training sequence optimization are studied in [57] and [58]. Diggavi et al. [59] focused on ICI modelling and adapted their results to MIMO-OFDM systems. There is a great effort in the field of optimal receiver equalization and antenna combining. Alamouti [60] presents a simple two-branch transmit diversity scheme. Using two transmit antenna and one receive antenna the scheme provides the same diversity order as maximal-ratio receiver combining (MRRC) with one transmit antenna and two receive antennas. He also shows a generalized method with two transmit antennas and M receive antennas to provide a diversity of order 2M. In this field, Chevreuil et al. [61] offered a good theoretical framework for further low-complexity studies. Kung et al. [62] investigated Bezout equalizer and pre-coders to mitigate the inevitable ISI/ICI in multipath MIMO systems, associated with space-time block codes (STBC) to achieve optimal error protection and fully exploit channel capacity. To take advantage of the added robustness offered by this approach, special space-time codes are being developed. Blum et al. [63], employing a 256-state code within a four transmit-four receive antennas system with QPSK modulation, achieve performances only 2dB lower than outage capacity.

2.7 Adaptive modulation

The bit error probability of different OFDM subcarriers transmitted in time dispersive channels depends on the frequency domain channel transfer function. The occurrence of bit errors is normally concentrated in a set of severely faded subcarriers, while in the rest of the OFDM spectrum often no bit errors are observed. If the subcarriers that will exhibit high bit error probabilities in the OFDM symbol to be transmitted can be identified and excluded from data transmission, the overall BER can be improved in exchange for a limited loss of system throughput. As the frequency domain fading deteriorates the SNR of certain subcarriers, but improves that of others above the average SNR value, the potential loss of throughput due to the exclusion of faded subcarriers can be mitigated by employing higher-order modulation on the subcarriers exhibiting higher SNR values.

In addition to excluding a set of faded subcarriers and varying the employed modulation order, other parameters such as the coding rate of error correction coding schemes can be adapted at the transmission according to the perceived channel transfer function.

Adaptive modulation is only suitable for duplex communication between two stations, since the transmission parameters have to be adapted using some form of two-way transmission in order to allow channel measurements and signalling to take place. Transmission parameter adaption is a response to time-varying channel conditions. In order to efficiently react to the changes of channel conditions, three following steps have to be taken:

- channel quality estimation;

- choice of the appropriate parameters for the next transmission;

- signalling or blind detection of the employed parameters.

Historically, interest in techniques of adapting the modulation and transmission rate parameters began in 1968, when Hayes [64] adapted the signal amplitude according to the prevalent channel environment by utilizing a feedback channel between the transmitter and receiver that was assumed noiseless and free from latency.

Recent work was pioneered by Webb and Steele [65], where the modulation adaption was analyzed in a flat Rayleigh fading environment with applications in a Digital European Cordless Telecommunications (DECT) system. Star QAM was used instead of square QAM and the channel reciprocity was exploited in a TDD scenario in order to adapt the modulation parameters. The metric used to quantify the channel quality was the received signal strength and the BER. There were also recorded the effect of block size, fading rate and co-channel interference on the performance.

The numerical upper bound performances of adaptive modulation in a slow Rayleigh fading channel was then evaluated by Torrance et al. [66].

Subsequent papers were published with more emphasis on the system aspects of adaptive modulation in a narrow-band environment. A reliable method of transmitting the modulation control parameters was proposed by Otsuki et al. [67], where the parameters were embedded in the transmission frame using Walsh code. Subsequently, at the receiver the Walsh sequence were decoded using maximum likelihood detection.

2.8 Review of the DVB-T standard

For digital terrestrial broadcasting, the DVB project opted to support OFDM, rather than single carrier, because of the very dense relay population in Europe. Also it was felt that high definition was not the strong driver that it had been in the USA. However, the scheme does allow for a future upgrade to include HDTV. The group considered the number of carriers in the OFDM transmission and opted to make this a user specified parameter, allowing for an early implementation at 2,000 carriers, with the possibility to increase to 8,000 when technology and commercial considerations allowed. The requirement for flexibility in frequency planning and the possibility to trade data-rate against coverage, was built in by requiring different forms of modulation (QPSK, 16QAM and 64QAM) and different code rates to be implemented in the receiver. The parameters of DVB-T standard can be summarized in table 2.8.

Parameter	Required value	Units
Useful channel bandwidth (BW)	8	MHz
Total number of subcarriers (N)	8192 (8k) or 2048 (2k)	-
Sampling frequency (f_s)	64/7	MHz
Subcarrier spacing (Δf)	1.116 (8k) or 4.464 (2k)	KHz
Active subcarriers	6817 (8k) or 1705 (2k)	-
Data subcarriers	6048 (8k) or 1512 (2k)	-
Signalling subcarriers	68 (8k) or 17 (2k)	-
Continual pilots	177 (8k) or 45 (2k)	-
Scattered pilots	1 over 12	-
Spacing of scattered pilots in time (N_l)	4	OFDM symbols
Spacing of scattered pilots in frequency (N_k)	3	subcarriers
Useful symbol duration (T_s)	896 (8k) or 224 (2k)	μs
Guard interval (T_g/T_s)	1/4, 1/8, 1/16, 1/32	-
Modulation	QPSK, 16QAM, 64QAM	-
Hierarchy α	1 , 2 , 4	-
Forward-error coding	convolutional + RS	-

Table 2.1: Main parameters of DVB-T.

Hierarchical modulation

Beside, the traditional uniform QPSK, 16QAM, 64QAM modulations, the standard supports non-uniform constellations. Non-uniform constellations are always associated with hierarchical transmission; in this case, two streams of data are simultaneously transmitted, possibly coded with different code rates to provide different robustness. In the case of figure 2.7, a 64QAM non-uniform constellation with $\alpha = 4$ conveys the very robust high-priority stream by means of the bits y_0, y_1 that determine the quadrant; the low-priority stream is less protected from channel impairments and is conveyed by the remaining bits y_2, y_3, y_4 and y_5 that determine the point of the constellation inside the quadrant.
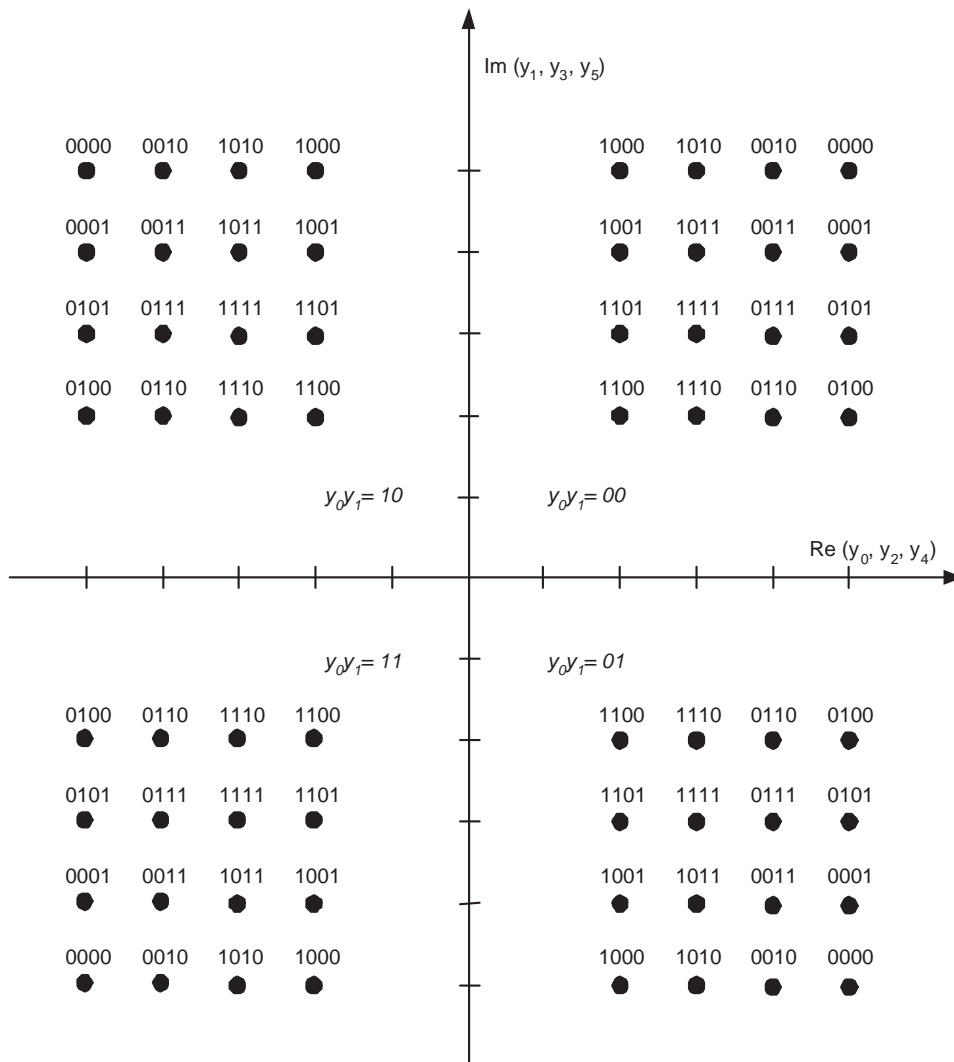
Figure 2.7: 64QAM non-uniform constellation, $\alpha = 4$.

By employing hierarchical modulation, the TV broadcasters are able to tailor the coverage to the specific needs. In the above example, the high-priority low-bitrate stream has a larger coverage while the low-priority high-bitrate stream is available only for users closer to the emitter.

The demodulator is supposed to decode only one out of the two streams.

Forward-Error Correction

The forward-error correction relies on a concatenated scheme common to the other DVB standards (DVB-S [2], DVB-C [3]) that employs a convolutional inner coder coupled with a Reed-Solomon outer coder. The block diagram of the encoding chain is shown in figure 2.8.
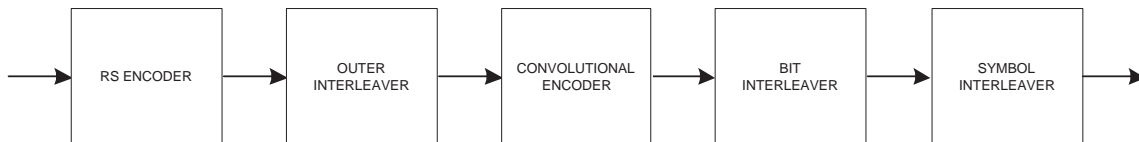
Figure 2.8: DVB-T forward-error correction block diagram.

The scheme exploits convolutional inner coder whose structure has already been shown in figure 2.4. This convolutional code can be represented by the two polynomial $G_1 = 171, G_2 = 133$ where the numbers express the connections to the adders in octal notation.

The bit- and symbol-interleavers play an important role for the performance of this error correction scheme. In the receiver, data obtained by demapping the data subcarriers are deinterleaved by the *symbol* and *bit* deinterleavers before convolutional decoding – usually soft-metric Viterbi algorithm is employed. The symbol interleaver shuffles the subcarriers in order to spread errors coming from multipath propagation, that causes deep fades in the frequency domain. The bit interleaver further spread the bits mapped on the same subcarrier (2, 4 or 6 depending on the constellation).

The outer interleaver is convolutional and spreads inner decoder residual errors, usually grouped in bursts, over 12 consecutive transport-stream packets.

2.9 Review of the 802.16 standard

Development of IEEE Standard 802.16 and the included WirelessMAN air interface, along with associated standards and amendments, is the responsibility of IEEE Working Group 802.16 on Broadband Wireless Access standards. The Working Groups initial interest was the 10-66 GHz range. The 2-11 GHz amendment project that led to IEEE 802.16a was approved in March 2000. The 802.16a project primarily involves the development of new physical layer specifications, with supporting enhancements to the basic MAC.

2.9.1 Medium Access Control (MAC) layer

The IEEE 802.16 MAC protocol was designed for point-to-multipoint broadband wireless access applications. It addresses the need for very high bit rates, both uplink (to the BS) and downlink (from the BS). Access and bandwidth allocation algorithms must accommodate hundreds of terminals per channel, with terminals that may be shared by multiple end users. The services required by these end users are varied in their nature and include legacy time-division multiplex (TDM) voice and data, Internet Protocol (IP) connectivity, and packetized voice over IP (VoIP). To support this variety of services, the 802.16 MAC must accommodate both continuous and bursty traffic. Additionally, these services expect to have an assigned Quality of Service (QoS) according to the specific traffic type.

While extensive bandwidth allocation and QoS mechanisms are provided, the details of scheduling and reservation management are left unstandardized and provide an important mechanism for vendors to differentiate their equipment.

Along with the fundamental task of allocating bandwidth and transporting data, the MAC includes a privacy sub-layer that provides authentication of network access and connection establishment to avoid theft of service, and it provides key exchange and encryption for data privacy. To accommodate the more demanding physical environment and different service requirements of the frequencies between 2 and 11 GHz, the 802.16a project is upgrading the MAC to provide automatic repeat request (ARQ) and support for mesh, rather than only point-to-multipoint, network architectures.

2.9.2 Physical layers

In the design of the physical (PHY) specification for 10-66 GHz, line-of-sight propagation was deemed a practical necessity. With this condition assumed, single-carrier modulation was easily selected; the air interface is designated WirelessMAN-SC.

Because of the point-to-multipoint architecture, the BS basically transmits a TDM signal, with individual subscriber stations allocated time slots serially. Access in the uplink direction is by time-division multiple access (TDMA). Following extensive discussions regarding duplexing, a burst design was selected that allows both time division duplexing (TDD), in which the uplink and downlink share a channel but do not transmit simultaneously, and frequency-division duplexing (FDD), in which the uplink and downlink operate on separate channels, sometimes simultaneously. This burst design allows both TDD and FDD to be handled in a similar fashion. Support for half-duplex FDD subscriber stations, which may be less expensive since they do not simultaneously transmit and receive, was added at the expense of some slight complexity. Both TDD and FDD alternatives support adaptive burst profiles in which modulation and coding options may be dynamically assigned on a burst-by-burst basis.

The 2-11 GHz bands, both licensed and license-exempt, are addressed in IEEE Project 802.16a. The standard specifies that compliant systems implement one of three air interface specifications, each of which provides for interoperability. Design of the 2-11 GHz physical layer is driven by the need for non-line-of-sight (NLOS) operation. Because residential applications are expected, rooftops may be too low for a clear sight line to a BS antenna, possibly due to obstruction by trees. Therefore, significant multipath propagation must be expected.

The three 2-11 GHz air interface specifications in 802.16a standard are:

- WirelessMAN-SCa: This uses a single-carrier modulation format.

- WirelessMAN-OFDM: This uses orthogonal frequency-division multiplexing with a 256-point transform. Access is by TDMA. This air interface is mandatory for license-exempt bands.

- WirelessMAN-OFDMA: This uses orthogonal frequency-division multiple access with a 2048-point transform. In this system, multiple access is provided by addressing a subset of the multiple carriers to individual receivers.

Because of the propagation requirements, the use of advanced antenna systems is supported.

WirelessMAN - SC

The PHY specification defined for 10-66 GHz uses burst single-carrier modulation with adaptive burst profiling in which transmission parameters, including the modulation and

coding schemes, may be adjusted individually to each subscriber station (SS) on a frame-by-frame basis. Both TDD and burst FDD variants are defined. Channel bandwidths of 20 or 25 MHz (typical U.S. allocation) or 28 MHz (typical European allocation) are specified, along with Nyquist square-root raised-cosine pulse shaping with a roll-off factor of 0.25. Randomization is performed for spectral shaping and to ensure bit transitions for clock recovery. The forward error correction (FEC) used is Reed-Solomon GF(N=256, K=239), with variable block size and error correction capabilities. This is paired with an inner block convolutional code to robustly transmit critical data, such as frame control and initial accesses. The FEC options are paired with quadrature phase shift keying (QPSK), 16-state quadrature amplitude modulation (16-QAM), and 64-state QAM (64-QAM) to form burst profiles of varying robustness and efficiency. The system uses a frame of 0.5, 1, or 2 ms. This frame is divided into physical slots for the purpose of bandwidth allocation and identification of PHY transitions. In the TDD variant of the PHY, the uplink subframe follows the downlink subframe on the same carrier frequency. In the FDD variant, the uplink and downlink subframes are coincident in time but are carried on separate frequencies.

WirelessMAN - SCa

The WirelessMAN - SCa PHY is based on single-carrier technology and designed for NLOS operation in the 2-11 GHz frequency bands. It brings some important modifications to the previously-addressed SC physical specifications. Some framing elements have been added that enable improved equalization and channel estimation performance over NLOS and extended delay spread environment, along with added Space-Time Coding (STC) transmit diversity option. The forward-error correction scheme employs a concatenated scheme with Reed-Solomon and Pragmatic Trellis Coded Modulation (TCM) and optionally Block Turbo Codes (BTC) or Convolutional Turbo Codes (CTC) for enhanced robustness.

WirelessMAN - OFDM

The WirelessMAN - OFDM PHY is based on OFDM modulation, that offers built-in support for NLOS operation, in the 2-11 GHz frequency bands.

Modulation parameters: the OFDM signal is extended by cyclic extension and the size of guard interval is decided by the BS and no more changed, since it would force all the SS to re-synchronize to the BS.

An OFDM symbol is made up from different carrier types:

- Data carriers

- Pilot carriers for various estimation purpose

- Null carriers for guard bands and DC carrier

The structure of the OFDM symbol in the frequency domain is shown in figure 2.9.
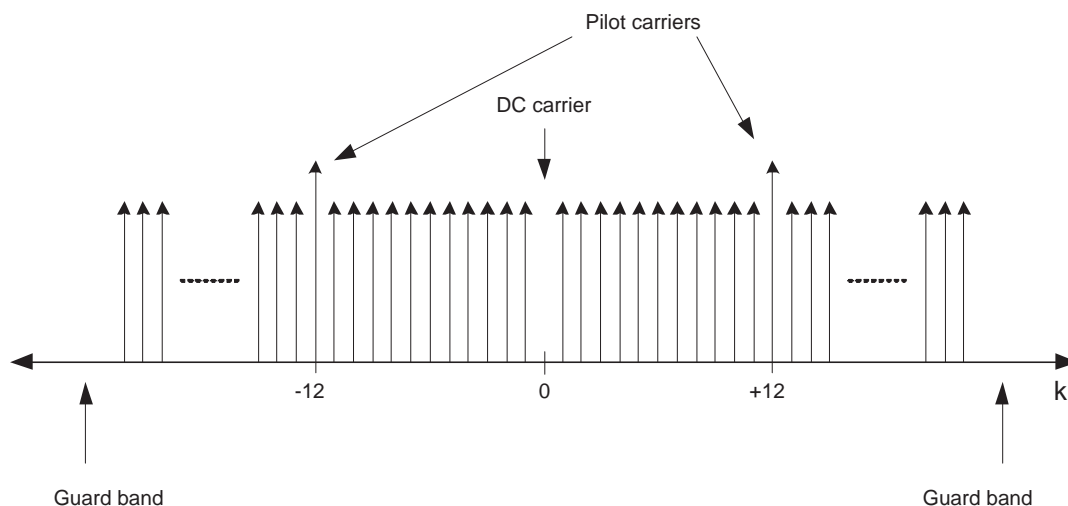
Figure 2.9: OFDM frequency description.

Table 2.2 resumes the parameters of the OFDM modulation.

Parameter	Required value
Total number of carriers (N)	256
Active carriers	200
Baseband excess bandwidth (f_s/BW)	8/7 or 7/6
Guard interval (T_g/T_s)	1/4, 1/8, 1/16, 1/32
Data carriers	192
Lower frequency guard carriers	28: from -128 to -101
Higher frequency guard carriers	27: from 101 to 127
Fixed locations pilot indexes	-84,-60,-36,-12,12,36,60,84

Table 2.2: Main parameters of WirelessMAN - OFDM PHY.

It must be noted that the sampling frequency f_s is determined by the nominal channel bandwidth BW. The carrier spacing is then determined by

$$\Delta f = f_s/N$$

Sub-channelization: the data carriers are divided into 4 sub-channels. Each subchannel accounts for 48 data carriers.

Error correction: the Forward Error Correction consists of a concatenation of a Reed-Solomon outer code and a rate-compatible convolutional inner code. This scheme must be supported on both uplink and downlink. Additional support for Block Turbo Codes and Convolutional Turbo Codes is optional.

Preamble structures: In the uplink, the data preamble consists of 2 times 128 samples preceded by a cyclic prefix whose length is the same as the cyclic prefix in the traffic mode. This preamble is referred to as *short preamble*. Figure 2.10 shows the structure of the UL preamble.
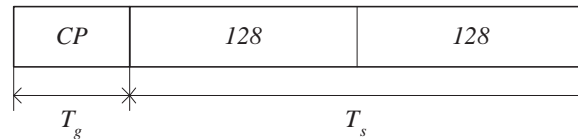
Figure 2.10: Short preamble structure.

The first preamble of the downlink phase consists of a cyclic prefix followed by 4 times 64 samples followed by a cyclic extension and finally followed by 2 times 128 samples. This preamble is referred to as the *long preamble* (refer to figure 2.11).
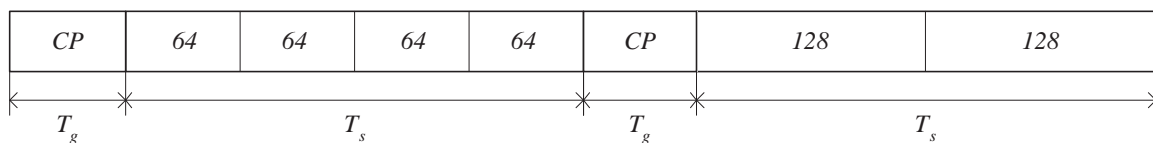
Figure 2.11: Long preamble structure.

Frame structure: The duplexing method is either FDD or TDD. In license-exempt bands, the duplexing method shall be TDD.

The OFDM physical supports a frame-based transmission. A frame consists of a DL sub-frame and an UL subframe. A DL sub-frame consists of only one DL physical Protocol Data Unit (PDU). An UL sub-frame consists of contention intervals scheduled for initial

ranging and bandwidth request purposes and one or multiple UL physical PDUs, each transmitted by a different SS.

WirelessMAN - OFDMA

The WirelessMAN - OFDMA PHY is based on OFDM modulation, that offers built-in support for NLOS operation, in the 2-11 GHz frequency bands.

Modulation parameters: the OFDM signal is extended by cyclic extension and the size of guard interval is decided by the BS and no more changed, since it would force all the SS to re-synchronize to the BS.

An OFDMA symbol is made up from different carrier types:

- Data carriers

- Pilot carriers for various estimation purpose

- Null carriers for guard bands and DC carrier

Pilot carriers are inserted in 32 fixed locations. For DL, other pilots are inserted each 12 carriers in a scheme similar to DVB-T.

In the OFDMA mode, the active carriers are divided into subsets of carriers, and each subset is termed a *sub-channel*. In the DL, a subchannel may be intended for different receivers; in the UL, a transmitter is assigned one or more sub-channels, and several transmitter may transmit in parallel. The data carriers are partitioned into groups of contiguous carriers. Each subchannel consists of one carrier from each of these groups. The number of groups is therefore equal to the number of carriers per subchannel, and it is denoted $N_{subcarriers}$. The number of the carriers in a group is equal to the number of subchannels, and it is denoted $N_{subchannels}$. The number of data carriers is thus equal to $N_{subcarriers} \cdot N_{subchannels}$. The exact partitioning into subchannels is determined by a permutation formula.

Table 2.3 resumes the DL parameters of the OFDMA modulation.

Error correction: the Forward Error Correction consists of a concatenation of a Reed-Solomon outer code and a rate-compatible convolutional inner code. This scheme must be supported on both uplink and downlink. Additional support for Block Turbo Codes and Convolutional Turbo Codes is optional.

Parameter	Required value
Total number of carriers (N)	2048
Active carriers	1702
Baseband excess bandwidth (f_s/BW)	8/7
Guard interval (T_g/T_s)	1/4, 1/8, 1/16, 1/32
Data carriers	1536
Lower frequency guard carriers	173
Higher frequency guard carriers	172
Fixed location pilots	32
Total number of pilots	166
$N_{subchannels}$	32
$N_{subcarriers}$	48

Table 2.3: Main parameters of WirelessMAN - OFDMA PHY.

2.10 Chapter summary

In this chapter, the fundamentals concept related to OFDM modulation have been recalled. The importance of error correction codes to achieve good performances for frequency selective channels has been stressed, and the main families of codes have been briefly presented.

The most critical part of an OFDM system is the receiver, that has to acquire and maintain time and frequency synchronization and provide channel estimation for coherent demodulation. A literature review of the most common synchronization method has been provided, along with channel estimation algorithms, with a special attention to pilot–assisted channel estimation schemes. Diversity has proven to be an efficient method to improve the system performances, and the literature main contributions have been summarized. For TDM systems, the possibility to employ adaptive modulation gives an additional advantage in term of system robustness and performance.

Even if the contributions presented above address and achieve excellent performances for each specific cited problem, the study and development of a proprietary OFDM system requires a careful tradeoff between performance and complexity.

Chapter 3

System Simulator

3.1   Chapter introduction

The study of wireless communication systems is a very complex task and requires the definition of many critical parameters; this is especially true for OFDM systems, whose complexity is generally higher than those employing single-carrier modulation schemes. Moreover, the choice of the modulation parameters is often a compromise between contradictory requirements and impacts directly on the design and complexity of the receiver. A simulator must be implemented to carefully evaluate the system design and the receiver complexity. The main requirements of such a simulator are fast execution times and accurate channel modelling. In fact, the impairments that a terrestrial propagation channel may exhibit are very different and adequate channel models must be used to stress the receiver design and ensure consistent comparisons between simulated and on-the-field performances.

3.2   C/C++ simulator

A simulator has been developed to evaluate the performances of the proposed OFDM systems. One of the primary goal of the simulator is to allow simulations runs embracing several seconds of real-world reception, in order to take into account slowly-varying effects as shadowing. For this reason, simulation speed was one of the main concerns.

During the initial planning phase, the first question that raised was the programming language to use. Among the several choices, we can cite:

- RTL simulation (Verilog, VHDL);

- MATLAB/Simulink environment;

- ANSI-C/C++.

Unfortunately, each of these options has advantages and drawbacks. The RTL simulation has one main advantage: it offers consistent performances between simulated and implemented design, but Verilog/VHDL code is difficult to handle and the simulation speed is very slow. The MATLAB/Simulink environment offers powerful mathematical tools for signal processing, visualization tools for result presentation and managing, but is not oriented toward low-level bit manipulation and thus would result in sub-optimal simulation speed. The ANSI C/C++ offers the highest simulation speed, at least one order of magnitude faster than Matlab and several order of magnitude faster that RTL code; it is a high-level language and allow to write signal processing routines is a very

compact and optimized way. Anyway, results are not so easily presented because of the lack of graphical data interfaces.

After carefully balancing the *pros* and *contros* of each language, the choice was for implementing the OFDM system with the ANSI C/C++ language due to its superior speed. Anyway, some functions have been developed to interface with the Matlab world and take advantage of its powerful data visualization tools.

Object-oriented programming

The simulator could have been written in standard C language, but we choose to exploit the concepts of object-oriented programming and implement each processing block as a different *object (class)*, with its own private data and functions, constructor and destructor. The main advantages of this kind of approach can be summarized as follows.

- Private data are dynamically allocated at object instantiation, thus reducing the used memory. The destructor is automatically invoked when the object is destroyed and the memory is freed.

- Private data initializations can be placed in the constructor, that is automatically called at object instantiation.

- The amount and type of private data storage give direct information about memory requirements of the derived VHDL design.

Another advantage is that implementing each block as a class results in a cleaner code, where each function works on a clearly referred object. For example, after instantiation of the *scrambler* block:

```
scrambler myscrambler;
```

we can invoke the scrambler process on packet *xb* as:

```
myscrambler.compute (yb,xb);
```

where the reference to scrambler block is evident.

One of the main general classes introduced in the simulator is the *packet* class template. This class provides the basic instruments to exchange packets of data between functions without worrying about pointers management.

```cpp
template <class T> class packet {
  public:
    uint     size;                        // size (no. of element)
    T*       data;                        // array of data
    packet   ();                             // generic instantiation
    packet   (uint csize);                   // explicit size instantiation
    packet   (packet<T> const &x);           // copy operator
    ~packet  ();                             // destructor
    alloc    (uint csize);                   // explicit memory allocation
    dealloc  ();                             // explicit memory free
    zeros    ();                             // init to zero
    packet<T>  operator + (packet<T> const &y);      // concatenation
    packet<T>& operator = (packet<T> const &y);      // assignment
    packet<T>& operator += (packet<T> const & y);    // data append
    packet<T>  operator () (uint start, uint stop);  // range selection
    };
```

This object contains the size of the packet (in number of elements) and the pointer of the data array. Several methods and operators have been implemented in order to hide the memory allocation and to ease the data manipulation. Moreover, this class has been implemented as a *template* to implicitly handle different data types exploiting the same user interface.

VHDL support

Some other features have been included to ease the development and the verification of VHDL implementation. Several fixed-point intermediate signals can be saved to file in *text* format after appropriate scaling and rounding. By simulating the C/C++ blocks in parallel with the VHDL design, we can verify the results consistency of the implemented VHDL fixed point design with the C/C++ floating point one.

Moreover, several look-up-tables have to be initialized in the VHDL code. Among those, we can recall FIR filters coefficients for channel estimator, baseband downsampling and filtering and demapper parameters. Some functions have been developed to automatically generate VHDL code with the initializations of the sensitive parameters. This have been done for two main reasons:

- to avoid mistakes that would have been difficult to find out and would have degraded the performances;

- to speed up the initial design and especially subsequent redesign that would require modifying the parameters.

3.2.1 Simulator components

The simulator is composed by three main components:

- transmitter;

- channel;

- receiver.

The transmitter generates 188-bytes long transport stream packets with random data and produces a baseband complex signal. The baseband data outputted by the transmitter is saved to a file called *tx.bin* in binary format.

The channel simulator provides for different channel models. It loads the data from the file *tx.bin* and saves the channel-impaired baseband signal to a binary file called *rx.bin*.

The receiver loads the input data from the file *rx.bin*, adds the noise contribution, and processes the received baseband data without *a-priori* knowledge about modulation parameters.

Each of these blocks have been developed with an approach as similar as possible to RTL design. The main problem is that C/C++ is a sequential language, while RTL is a concurrent one. These are completely different programming paradigm, but pseudo-concurrent processing is achieved if the C/C+ design is subdivided in sub-blocks and each sub-block processes the data as soon as its inputs are ready. This approach helps the subsequent RTL design and has the primary advantage of avoiding the accumulation of big amount of intermediate data, thus minimizing memory requirements.

Basic setup

The basic setup for system simulation is depicted in figure 3.1.
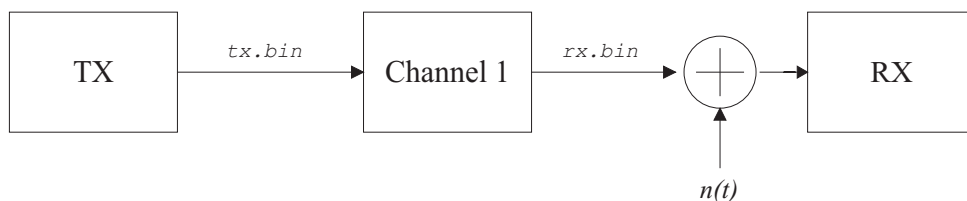
Figure 3.1: Simulator basic setup.

Sometimes it is useful to disable some elements; for example, several simulation runs with different noise levels are required to evaluate the behavior of the digital wireless

system around the minimum operating point. In this case the transmitter and the channel are enabled just for the first simulation run to generate the file *rx.bin*; afterwards, the receiver processes the same file several times inserting different amount of noise.

Diversity setup

The simulator can be modified to simulate different system configurations. Among these configurations, the most interesting involves the capacity of simulating receivers with antenna diversity.

In this case, the same transmitted signal is applied to two independent channel simulators, and then the signals *rx1.bin* and *rx2.bin* are applied to the diversity receiver, as depicted in figure 3.2. Since normally the receiving antennas are spaced by a distance $\Delta l << d$, where d is the distance between the transmitter and the receiver, we can assume that the two channel elements employ the same channel model and the two received signals are impaired by the same amount of noise. Anyway, it must be noted that is fundamental to impose independent multipath fading and noise sequences. The shadowing term can be common to the two paths since the shadow fading exhibited by the two received signal in line-of-sight conditions is correlated [68].
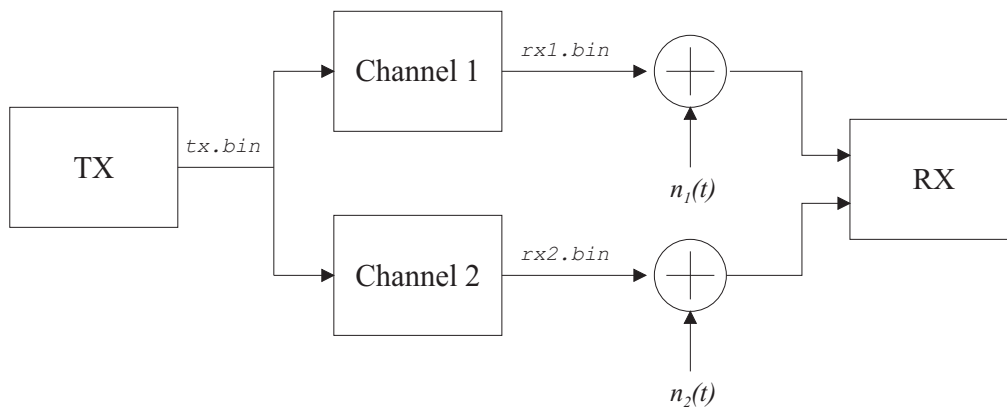
Figure 3.2: Simulator block diagram - diversity setup.

3.3 Channel simulator

To verify the performance of mobile communication systems, computer simulations considering the particular channel-properties need to be carried out. Care must be taken in the selection of the channel model used to characterize system performances. Using an inadequate channel model would result in misleading figures and inconsistent on-the-field performances. Moreover, during the development of a wireless systems, several components have to be studied and evaluated in terms of their peculiar performances. In particular, the receiver design requires the development and tuning of multiple synchronization and channel analysis blocks that have to be stressed by real-world conditions.

A mobile radio channel is usually characterized by the superposition of three different, mutually independent, multiplicative and approximately separable components that accounts for small-, medium-, and large-scale propagation effects [69]. The small-scale variations, mostly referred to as *multipath fading*, are fairly rapid in space, with significant changes occurring within the order of one wavelength. Medium-scale effect, mostly referred to as *shadowing*, is influenced by the spatial movements of the order of tens of wavelengths and creates random variations in the average power of the received signal which typically follows a lognormal distribution. In the large scale effect, spatial movements of the order of hundreds of meters make the median average power level vary in power-law fashion with path length. Large-scale variations is mostly referred to as *path loss*.

The received power P_{rx} can be expressed as:

$$P_{rx} = P_{tx}g_p g_s g_m \tag{3.1}$$

where P_{tx} is the transmitted power, g_p is the distance-dependent path loss, g_s is the gain due to shadow fading and g_m is the gain due to multipath fading.

The block diagram of the channel simulator is depicted in figure 3.3.
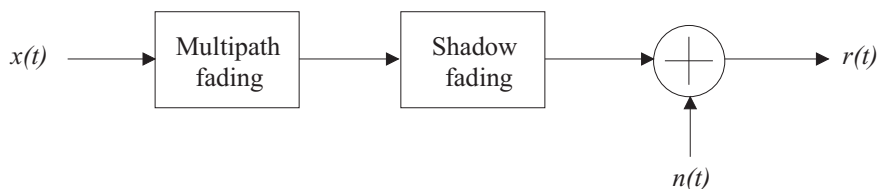
Figure 3.3: Channel simulator block diagram.

3.3.1   Path loss and AWGN contribution

The distance-dependent path loss can be expressed as:

$$g_p = G_{tx}G_{rx}\left(\frac{\lambda}{4\pi r}\right)^2 \tag{3.2}$$

where G_{tx} and G_{rx} represent the gain of the transmission and reception antennas, λ is the carrier wavelength and r is the distance between emitter and receiver. The above equation holds well for free-space propagation (eg, satellite communications) but must be corrected to take into account atmospheric attenuation and Earth geometry. We can thus rewrite equation 3.2 as:

$$g_p = G_{tx}G_{rx}\left(\frac{\lambda}{4\pi}\right)^2 r^{-\gamma} \tag{3.3}$$

where appropriate γ must be used. $\gamma = 4$ fits the plane-Earth model, while $\gamma = 4.16$ can be used for line-of-sight applications in the S-band [75].

The path loss is assumed to be constant for each simulation run, and results in a white noise contribution at the demodulator input. The Automatic Gain Control (AGC) of the RF part keeps constant the power of the signal at the demodulator input; the path loss contribution can thus be accounted by a variable power noise contribution superimposed to a constant power signal. Thus, the Additive White Gaussian Noise (AWGN) contribution $n(t)$ adds linearly to the received signal.

The power of the signal $n(t)$ in figure 3.3 can be adjusted to meet the desired C/N figure. It must be noted that the C/N figure specify the ratio in decibels (dB) between the power of the carrier of the desired signal and the total received noise power.

3.3.2   Shadow fading

For mobile wireless links, the receiver cannot always exploit direct line-of-sight signal, due to the presence of obstacles that interpose between transmitter and receiver antennas. This effect is called *shadow fading* and, with the common hypothesis of fixed obstacles, is dependent on the speed of the transmitter and receiver.

Log-normal shadow fading

Several studies have been accomplished on shadow fading in the scope of mobile radio channels, mainly for cellular applications [70], [71], [72]. In this case, both transmitter and receiver are on the ground, and the term g_s of equation 3.1 can be expressed by a

log-normal probability density function (g_s expressed in dB):

$$p(g_s) = \frac{1}{\sigma_s \sqrt{2\pi}} \, e^{\frac{g_s^2}{2\sigma_s^2}} \tag{3.4}$$

where the model parameters are obtained empirically. The log-standard deviation σ_s is normally between 8 and $12dB$. The autocorrelation of the shadowing process depends on the speed of the transmitter and receiver. A log-normally distributed sequence obeying equation 3.4 has been derived with Matlab for a receiver speed of $300km/h$. The evolution of g_s over $220ms$ is shown in figure 3.4.
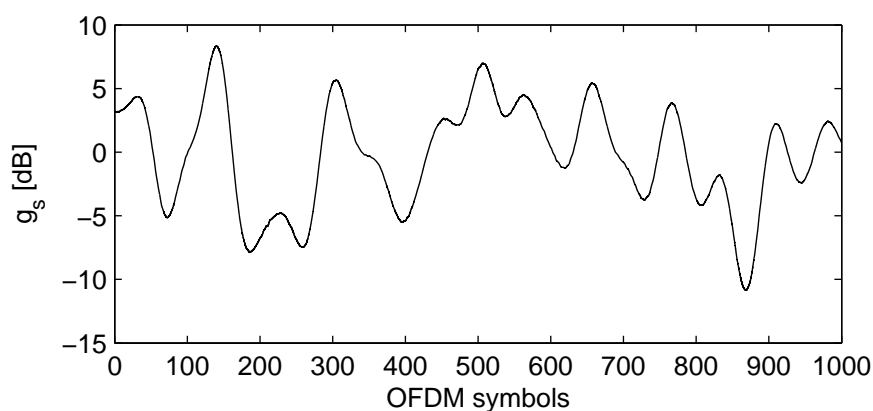
Figure 3.4: Shadow fading g_s.

As can be noted, around OFDM symbols 50 and 160 the slope of g_s is about $0.5dB/$symbol, thus leading to a considerable amount of ICI. To simulate slower shadow fading processes, the sequence of figure 3.4 is stretched in time, applying appropriate upsampling.

Sparse shadow fading

During field tests in Athens for Olympic games 2004, different shadowing behavior has been observed for the uplink between motorcycles and helicopter. The observed shadow fading exhibited strong attenuation values for short time intervals, due to obstacles such as small bridges and trees, while for the rest of the time the link was of line-of-sight (Ricean) nature, without noticeable attenuation due to shadowing. This generated singular errors that adversely affected the link perceived quality. Since one of the main goals of the proposed systems is to overcome such impairments, a different sparse shadow fading model has been developed. The block diagram of the proposed shadow fading model is shown in figure 3.5.
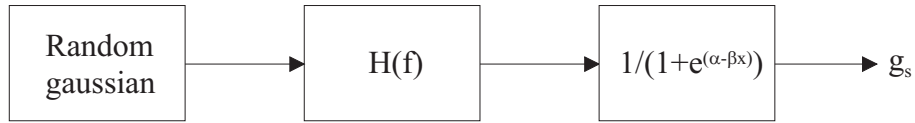
Figure 3.5: Shadow fading block diagram.

The filter $H(f)$ has been retained from previous model and the parameters α and β have been adjusted to obtain four different shadow fading evolutions. Once again, to simulate slower shadow fading processes, the sequence is stretched in time, applying appropriate upsampling.

The first choice generated the fading process depicted in figure 3.6.
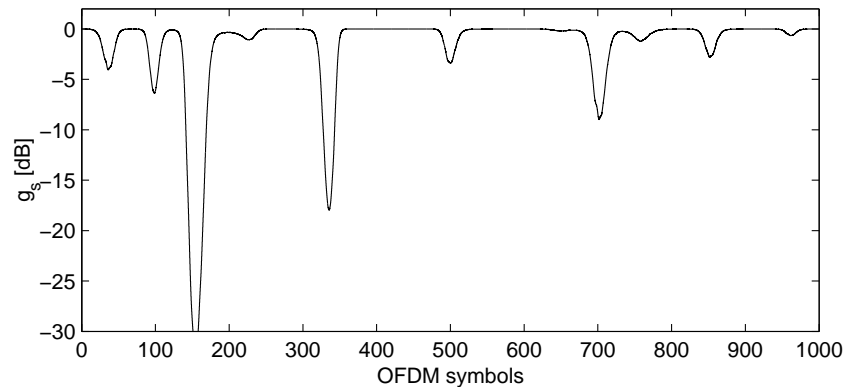
Figure 3.6: Shadow fading g_s, expressed in dB.

There are some sparse shadowing events, with high attenuation. Around symbol number 150, the attenuation is over 30dB. This model can be considered a good approximation of propagation experiencing shadow events due to small obstacles.

Two other independent shadowing processes were generated using the same parameters. Their evolutions are depicted in figure 3.7 and 3.8.

To simulate the fading process generated by shadowing of trees, a lower standard deviation has been used. The resulting shadowing process is shown in figure 3.9.

In this case, the attenuation peaks have lower magnitude, but are more closely spaced.

These four different realizations of the sparse shadow fading process, even if not representative of all possible real cases and not statistically accurate, have been extensively used in the simulations to account for single points of failure caused by obstacles interposition between transmitter and receiver.
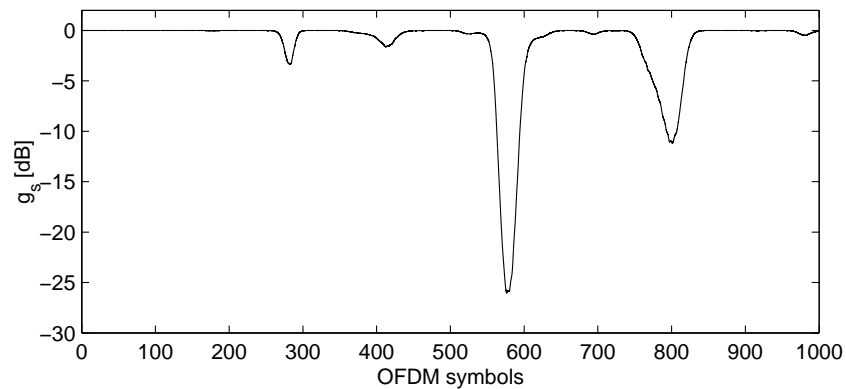
Figure 3.7: Shadow fading g_s, expressed in dB.
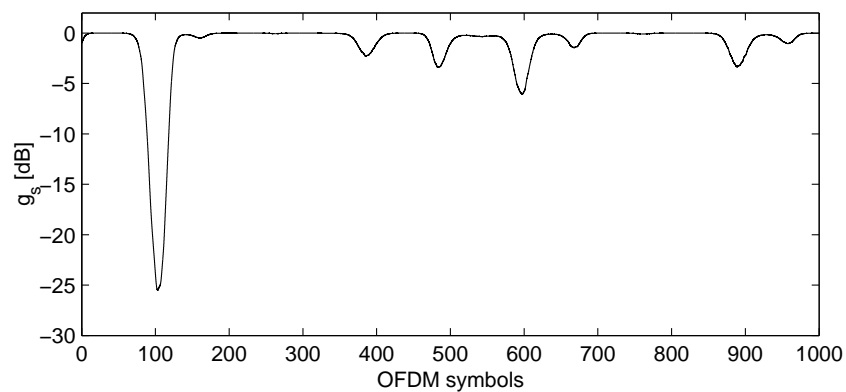
Figure 3.8: Shadow fading g_s, expressed in dB.
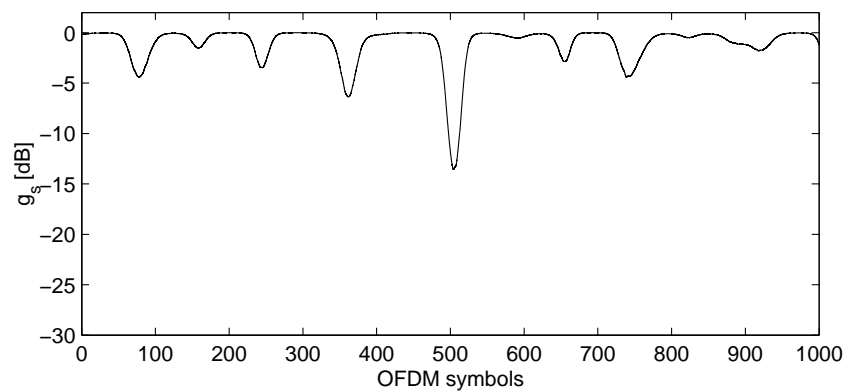
Figure 3.9: Shadow fading g_s, expressed in dB.

3.3.3 Multipath fading

Rice and Rayleigh stationary models

To evaluate the performances for multipath channels, the two channel models described in the DVB-T standard [4], annex B, have been implemented. They are stationary models,

and they are described by the following equation, where $x(t)$ and $y(t)$ are input and output signals respectively:

$$y(t) = \frac{\rho_0 x(t) + \sum_{i=1}^{N} \rho_i e^{-j\theta_i} x(t - \tau_i)}{\sqrt{\sum_{i=0}^{N} \rho_i^2}} \qquad (3.5)$$

where ρ_0 is the line-of-sight contribution, N is the number of echo paths, ρ_i, θ_i and τ_i are respectively amplitude, phase and delay of the $i - th$ path. A block diagram is shown in figure 3.10, where the $y(t)$ normalization factor is omitted for clarity.
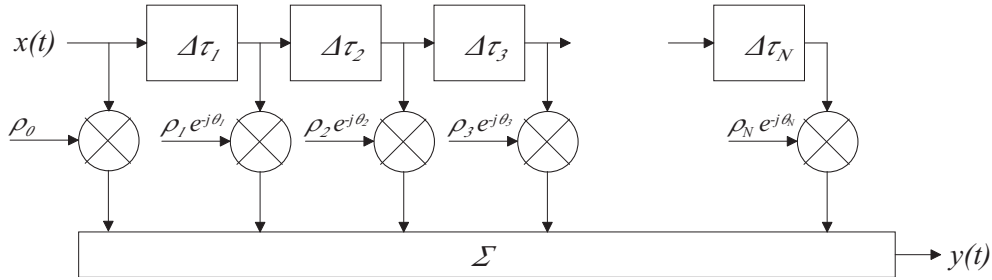
Figure 3.10: DVB-T Ricean and Rayleigh channel models block diagram.

The Ricean factor K express the ratio between the power of the direct path (the line-of-sight ray) and the total power of the reflected paths, and is given by:

$$K = \frac{\rho_0^2}{\sum_{i=1}^{N} \rho_i^2} \qquad (3.6)$$

Using these equations and the values for ρ_i, θ_i and τ_i listed in table 3.3.3, two different channel models have been generated:

- **Ricean channel** - ρ_0 has been calculated using 3.6 with ricean factor $K = 10$. This is the case of a line-of-sight (LOS) stationary environment.

- **Rayleigh channel** - ρ_0 has been forced to zero. This represent the case of a non-line-of-sight (NLOS) stationary environment.

The impulse response of the Rayleigh channel is shown in figure 3.11. The Ricean channel differs only because of the line-of-sight contribution ρ_0 at time $t = 0$ and is not shown.

The frequency-domain responses of Rayleigh and Ricean channels are shown in figure 3.12.

i	ρ_i	$\tau_i[\mu s]$	$\theta_i[rad]$
1	0,057662	1,003019	4,855121
2	0,176809	5,422091	3,419109
3	0,407163	0,518650	5,864470
4	0,303585	2,751772	2,215894
5	0,258782	0,602895	3,758058
6	0,061831	1,016585	5,430202
7	0,150340	0,143556	3,952093
8	0,051534	0,153832	1,093586
9	0,185074	3,324866	5,775198
10	0,400967	1,935570	0,154459
11	0,295723	0,429948	5,928383
12	0,350825	3,228872	3,053023
13	0,262909	0,848831	0,628578
14	0,225894	0,073883	2,128544
15	0,170996	0,203952	1,099463
16	0,149723	0,194207	3,462951
17	0,240140	0,924450	3,664773
18	0,116587	1,381320	2,833799
19	0,221155	0,640512	3,334290
20	0,259730	1,368671	0,393889

Table 3.1: DVB-T Channel models parameters.

Wide-Sense Stationary Uncorrelated Scattering (WSSUS) channel models

Let's now consider a frequency-selective and time-variant transmission channel $h(f, t)$. Although not being exhaustive for all classes of channels, describing the statistics of wireless channel by means of first and second order moments gives already good insight on their behavior [73]. Channels are said to be wide-sense stationary if the first order moments are independent of time, and the second order moments only depend on the time difference Δt. Similarly, channels that fulfill the same requirement with respect to the frequency variable are said to exhibit uncorrelated scattering. Finally, channels that combine both characteristics are known as Wide-Sense Stationary Uncorrelated Scattering (WSSUS) channels.

The complex baseband representation [74] of a mobile wireless channel impulse re-
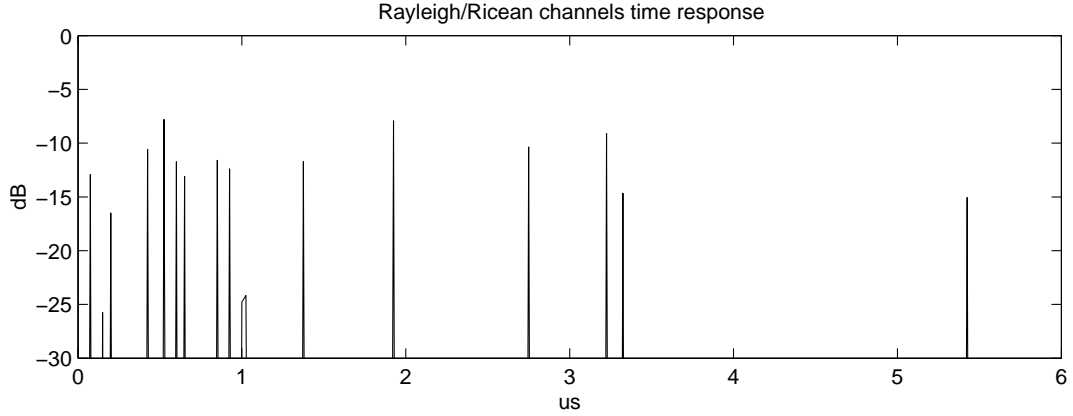
Figure 3.11: Rayleigh channel model impulse response.
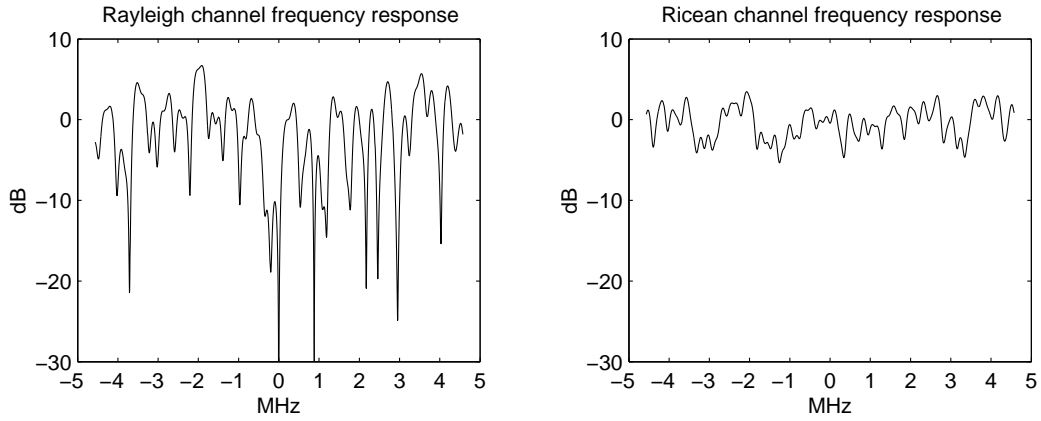
Figure 3.12: Rayleigh and Ricean frequency response over a 8MHz-channel.

sponse can be described by

$$h(t, \tau) = \sum_k \gamma_k(t)\delta(\tau - \tau_k) \tag{3.7}$$

where τ_k is the delay of the kth path and $\gamma_k(t)$ is the corresponding complex amplitude. Due to the motion of the vehicle, $\gamma_k(t)$'s are wide-sense stationary (WSS) narrow-band complex Gaussian processes, which are independent for different paths.

We assume that $\gamma_k(t)$ has the same normalized correlation function $r_t(\Delta t)$ for all k and, therefore, the same normalized power spectrum $p_t(\Omega)$. Hence

$$r_{\gamma k}(\Delta t) = E\{\gamma_k(t + \Delta t)\gamma_k^*(t)\} = \sigma_k^2 r_t(\Delta t) \tag{3.8}$$

where σ_k^2 is the average power of the kth path. Using 3.7, the frequency response of the

time-varying radio channel at time t is

$$H(t, f) = \int_{-\infty}^{\infty} h(t, \tau)e^{-j2\pi f\tau}d\tau = \sum_k \gamma_k(t)e^{-j2\pi f\tau_k} \tag{3.9}$$

Hence, the correlation function of the frequency response for different times and frequencies is

$$
\begin{aligned}
r_H(\Delta t, \Delta f) &= E\{H(t + \Delta t, f + \Delta f)H^*(t, f)\} \\
&= \sum_k r_{\gamma k}(\Delta t)e^{-j2\pi\Delta f\tau_k} \\
&= r_t(\Delta t)\left(\sum_k \sigma_k^2 e^{-j2\pi\Delta f\tau_k}\right) \\
&= \sigma_H^2 r_t(\Delta t)r_f(\Delta f)
\end{aligned}
\tag{3.10}
$$

where is the total average power of the channel impulse response defined as

$$\sigma_H^2 = \sum_k \sigma_k^2 \tag{3.11}$$

Without loss of generality, we assume that $\sigma_H^2 = 1$, which, therefore, can be omitted. From 3.10, the correlation function of $H(t, f)$ can be separated into the multiplication of a time-domain correlation $r_t(\Delta t)$ and a frequency-domain correlation $r_f(\Delta f)$. $r_t(\Delta t)$ is dependent on the vehicle speed or, equivalently, the Doppler frequency, while $r_f(\Delta f)$ depends on the multipath delay spread.

COST207 models

One of the major achievements in the COST-207 European project was the definition of time dispersive test channels for evaluation of equalizer performance in GSM systems. The strength of the COST-207 test profiles, Rural Area (RA), Typical Urban (TU), Bad Urban (BU) and Hilly Terrain (HT), has been their wide acceptation even outside Europe. The anticipation of such unique channel models has allowed researchers to compare results from link level simulations almost globally. The COST-207 models characterize the multipath channel for the case of Wide Sense Stationary Uncorrelated Scattering. Thus, they assume stationarity of the radio channel at least on the short term. Simulated channel responses for a 8MHz channel for a mobile speed of 80km/h are shown in fig. 3.13, 3.14, 3.15 and 3.16.

a) COST207 – Typical rural (non–hilly) area
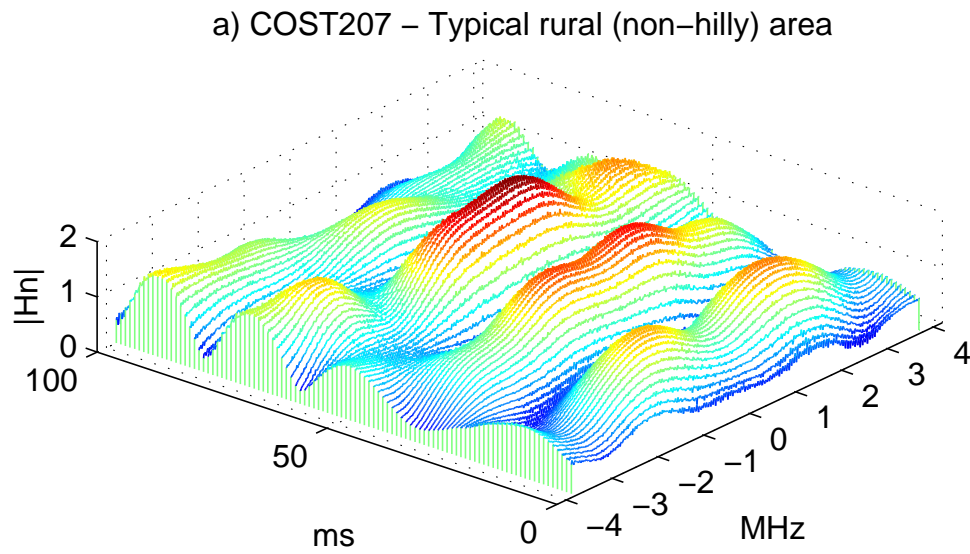
Figure 3.13: COST207-Rural Area (RA): frequency response over a 8MHz-channel, 80km/h.

b) COST207 – Typical urban (non–hilly) area
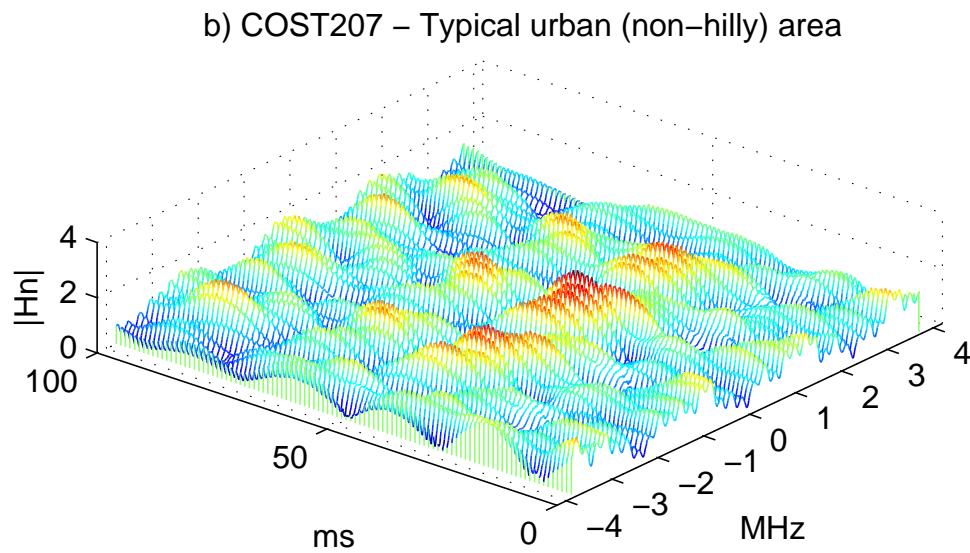
Figure 3.14: COST207-Typical Urban (TU): frequency response over a 8MHz-channel, 80km/h.

c) COST207 – Bad case hilly urban area
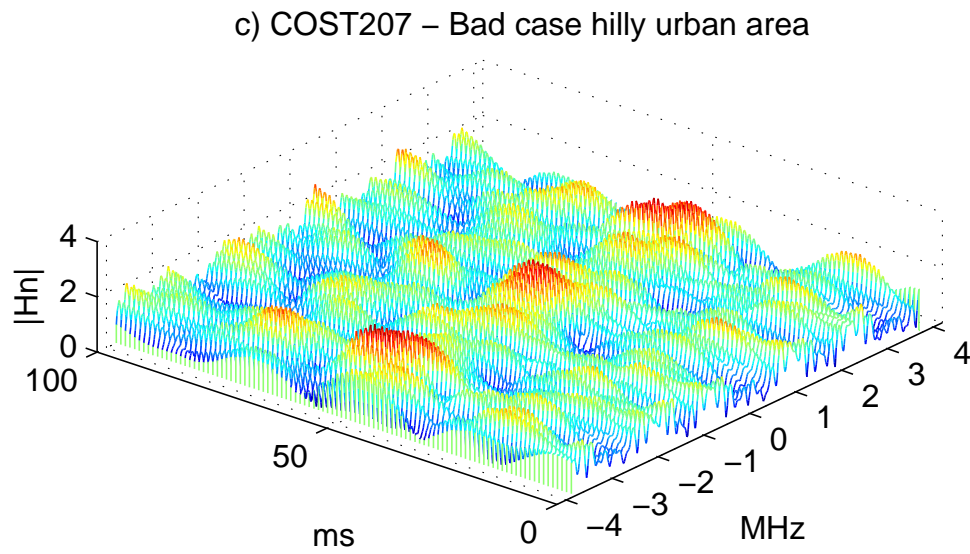
Figure 3.15: COST207-Bad Urban (BU): frequency response over a 8MHz-channel, 80km/h.

d) COST207 – Typical hilly terrain
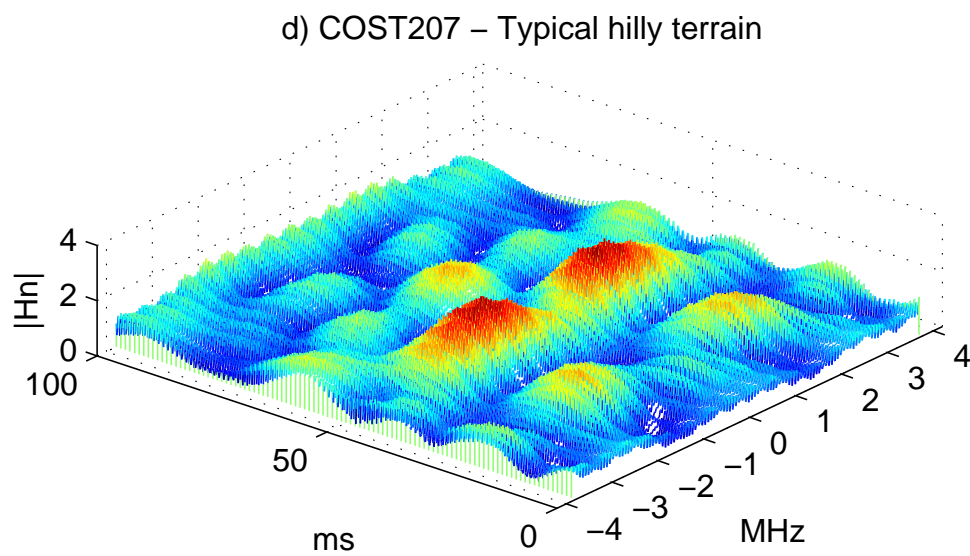
Figure 3.16: COST207-Hilly Terrain (HT): frequency response over a 8MHz-channel, 80km/h.

3.4   Chapter summary

A C/C++ simulator has been written to evaluate the performances of the proposed solutions. Object-oriented programming has been used to enhance code readability and to hide private data of each processing block. Some special interfaces have been implemented to exploit Matlab powerful visualization tools.

Several channel models have been implemented. Among those, Ricean and Rayleigh multipath channel models as described in annex B of the DVB-T standard and COST207 mobile models. From field trials in Athens, during the Olympic Games 2004, a particular shadow fading behavior has been observed. For this reason, beside the well-known lognormal shadow fading model, a sparse shadow fading model able to reproduce the observed channel behavior has been proposed.

Chapter 4

Enhanced-mobility COFDM modulation

4.1   Chapter introduction

In this chapter an enhanced-mobility COFDM system is proposed, aimed to satisfy the requirements of unidirectional long and medium range wireless applications, like outdoor events and multimedia relays. The requirements of these applications are analyzed and the limitations of the 2k mode of the DVB-T standard are identified. The enhanced-mobility COFDM modulation parameters are then completely specified, with a particular attention to the specific added features. The TPS format has been modified in order to convey the additional configuration information preserving backward compatibility toward non-hierarchical DVB-T 2k mode.

4.2   Applications analysis

The enhanced-mobility COFDM system presented in this chapter does not cover all the application range and does not fulfill all the different and sometimes contradictory requirements already identified in chapter 1. There are several applications for which long-range (up to 50km) audio/video transmission links are required; among these, we can cite television productions of outdoor sport events, multimedia links to/from airplanes, military surveillance. The relatively long propagation times precludes the possibility to efficiently employ time-division multiplexing to share the RF channel between multiple terminals and implement a backward channel.

The DVB-T standard, born for unidirectional broadcasting, represents a good starting point for the development of a specialized system. Anyway, several modifications must be considered to extend the 8MHz bandwidth and to overcome the lack of explicit support for mobile reception. The bandwidth allocated for television production events is usually wider: 12MHz is a common figure, but often 20MHz are reserved for each contribution channel. The enlarged bandwidth could be efficiently exploited to convey higher bitrates and hence higher quality audio/video streams or alternatively to implement stronger error correction schemes.

The lack of explicit support for mobility translates especially in reduced protection to shadow fading. Even short shadowing events cause unrecoverable transmission errors, generating annoying punctual system failures. Some different solutions must be studied to address this kind of problems.

In these applications the propagation loss term g_p in equation 3.1 is the dominant factor of the RF power budget. As a consequence, the transmission power is often boosted over $1W$, and the size and power consumption of the system has to be increased as well.

Directional antenna have to be used for one or both ends of the link.

The terms g_s and g_m in equation 3.1 are dependent on the terrain conditions and can vary over a wide range. The only way to take into account these effects is to provide an additional **power margin** to ensure reliable communication for most of the practical cases: values of $12dB$ or above are commonly used for coverage planning of DVB-T systems. The goal of the time interleaver is to reduce the this power margin figure in order to keep the required RF power below 1W for most of the applications targeted by this system. They can be divided in two main classes: long distance and medium distance applications.

4.2.1 Long-distance applications

A typical example of long-range application is the relay downlink for television productions; in this case, the signals of several mobile cameras are collected by an helicopter and then relayed down to the ground. The reception point is usually constituted by a regia van placed on a high location that can be some tens of kilometers far away. To ensure transmission over these distances, the higher-possible RF power should be used, since the power budget is dominated by path loss. Moreover directional antennas are often employed, at least for reception.

For portable/mobile applications, the RF power is limited by power consumption and heat dissipation. Moreover, due to the back-off and linearity requirements of OFDM modulated signals, the efficiency of an amplifier with good performances can be expected to be less than 10%, and typically [76] around 5%. This limit the available output power to a maximum of $10W$ for emitters mounted on vehicles or helicopters, and around $1W$ for portable systems.

With these figures, the power budget is limited and we could expect to successfully guarantee wireless links only in line-of-sight (LOS) scenarios, since the additional power margin is limited by the available transmission power. Anyway, the imperative use of directional antennas limits the amount of multipath scattering experienced by the receiver. In this case, the channel can be well approximated by Ricean channel model. Additional slow-shadowing effects can be added to simulate a temporary misalignment of the tracking mechanism of transmission or reception antennas.

The main requirements of this type of applications can be listed, by order of relevance, as:

- AWGN robustness

- Payload capacity

- Protection to multipath fading

4.2.2   Medium-distance applications

Shorter-range applications are relay uplink, that account for link distances up to 1 km, stadium applications ad eventually even indoor studio productions. For these application, the power budget is normally more relaxed, and a higher amount of multipath fading can be tolerated.

Using equation 3.2 in a typical case where the distance is around 400m ($g_p = -140dB$), with omnidirectional transmission antenna ($g_{TX} = 4dB$), directional reception antenna ($g_{RX} = 20dB$) and 1W amplifier ($P_{TX} = 30dBm$), we can estimate the fading margin to be in the order of $10dB$.

In this case, Ricean, Rayleigh, COST207 and WSSUS models are applicable. In addition, fast sparse shadowing effects can be added to account for small obstacles that can interpose in the line-of-sight.

The main requirements of this type of applications can be listed, by order of relevance, as:

- Protection to shadow fading

- Protection to multipath fading

- Low latency

- Payload capacity

- Low power consumption

- Compact size

4.3 System specifications

The experienced gained on DVB-T modulation drove the study of the proposed system, that differs from DVB-T by several aspect, while retaining backward compatibility if the advanced features are disabled. Three main modifications have been provided.

- **Deep time-interleaving** has been added to provide protection to multipath fading and especially sparse shadow fading for applications where latency is not the primary issue.

- The **modulated bandwidth is variable** to fully exploit the allocated radio resource and adapt to channels bandwidths up to $24MHz$.

- **Turbo codes** have been added to further improve error correction capacities beyond those provided by the convolutional scheme.

Moreover, the enhanced-mobility COFDM system has been designed to maintain backward-compatibility toward existing DVB-T 2k systems. Since the number of available *reserved* bits inside DVB-T Transmission Parameter Signalling (TPS) stream is not sufficient to host the additional parameters, the TPS format must be carefully modified to preserve the backward compatibility when the advanced features are disabled. The modulator block diagram is depicted in figure 4.1.
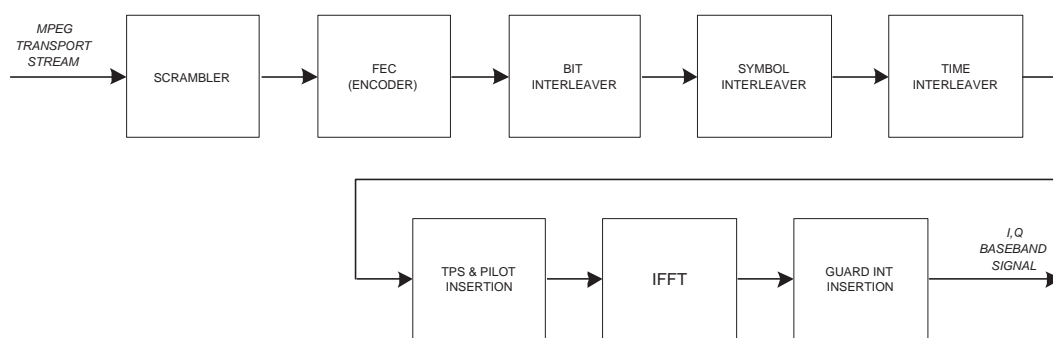
Figure 4.1: Block diagram of enhanced-mobility COFDM modulator.

4.3.1 Performance targets

The performance targets of the developed enhanced-mobility COFDM system are summarized in table 4.1.

Useful channel bandwidth (BW)	$8MHz$ to $24MHz$
Multipath fading tolerance	up to $300km/h$, COST207 channels
Shadow fading tolerance	signal loss up to $1s$
Minimum latency	$< 10ms$
Payload capacity	$< 74Mbps$ (64QAM, GI=1/16, R=3/4, BW=$24MHz$)
	$> 3.1Mbps$ (QPSK, GI=1/4, R=1/3, BW=$8MHz$)
Complexity of VHDL design	Modulator: XC2V2000
	Demodulator: 2 x XC2VP30

Table 4.1: Requirements of Enhanced-mobility COFDM system.

The insertion of the time interleaver can effectively conceal loss of signal up and beyond one second exploiting the maximum interleaver depth; anyway, it must be noted that the latency is lower-bounded by the interleaver depth, thus shadow and multipath fading protection by means of time interleaving has to be trade with the latency.

The payload capacity can be adjusted in a range that spans more than one order of magnitude and is a function of the modulated bandwidth and of the desired link robustness. The wider-bandwidth and less protected mode can be exploited to convey high definition television signals with very high quality or multiple multiplexed standard definition signals.

The complexity requirements are given by the physical hardware platform in which the system has been implemented, that employs Xilinx Virtex2 and Virtex2Pro devices.

4.3.2   Modulation parameters

The modulation parameters of the enhanced-mobility COFDM system are summarized in table 4.2.

4.3.3   Carrier number N

To adapt the system to different channel bandwidth, the simplest method is to vary the sampling frequency. The sampling frequency can be varied between $f_s = 9.142857MHz$ for a 8 MHz channel and $f_s = 27.428571MHz$ for a 24 MHz channel. Conceptually, the sampling frequency can vary continuously between the minimum and maximum value. Let's denote as **case A** the situation corresponding to the minimum sampling frequency and as **case B** the other extreme. These would be the corner cases for our study.

Parameter	Required value	Units
Sampling frequency (f_s)	9.142857 to 27.428571	MHz
Total number of subcarriers (N)	2048	-
Subcarrier spacing (Δf)	4.464 to 13.392	KHz
Active subcarriers	1705	-
Data subcarriers	1512	-
Spacing of scattered pilots in time (N_l)	4	OFDM symbols
Spacing of scattered pilots in frequency (N_k)	3	subcarriers
Useful symbol duration (T_s)	224 down to 74.6	μs
Guard interval (T_g/T_s)	1/4, 1/8, 1/16	-
Modulation	QPSK, 16QAM, 64QAM	-
Inner code	Convolutional or Turbo	-
Inner interleaver	Same as DVB-T	-
Symbol interleaver	Same as DVB-T	-
Time interleaver depth	0 or $2^n 96$ ($n \leq 7$)	OFDM symbols
Outer interleaver	Convolutional: 12, 17 or 34	TS packets
Outer code	Same as DVB-T	-
Scrambling	Same as DVB-T	-

Table 4.2: Parameters of Enhanced-mobility COFDM system.

If we recall that the subcarrier spacing Δf is equal to:

$$\Delta f = \frac{1}{NT} = \frac{1}{T_s} \tag{4.1}$$

then, with the above numbers, Δf would be bounded between 4.464KHz (case A) and 13.392KHz (case B).

Mobile channels

The subcarrier spacing has a direct impact on mobile tolerable speed. As shown by Russell and Stüber [37], the degradation due to inter-carrier interference induced by the Doppler spread for a 2K OFDM system is about 25dB for

$$f_D T_s = 0.2 \tag{4.2}$$

where f_D is the maximum Doppler frequency and depends on the mobile speed v and on the RF carrier frequency f_c:

$$f_D = f_c \frac{v}{c} \tag{4.3}$$

T_s is the OFDM symbol period and depends on the system sampling frequency. Combining the above equations, we obtain:

$$f_c \frac{v}{c} \frac{N}{f_s} = 0.2 \tag{4.4}$$

For case B, the sampling frequency f_s is three times higher than case A; this translates in a three-fold increase in tolerable mobile speed v.

Multipath protection

As a direct consequence of the orthogonality condition, the useful symbol period T_s in inversely proportional to subcarrier spacing Δf. Thus, case B offers less protection to long echo; using the longest guard interval $T_g = T_s/4$, the maximum echo spread is limited to $18\mu s$, when case A allows echo spreads up to $56\mu s$. In other words, the maximum bandwidth of 24MHz can not be used if echo spread of more than $18\mu s$, corresponding to about $5.4km$, are expected.

If we define the guard interval efficiency η_g

$$\eta_g = \frac{T_s}{T_s + T_g} \tag{4.5}$$

it must be noted that even for echoes shorter than $5.4km$, when both cases can withstand the echo delay spread with an appropriate choice of the guard interval, case B suffers from reduced efficiency, since longer guard interval has to be used to guarantee the same degree of protection as case A. Figure 4.2 clarifies this behaviour; over $16.2km$ for case A and $5.4km$ for case B efficiency has been dropped to zero, to show that no more multipath protection is guaranteed by the guard interval insertion process.

4.3.4   Pilot structure

Various carriers within the OFDM frame are modulated with reference information whose transmitted value is known to the receiver. These cells contain scattered or continual pilot subcarriers and are transmitted at "boosted" power level.

Each continual pilot coincides with a scattered pilot every fourth symbol; the number of useful data carriers is constant from symbol to symbol. There are a total of 1512 useful carriers.

Definition of reference sequence

The continual and scattered pilots are modulated according to a PRBS sequence w_k, corresponding to their respective carrier index k.
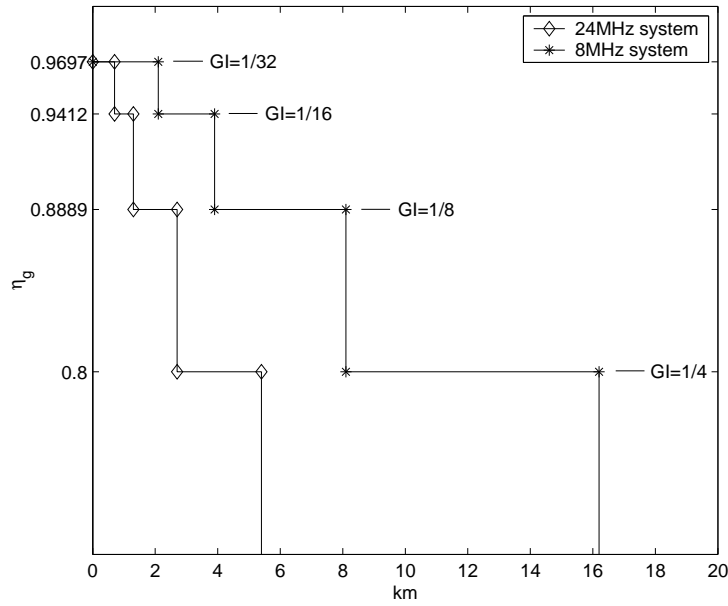
Figure 4.2: Guard interval efficiency VS maximum echo spread.

The PRBS sequence is generated according to figure 4.3 and is initialized to all-one sequence "11111111111" at the beginning of each new OFDM symbol.
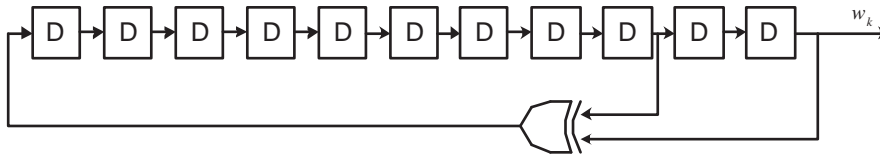
Figure 4.3: Reference sequence generator.

The polynomial for the Pseudo Random Binary Sequence (PRBS) generator is:

$$X^{11} + X^2 + 1$$

Continual pilots

Continual pilots are inserted in fixed positions, for $k \in CP$ according to table 4.3.

All 45 continual pilots are modulated according to the reference sequence w_k defined before. The continual pilots are transmitted at "boosted" power level. The corresponding

Location of continual pilots
0 48 54 87 141 156 192 201 255 279 282 333 432 450 483 525 531 618 636 714
759 765 780 804 873 888 918 939 942 969 984 1050 1101 1107 1110 1137 1140
1146 1206 1269 1323 1377 1491 1683 1704

Table 4.3: Location of continual pilots.

modulation is given by:

$$c(l, k) = 4/3 \cdot 2(1/2 - w_k) \tag{4.6}$$

Scattered pilots

Reference information, taken from the reference sequence, is transmitted in scattered pilot subcarriers in every symbol. Scattered pilot cells are always transmitted at the "boosted" power level. For OFDM symbol of number l (ranging from 0 to 67), carriers for which index $k \in SP$, where $SP = \{k = 3(l \bmod 4) + 12p \mid p \in N, k \in [0 : 1704]\}$, are scattered pilots, where p is an integer that takes all possible values greater than or equal to zero, provided that the resulting value for k does not exceed the valid range $[0 : 1704]$. The pilot insertion pattern is shown in figure 4.4.
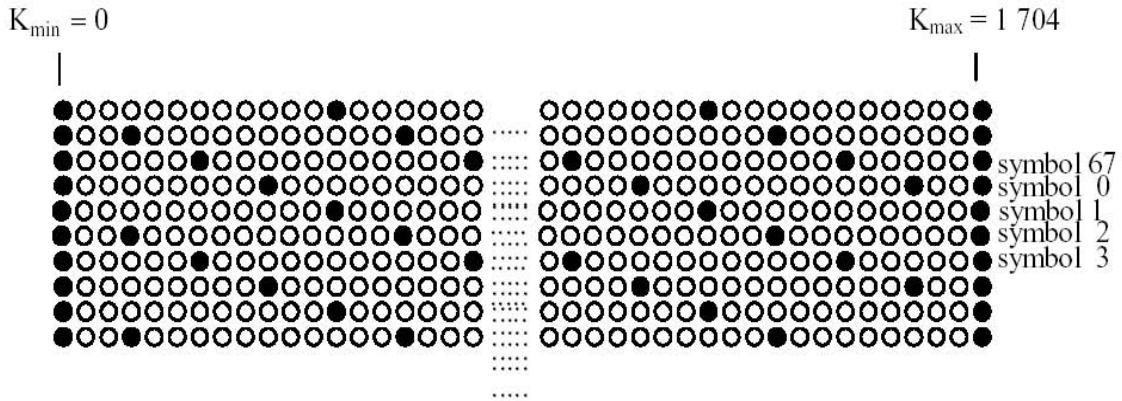
Figure 4.4: Scattered pilots position.

The pilot insertion structure has been retained from the DVB-T standard. Anyway, due to the change of sampling frequency, the performances vary. Said et al. [80] gives a simple yet effective way to calculate the maximum Doppler frequency and delay echo spread from N_l and N_k, respectively. If we recall:

$$f_D \cdot T_s \cdot N_l \leq 1/2 \tag{4.7}$$

with $N_l = 4$, then the condition becomes $f_D \leq 558Hz$ for case A and $f_D \leq 2230Hz$ for case B. For a wireless link in the 2.5GHz band, this correspond to a speed of about $100km/h$ for case A and to a speed of about $300km/h$ for case B.

Regarding the delay spread, we could calculate the maximum echo spread recalling [80]:

$$T_m \cdot \Delta f \cdot N_k \leq 1 \tag{4.8}$$

Since $\Delta f = 1/T_s$, we can write it:

$$N_k \leq T_s/T_m \tag{4.9}$$

and note that this is independent of sampling frequency. In fact, since $N_k = 3$, the pilot spacing in the frequency domain allows to discriminate echoes whose maximum distance is $T_m = 1/3T_s$. This fulfills the requirement given by the maximum guard interval of $T_g = 1/4T_s$.

Transmission Parameter Signalling (TPS)

The TPS carriers are used for the purpose of signalling parameters related to the transmission scheme, i.e. channel coding and modulation. The TPS is transmitted in parallel on 17 TPS subcarriers according to the indexes of table 4.4. Every TPS carrier in the same symbol conveys the same differentially encoded information bit.

Location of TPS pilots
34 50 209 346 413 569 595 688 790 901 1073 1219 1262 1286 1469 1594 1687

Table 4.4: Location of TPS pilots.

The TPS subcarriers convey information on:

- modulation order (constellation);

- guard interval;

- inner coder type (convolutional or turbo);

- inner code rates;

- frame number in a super-frame;

- time interleaver depth;

- outer interleaver depth.

The TPS is defined over 68 consecutive OFDM symbols, referred to as one OFDM frame. Four consecutive frames correspond to one OFDM super-frame. The reference sequence corresponding to the TPS carriers of the first symbol of each OFDM frame is used to initialize the TPS modulation on each TPS carrier. Each OFDM symbol conveys one TPS bit.

Each TPS block (corresponding to one OFDM frame) contains 68 bits, defined as follows:

- 1 initialization bit;

- 16 synchronization bits;

- 37 information bits;

- 14 redundancy bits for error protection.

The transmission parameter information is formatted as shown in table 4.5.

Bit number	Format	Purpose/Content
s_0	see subclause 4.6.2.1	Initialization
$s_1 - s_{16}$	0011010111101110 or 1100101000010001	Synchronization word
$s_{17} - s_{22}$	100011 or 010111	Length indicator
$s_{23} - s_{24}$	see table 4.6	Frame number
$s_{25} - s_{26}$	see table 4.7	Constellation
$s_{27} - s_{29}$	000	Hierarchy information
$s_{30} - s_{32}$	see table 4.8	Code rate
$s_{33} - s_{35}$	see table 4.9	Encoder type
$s_{36} - s_{37}$	see table 4.10	Guard interval
$s_{38} - s_{39}$	00	Transmission mode
$s_{40} - s_{47}$	00000000	Cell identifier
$s_{48} - s_{51}$	see table 4.11	Time interleaver depth
$s_{52} - s_{53}$	all set to "0"	Reserved for future use
$s_{54} - s_{67}$	BCH code	Error protection

Table 4.5: TPS format.

The first 6 bits of the TPS information is used as a TPS length indicator (binary count) to signal the number of used bits of the TPS. For backward compatibility, the

length indicator has the value $s_{17} - s_{22} = 010111$ if the time interleaver is bypassed and the value $s_{17} - s_{22} = 100011$ if the time interleaver is activated.

The frames inside the super-frame are numbered from 0 to 3 and the actual frame number is signalled according to table 4.6.

Bits s_{23}, s_{24}	**Frame number**
00	Frame number 1 in a superframe
01	Frame number 2 in a superframe
10	Frame number 3 in a superframe
11	Frame number 4 in a superframe

Table 4.6: Frame number field.

The constellation shall be signalled by 2 bits according to table 4.7.

Bits s_{25}, s_{26}	**Constellation**
00	QPSK
01	16QAM
10	64QAM
11	reserved

Table 4.7: Constellation field.

The code rate shall be signalled by 3 bits according to table 4.8. It must be noted not all combinations of code rate and encoder type are allowed.

The forward-error correction structure shall be signalled by 3 bits according to table 4.9. The parameter B refer to the depth of the outer interleaver for concatenated error-correction schemes. It must be noted not all combinations of code rate and encoder type are allowed.

The value of the guard interval is signalled according to table 4.10.

The value of the time interleaver depth is signalled according to table 4.11.

The 53 bits containing the TPS synchronization and information (bits s1 - s53) are

Bits s_{30}, s_{31}, s_{32}	Code rate
000	1/2
001	2/3
010	3/4
011	5/6
100	7/8
101	1/3
110	2/5
111	reserved

Table 4.8: Code rate field.

Bits s_{33}, s_{34}, s_{35}	Encoder type
000	convolutional + RS, B=12
001	convolutional + RS, B=17
010	convolutional + RS, B=34
011	reserved
100	PCCC + RS, B=12
101	PCCC + RS, B=17
110	PCCC + RS, B=34
111	reserved

Table 4.9: Encoder type field.

Bits s_{36}, s_{37}	Guard interval
00	1/32
01	1/16
10	1/8
11	1/4

Table 4.10: Guard interval.

extended with 14 parity bits of the BCH (67,53, t = 2) shortened code, derived from the original systematic BCH (127,113, t = 2) code. Code generator polynomial:

$$h(x) = x^{14} + x^9 + x^8 + x^6 + x^5 + x^4 + x^2 + x + 1. \qquad (4.10)$$

The shortened BCH code may be implemented by adding 60 bits, all set to zero, before

Bits $s_{48}, s_{49}, s_{50}, s_{51}$	**Time interleaver depth**
0000	time interleaver bypassed
0001	$M = 96 \cdot 2^0$
0010	$M = 96 \cdot 2^1$
0011	$M = 96 \cdot 2^2$
0100	$M = 96 \cdot 2^3$
0101	$M = 96 \cdot 2^4$
0110	$M = 96 \cdot 2^5$
0111	$M = 96 \cdot 2^6$
1000	$M = 96 \cdot 2^7$
1001	reserved
1010	reserved
1011	reserved
1100	reserved
1101	reserved
1110	reserved
1111	reserved

Table 4.11: Time interleaver depth.

the information bits input of a BCH (127,113, t = 2) encoder. After the BCH encoding these null bits shall be discarded, leading to a BCH code word of 67 bits.

The structure of the TPS information and the bit encoding has been modified respect to the DVB-T standard in a way that backward compatibility is retained for 2K, non-hierarchical systems.

In particular, this system can receive the OFDM signal emitted by a previous-generation conventional DVB-T system. In this case, we can note that bits $s_{33} - s_{35}$ ("LP code rate" in DVB-T) are set to zero, thus selecting convolutional encoding with $B = 12$ outer interleaver depth as required by the DVB-T standard; moreover, bits $s_{48} - s_{51}$ ("Reserved - all 0" in DVB-T) bypass the time interleaving.

Equivalently, this system generates a 2K, non-hierarchical DVB-T signal with correctly-formatted TPS information if the advanced features are disabled.

4.3.5 Inner Interleaving

Interleaving is essential to obtain the best performance for frequency-selective channels. From figure 4.1, there are three cascaded inner interleaver blocks.

- **Bit interleaver**: takes the encoded bits from the FEC encoder (Convolutional or turbo) and spreads them in order to avoid that consecutive bit were packed into the same subcarrier. It is block-based with block size of 126 subcarriers. The structure is the same as DVB-T.

- **Symbol interleaver**: it shuffles the subcarrier in a pseudo-random order, to avoid consecutive bits were mapped into adjacent subcarriers. This is particularly important for channel that exhibit frequency selective fading, because the frequency nulls corrupt the data carried by several adjacent subcarriers. The structure is the same as DVB-T.

- **Time interleaver**: the scope of this interleaver is to mitigate the effects of fast-shadowing. Subcarriers are shuffled between several OFDM symbols in order to evenly spread errors due to shadowing over a large number of OFDM symbols.

Time interleaver

The time interleaver receives the data (2, 4 or 6 bit for each subcarrier, depending on constellation employed) from the symbol interleaver. For each OFDM symbol, there are 1512 data-modulated subcarriers. Employing a time interleaver gives the advantage that the errors deriving from few OFDM symbols corrupted by shadow and multipath fading are spread across hundreds or thousands of OFDM symbols. Doing so, the error burst deriving from the corrupted OFDM symbols is transformed in sparse errors over a longer time period, allowing the channel coding mechanism to recover the missing data. Increasing the memory depth improves the performances due to the increased averaging period, but at the same time introduces significant end-to-end delay. In applications where the latency is the primary issue, the time interleaver should be bypassed.

The choice of time interleaver structure is conditioned by the data rate and by the maximum amount of data to store. For the transmitter, if we consider the maximum data rate, corresponding to 64QAM modulation, sampling frequency $f_s = 27.43 MHz$ and guard interval $T_g = T_s/32$, the coded data rate R_{ti} correspond to:

$$R_{ti} = 6 \ f_s \ \frac{1512}{2048} \ \frac{T_s}{T_s + T_g} = 118 Mb/s.$$

The time interleaver depth should be enough to store an amount of data N_{ti} corresponding of at least $D = 1$ second of transmission, at the maximum data rate:

$$N_{ti} \geq \frac{1}{2} \, R_{ti} \, D = 59Mb.$$

The receiver de-interleaves the data coming from the de-mapper block. In this case, every transmitted bit becomes a soft-metric information s_i, generally quantized over 3 to 5 bits. We used 4-bits soft-metrics as a good compromise between complexity and performances [78]. For this reason, the data rate R_{ti} and data amount N_{ti} are four times higher than the transmitter ones.

The huge amount of data storage claims for external Synchronous Dynamic-RAM (SDRAM) chips. This imposes some constraints on data accesses, that should be grouped in burst to exploit the memory bandwidth of this kind of memories. Moreover, the interleaver works on a continuous stream of data, framed only by OFDM symbol boundaries, and eventually by the superframe structure.

The proposed interleaver is of convolutional type. It has the advantage of requiring only OFDM-symbol synchronization. Its structure is shown in figure 4.5.
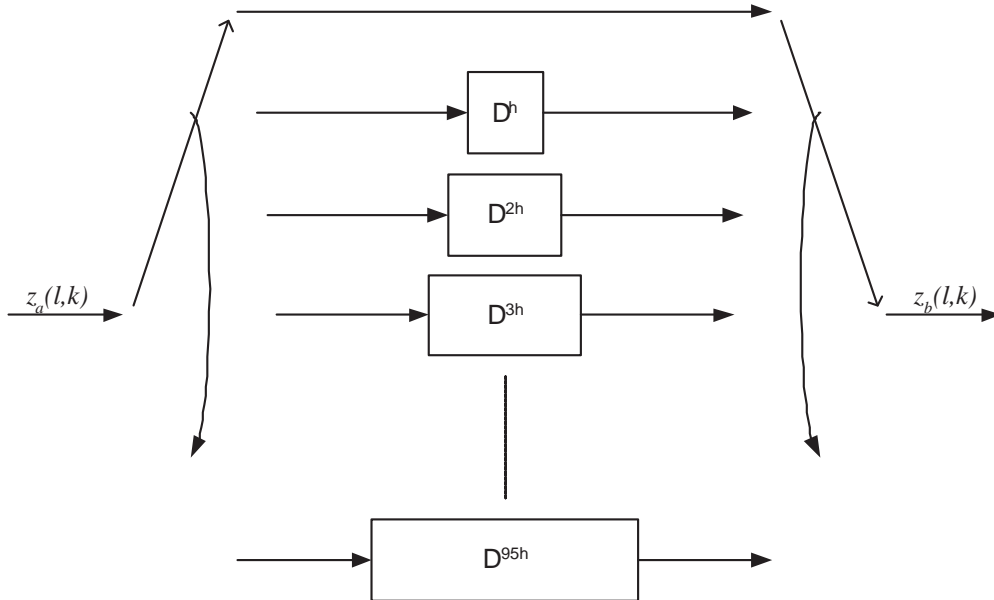
Figure 4.5: Time interleaver block diagram.

The input data are first grouped in $B = 96$ groups of 16 subcarriers, for a total of 1536 subcarriers. Since the data-modulated subcarriers are 1512, the last 24 subcarriers

are set to zero. The selector is synchronized on the OFDM symbol boundaries, so the position shown in figure 4.5 correspond to the first data group of each OFDM symbol. There are 96 branches, and each branch contains a FIFO with depth bh where b is the branch number in the range $[0, 95]$ ad h is the parameter which defines the interleaver maximum depth.

The interleaver output subcarrier $z_b(l, k)$ can be expressed as:

$$z_b(l, k) = z_a(l - h \cdot floor(k/16), k) \tag{4.11}$$

For the de-interleaver, the reverse process is applied, as shown in figure 4.6, when the output $z_c(l, k)$ can be expressed as:

$$z_c(l, k) = z_b(l - h \cdot (95 - floor(k/16)), k). \tag{4.12}$$
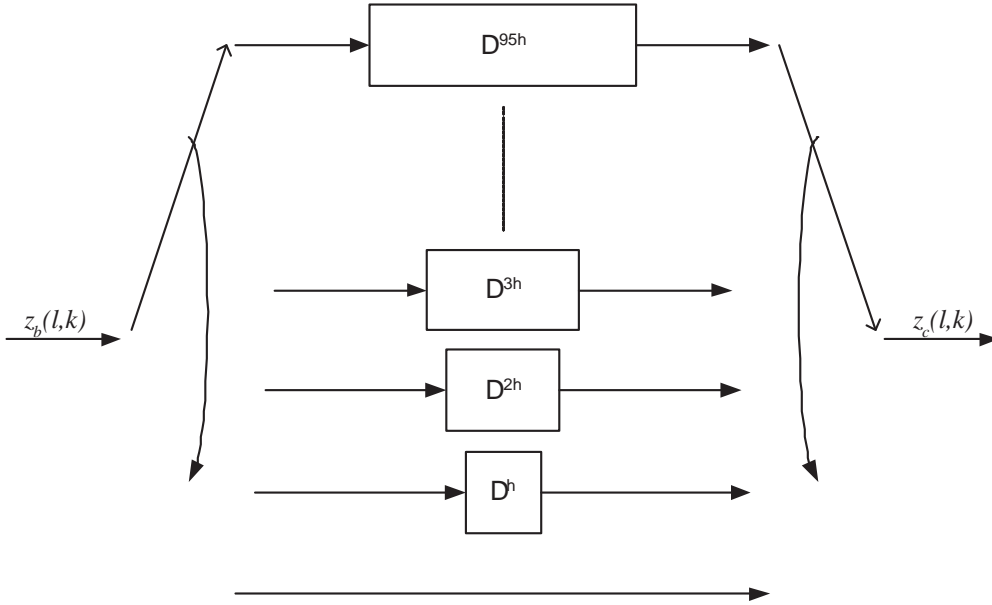
Figure 4.6: Time de-interleaver block diagram.

Combining equations 4.11 and 4.12, it can be noted that after the interleaving/de-interleaving process each subcarrier has been delayed by $95h$ OFDM symbols:

$$z_c(l, k) = z_a(l - 95h, k). \tag{4.13}$$

The main characteristic of this kind of interleaver is its inherent time-continuity. One faulty OFDM symbol would be spread over Bh OFDM symbols, as shown in figure 4.7, where $h = 1$ and OFDM symbols with only $B = 8$ groups of 2 subcarriers are used for clarity.
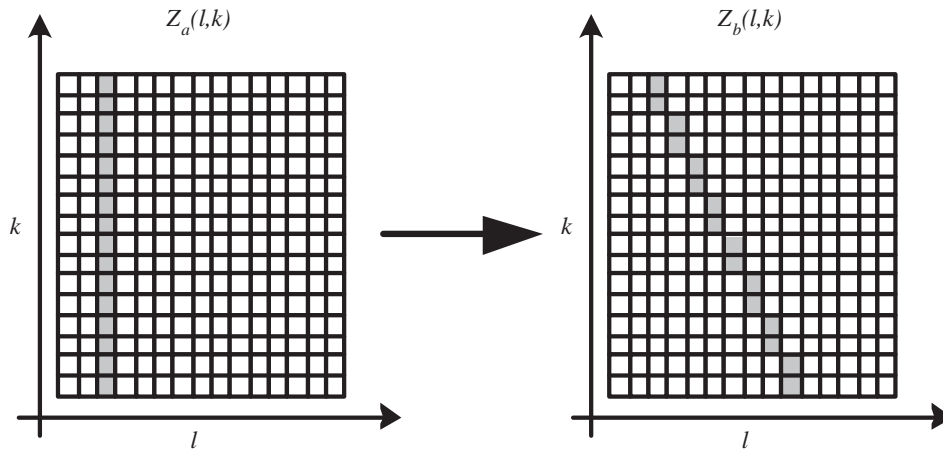
Figure 4.7: Time interleaver example: $B = 8$, $h = 1$, groups of 2 subcarriers.
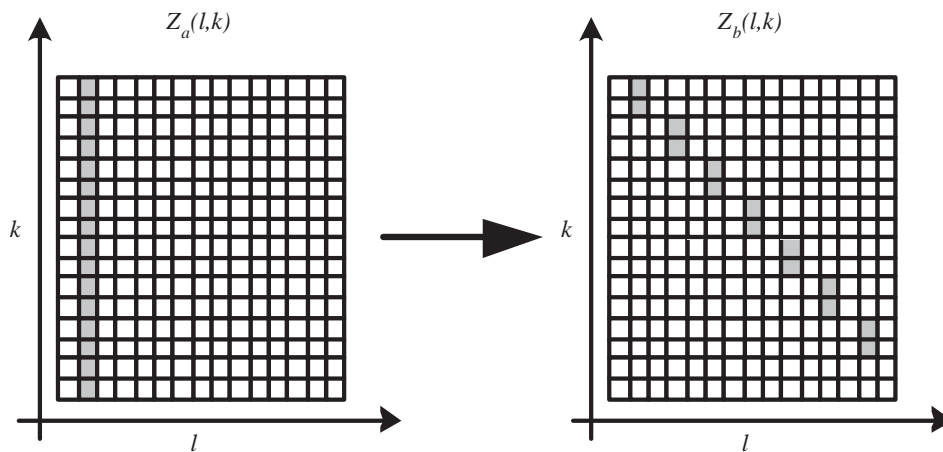
Figure 4.8: Time interleaver example: $B = 8$, $h = 2$, groups of 2 subcarriers.

The same simplified interleaver is shown in figure 4.8 with $h = 2$.

A group of E consecutive faulty OFDM symbols would be spread over $Bh+E$ symbols. The advantage of the convolutional interleaver is that it spreads time-consecutive errors evenly over the whole interleaver depth, thus achieving optimal performances of the error correction scheme.

4.3.6 Forward Error Correction

Two different Forward Error Correction (FEC) schemes can be selected for this system. For backward compatibility, the original DVB-T concatenated scheme of figure 4.9 with

inner convolutional encoder ($n = 7, G_1 = 171, G_2 = 133$) and outer Reed-Solomon encoder ($n = 204, k = 188$) has been retained.
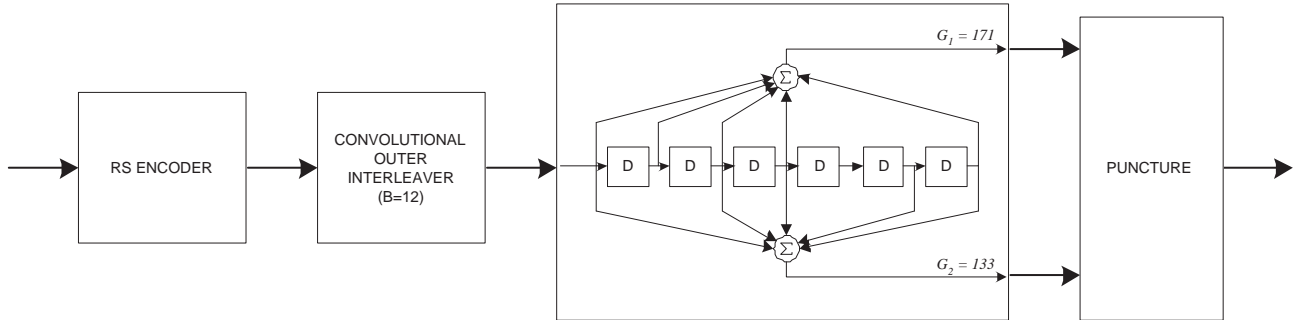
Figure 4.9: Concatenated convolutional+RS FEC scheme.

Lattuada [79] analyzed different turbo codes families in terms of performance and complexity, with the goal of improving the original DVB-T FEC. The Parallel-Concatenated Convolutional Code (PCCC) has been chosen; even if this code offers very good performances, some residual output errors can survive. For this reason, the FEC is based on a concatenated scheme where the Reed-Solomon outer coder has been retained. The performances have been extensively analyzed [93] and the results are shown in the following chapters.

To better adapt the RS correction capabilities to the characteristics of the inner turbo coder, the outer interleaver (sometime referred as *Forney* interleaver) can be modified increasing its depth. While the original DVB-T interleaver had a fixed $B = 12$ branches and consequently interleaver depth equal to 12 Transport-Stream packets, for the proposed error correction scheme the parameter B can be chosen between $B = 12, 17$ or 34.

The inner coder is a Parallel Concatenated Convolutional Code, with polynomials (15,13) constituent convolutional encoders. The structure is depicted in figure 4.10.

The puncturing block provides for rates of 1/3, 2/5, 1/2, 2/3, 3/4. The choice of coding rate below 1/2 allows to enforce the link robustness down to very low C/N figures, as will be shown by the simulation results presented in the following chapters.

4.4 Chapter summary

In this chapter, a COFDM system has been proposed, that modifies the existing DVB-T standard to improve the performances especially for mobile scenarios and capable to
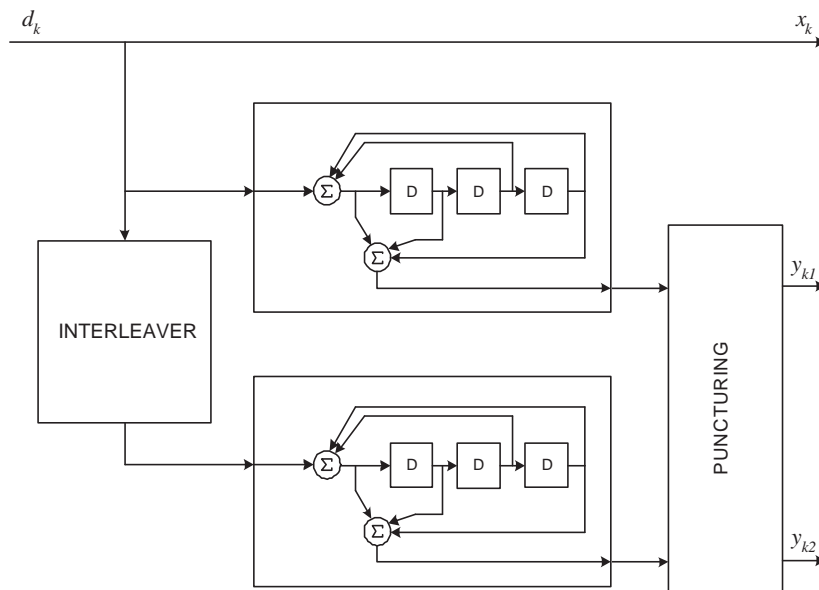
Figure 4.10: Turbo PCCC encoder block diagram.

adapt to larger channel bandwidths. In particular, a special time interleaving scheme has been added, that allow to overcome strong shadow fading without loss of data. Turbo codes have been added, obtaining further improvements in terms of link robustness. The Transmission Parameter Signalling (TPS) structure and data format have been modified to include the additional information needed to correctly decode the time-interleaved and turbo-encoded signal while retaining compatibility toward 2K non-hierarchical mode when the advanced features are disabled.

Chapter 5

System verification and demodulator design

5.1 Chapter introduction

In this chapter the study of the demodulator tasks related to the enhanced-mobility COFDM system is presented. Moreover, an hardware platform is briefly described and some implementation aspects are analyzed, as long as algorithm optimization aimed to reduce the receiver hardware complexity.

The system specifications presented in chapter 4 do not include the description of the receiver specific tasks. The specifications can describe accurately the transmitted signal, but the received one will experience a variable degree of attenuation, frequency domain distortion, frequency offset; moreover, timing reference is not directly available to the receiver and must be recovered from the signal itself. The study of appropriate automatic gain control, time and frequency synchronization, channel estimation and analysis algorithms is then required to develop a complete wireless system. Moreover, the complexity–performance tradeoff of the above cited algorithms must be carefully evaluated to provide consistent performances of the whole system. Additionally, the special features provided by the enhanced-mobility OFDM system, such as deep time interleaver and turbo codes, require specific demodulator development. In particular, the time interleaver, coupled with powerful error-correction algorithms, can effectively recover data lost by deep time fades several tenths of second long; however, the receiver must retain coarse time and frequency synchronization and provide robust and fast re-acquisition schemes. Turbo codes are powerful enough to guarantee correct reception for signals with very low SNR, but the receiver must be able to acquire and maintain time and frequency synchronization, provide good channel estimation and perform correct channel analysis even for such bad environment.

In the recent past, the evolution of semiconductor technology and in particular of Field Programmable Gate Arrays (FPGA) allowed the implementation of complex OFDM transmission standards as DVB-T in the form of Intellectual Property (IP) cores that can fit in these devices. The recently introduced Virtex2 family by Xilinx offers Digital Signal Processing capabilities by immersing specialized components as embedded hardware multipliers inside the FPGA cell matrix. A FPGA-based system has been designed to implement a complete wireless link in order to evaluate the performances and the feasibility of the proposed solutions and to perform on-field trials. Some preliminary tests already shows that the implemented design is able to successfully overcome the problems due to shadow fading.

5.2   Demodulator design

The detailed proposed architecture of the front-end is depicted in figures 5.1 and 5.2.
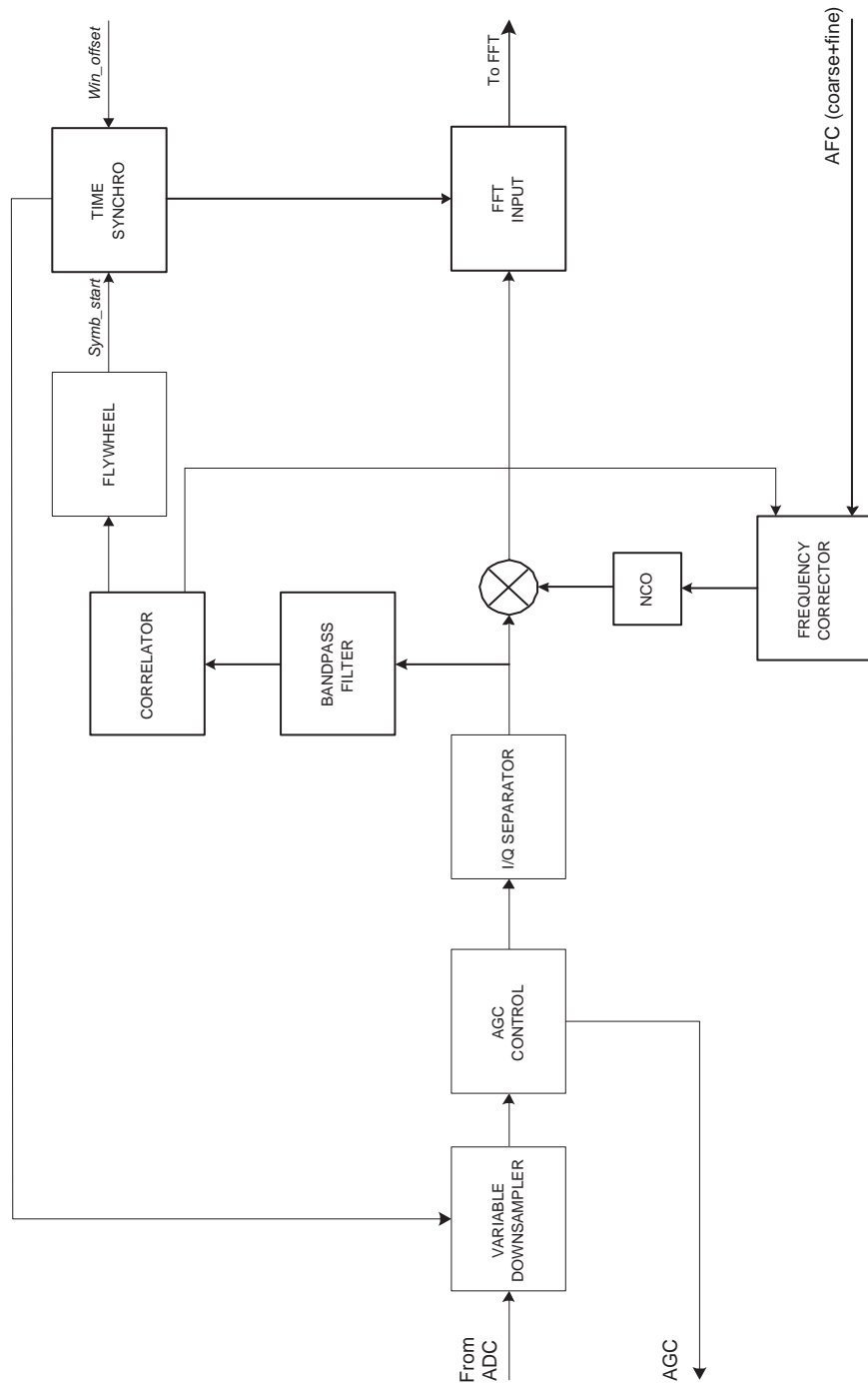
Figure 5.1: Receiver structure, part 1

The different units showed in the block diagram represent the main receiver tasks.

For the implemented system, physically changing the sampling frequency of the modulation and demodulation systems could not be practical. A different approach is represented by variable interpolation/decimation. The structure and performances of such algorithms are extensively analyzed in [84] and [85]. Anyway, the *variable decimator* block is coupled with adequate signal oversampling (not shown in the figure). For the implemented system, the higher applicable sampling frequency is limited to $25MHz$, since the master clock frequency is $100MHz$ and 4x signal oversampling has been employed.

The *AGC control* block maintains constant the average signal power level. The *I/Q separator* demodulates the real-valued signal coming from ADC and centered around $f_s/2$ and obtains a complex signal centered around DC. The *bandpass filter*, *correlator*, *flywheel* and *time synchro* blocks belong to time acquisition and tracking mechanism. *Frequency corrector* and *NCO* blocks is part of the frequency synchronization part.

In the second part of the block diagram the *FFT* block can be noted. After FFT computation, the *TPS extraction* and *TPS decoding* blocks demodulate and interpret the Transmission Parameter Signalling information. On the lower side, six blocks provide pilot-assisted channel estimation. The *soft-demapper* block processes the transformed complex data samples and extracts the probabilities of each transmitted bit expressed in the form of soft-metrics, that are sent to the error-correction part of the design (not shown in the figure).

The discussion of the specific demodulation tasks will be the object of the further paragraphs of this section.

Figure 5.2: Receiver structure, part 2

5.2.1   Automatic Gain Control (AGC)

The power of the signal at the receiver antenna can vary upon a wide range. A receiver should be able to adapt its internal gain in order to guarantee adequate amplification for weak signals and provide attenuation for strong ones.

The first amplification stage is responsible of the performances in terms of receiver sensitivity, since thermal noise inserted at early stage will be further amplified by following gain stages.

A simplified block diagram of a commercial tuner is shown in figure 5.3.
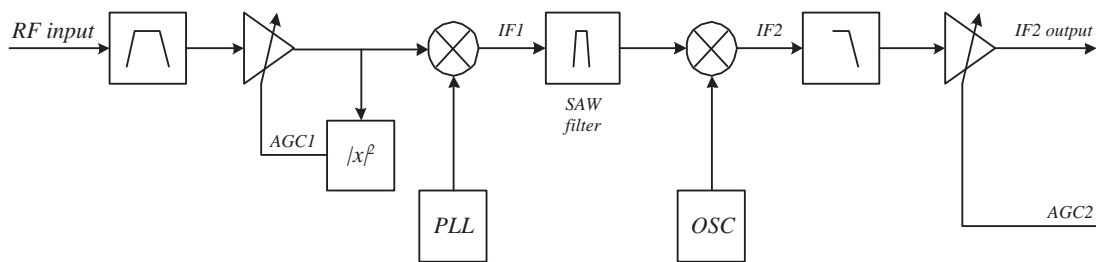
Figure 5.3: Simplified tuner block diagram.

The signal is first bandpass filtered to avoid out-of-band interferences. This is usually a fixed-frequency large-bandwidth filters that covers all the tuning band. The signal then undergoes amplifications by a first variable-gain amplifier, directly controlled to avoid saturations in following stages (AGC1). Then, the signal is mixed with a sine wave generated by a PLL whose frequency determines the tuned channel. The signal at (first) intermediate frequency (IF1) is sharply bandpass-filtered by the channel selector surface-wave (SAW) filter. A second down-conversion by a fixed frequency gives the second intermediate frequency signal, centered around 36.167MHz in our case. The amplitude of the output signal is controlled by the second gain control signal (AGC2) coming from the demodulator itself. The behaviour as a function of signal RF power of the two gain controls, AGC1 and AGC2, is depicted in figure 5.4 for the tuner used.

As can be noted, AGC1 acts for input RF power down to -70dBm, where it can no more provide additional gain. For RF power from -70dBm down to the noise limit, AGC2 provides a way to maintain a constant IF2 signal level to the demodulator input.

For a mobility-harnessed OFDM demodulator, the input signal power can vary over a wide range because of the multipath and shadow fading effects. Conventional slow AGC strategy developed for fixed reception cannot be employed with satisfactory results.
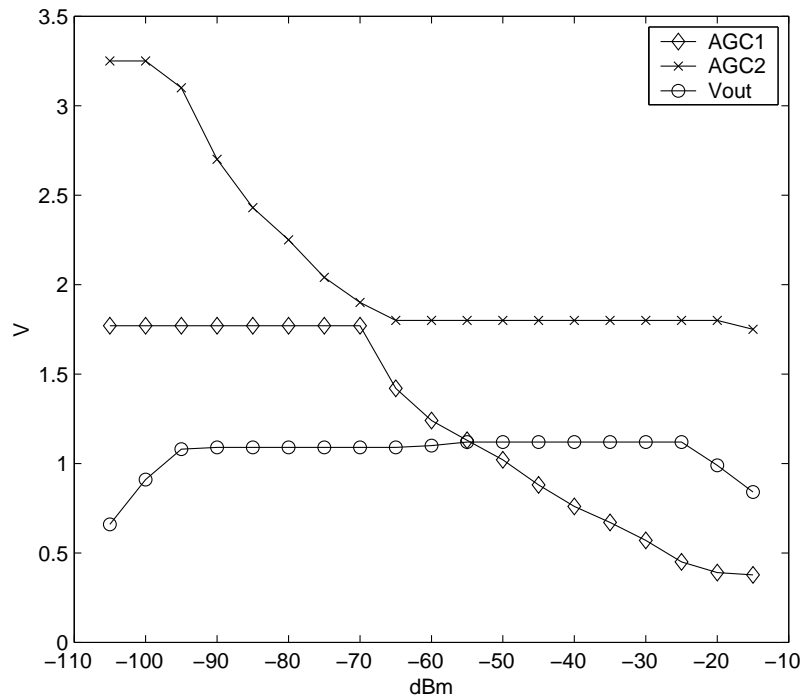
Figure 5.4: AGC1 and AGC2 as a function of RF input power.

Faster strategies are required, anyway the use of a commercial tuner limits the maximum AGC control speed. The data comes from the Analog-to-Digital Converter (ADC) and the demodulator has to provide the AGC signal to the tuner. This signal is a PWM-modulated 3.3V CMOS signal, and the external filtering to obtain an analog signal to control the tuner is performed by a simple RC network. The external filter limits the reaction speed of the AGC control. To be able to vary this speed, the method depicted in figure 5.5 has been employed, where one of two resistor can be selected enabling the relative output buffer, thus varying the time constant of the external RC network. Longer time constant provides better rejection of the PWM-induced noise, while shorter time constant can be used to follow fast transients.

Even employing the lower-value resistor, the AGC2 speed is limited by the RC timing constant and by the tuner itself. Moreover, since the AGC2 control loop is feedback-based, fluctuations of the input signal are required to provide a correction signal. For this reason, a two-stages control strategy have been studied. The simplified block diagram of the implemented AGC strategy is shown in figure 5.6.

The mean power of the signal coming from the tuner and converted by the ADC is extracted by strongly low-pass filtering the square-value of the signal. The estimated
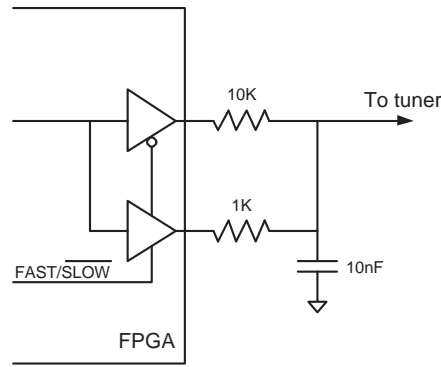
Figure 5.5: AGC resistor selection
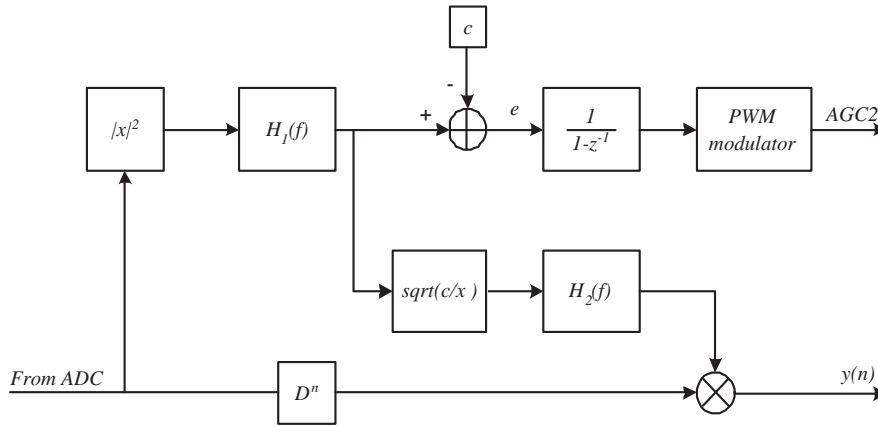
Figure 5.6: AGC block diagram

power is then compared to the desired level c and the AGC2 correction signal is obtained by integration of the error term e. The entity of the error term e is used to control the output buffers and switch between lower-valued resistor ($|e| > threshold$) or higher-valued resistor ($|e| < threshold$). This improves the speed of the AGC2 control strategy without affecting the performances for slowly-varying channels, when the use of the higher-value resistor yields better noise rejection.

Even employing this mechanism to adapt convergence speed, the incoming data can still experience power fluctuations. To correct the data, a digital corrector has been implemented. It must be noted that the function

$$\sqrt{\frac{c}{x}}$$

is approximated by the first-order Taylor series

$$1 - \frac{1}{2c}(x - c)$$

for $x \approx c$. Moreover, the $(1/2c)$ term can be implemented as bit-shifts and recalling $e = x - c$, the function is easily computed requiring just one adder.

The filters $H_1(f)$ and $H_2(f)$ are easily implemented as first-order IIR with power-of-two updating coefficients. In this way, multiplications are replaced by shift-and-add operations and the required resources are minimal.

5.2.2 Timing synchronization

The first task that an OFDM receiver has to accomplish is to acquire time synchronization of the received signal. For a continuous-transmission system, when no other information are known, only the cyclic extension (guard interval) of the OFDM signal can be exploited [86]. If we compute the correlation $G(n)$ of the input signal $r(n)$ as:

$$G(n) = \sum_{i=0}^{N_g} r(n+i)r^*(n+i+N)$$ (5.1)

then $G(n)$ is a complex estimator that exhibits its absolute value maximum for n corresponding to the beginning of the useful part of the OFDM symbol. The correlation absolute value $|G(n)|$ for an OFDM signal in ideal conditions (no noise, flat channel response) is depicted in figure 5.7.
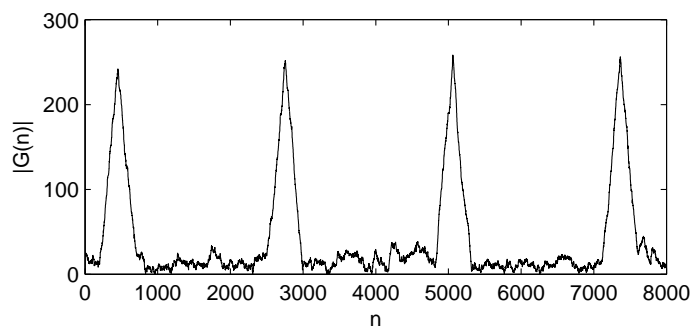
Figure 5.7: Correlation output in ideal conditions. $N = 2048, N_g = 256$.

Effects of narrow-band interferer

OFDM modulation is robust to narrow-band interferer, since only some subcarriers are corrupted by the interferer; in these conditions, the error-correction scheme is able to recover the corrupted data. Unfortunately the correlation process used for initial acquisition and time tracking can be impaired by coherent narrow-band interferers. To avoid this

drawback, narrow-band interferer must be detected and filtered out before the correlation process.

In fact, if we write the received signal $r(n) = x(n) + \alpha e^{j2\pi fn/N}$, substituting $r(n)$ in equation 5.1 we obtain:

$$
\begin{aligned}
G(n) &= \sum_{i=0}^{N_g} x(n+i)x^*(n+i+N) + x(n+i)\alpha e^{-j2\pi f(n+i+N)/N} + \\
&\quad + x^*(n+i+N)\alpha e^{j2\pi f(n+i)/N} + \alpha^2 e^{-j2\pi f}
\end{aligned}
\tag{5.2}
$$

where we can note that the second and third terms are uncorrelated over the N_g sum and then represent self-noise contributions. The fourth term is a constant, independent of n, thus giving DC component at the output of the correlator.

Another typical interference is constituted by co-channel PAL emission. Most of the energy of a PAL interferer is concentrated around the video carrier, located in the lower frequencies, and around the audio carrier, located in the higher frequencies. A typical RF spectrum for a PAL/NTSC analog modulation is depicted in figure 5.8.
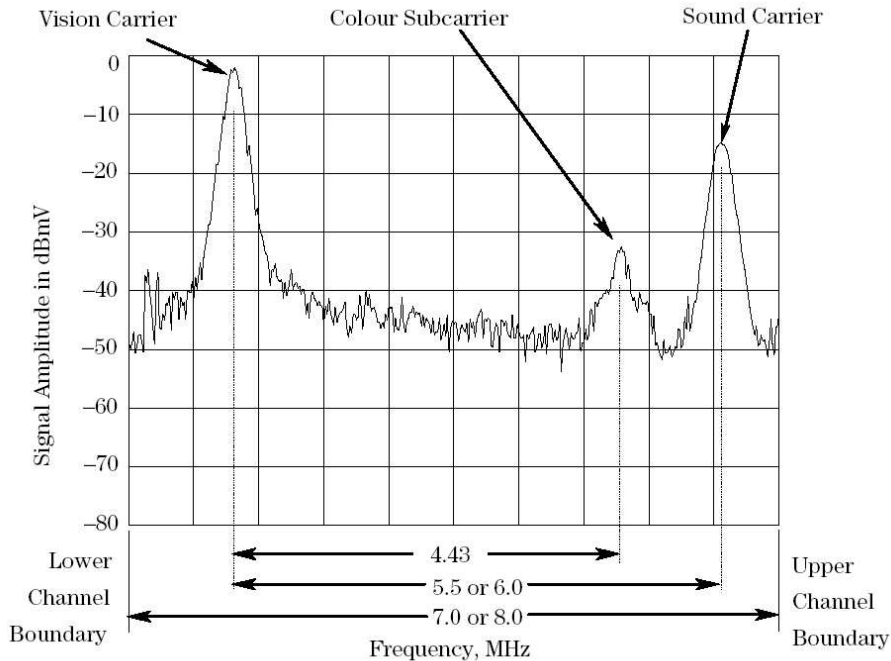
Figure 5.8: PAL/NTSC RF spectrum.

For the implemented design, the central DC leakage due to the I/Q analog modulator

impairs the correlation process. To suppress the DC leakage contribution, a high-pass filter has been studied. For efficient implementation, a second-order IIR architecture has been chosen, that requires a single hardware multiplier.

A future extension is constituted by the study and implementation of a bandpass filter (for instance, $f_{c1} = 0.5\text{MHz}$, $f_{c2} = 2.5\text{MHz}$) to suppress most of the energy deriving by a PAL/NTSC co-channel interferer and eventually provide adaptive filtering to effectively protect the correlation process from high-energy narrow-band interferers.

Implementation considerations

For each new input sample of the correlator, just one new term has to be added to the sum, while an old term must be subtracted. Thus, the sum over N_g terms can be simplified [87]. Equation 5.1 can thus be rewritten in a recursive fashion as

$$G(n) = G(n-1) + t(n) - t(n + N_g + 1)$$

where $t(n)$ is:

$$t(n) = r(n)r^*(n + N).$$

A block diagram of an efficient correlator implementation that exploits the recursive formula is depicted in figure 5.9.
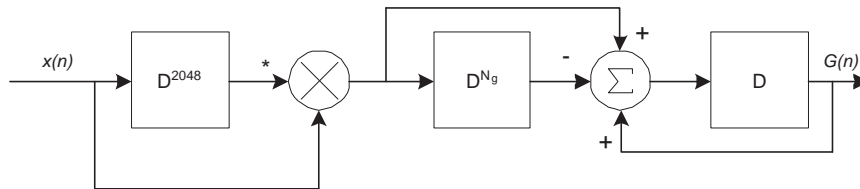
Figure 5.9: Correlator block diagram.

To search the correlation maximum, a complex absolute-value must be performed. Since the computation of:

$$|a + jb| = \sqrt{a^2 + b^2}$$

requires two real multiplications and a square-root operation, an low-complexity approximation is desirable. Since high precision is not required, the absolute value can be efficiently approximated by:

$$|a + jb| \simeq |a| + |b|$$

and a further simplification can be performed by implementing the absolute value of a and b as bit-wise inversion of the two's-complement fixed-point binary representations for negative terms.

To extract the peak position, an adaptive threshold algorithm has been used. For each OFDM symbol, the two crossing points n_1 and n_2 between the correlator pseudo-absolute value and the threshold are easily extracted, and the peak position is assumed to be $n_p = (n_1 + n_2)/2$. The correlator absolute value is low-pass filtered and this quantity, that represents the correlation mean power, is used as threshold. It must be noted, however, that the threshold value must not change in the interval between the points n_1 and n_2, so this value is "hold" when the signal is over the threshold. The IIR time constant and threshold scaling have been adjusted with the aid of several simulations. An example of the evolution of correlation and threshold over time is shown in figure 5.10.
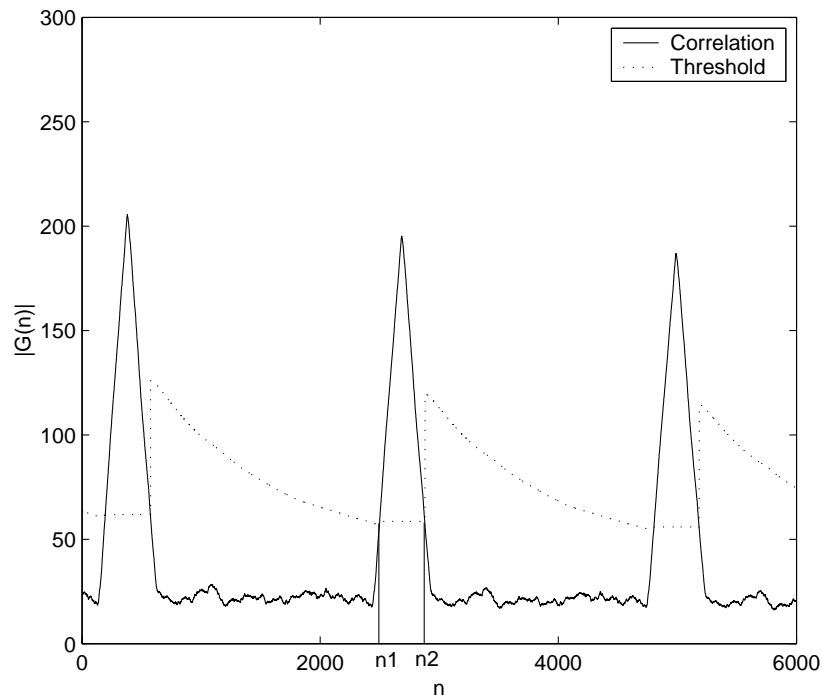
Figure 5.10: Correlation peak retrieval by adaptive threshold, GI = 1/8, C/N = 20dB.

Simulations show that the threshold method is simple and yet more reliable than looking for the actual correlator maximum.

Guard interval detection

At the beginning, the receiver has no information other than the correlation due to cyclic prefix insertion; moreover, the receiver has no *a-priori* knowledge about the used guard interval length N_g. In this case, the minimal N_g should be used, but the correlator output will exhibit a flat zone around the maximum. This behaviour is shown in figure 5.11, where $N_g = 64$ has been assumed by the receiver but the guard interval size was 1/8 ($N_g = 256$).
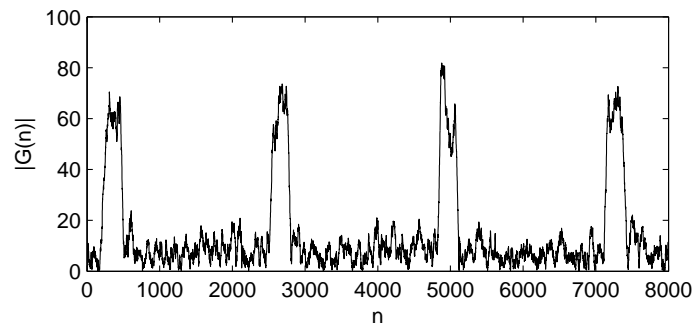
Figure 5.11: Correlation output. $N = 2048, N_g = 64$ instead of $N_g = 256$.

Once again, the method of using the crossing points over a threshold instead of looking for the actual correlator maximum is clearly more precise.

To recover the guard interval size N_g used by the transmitter, the receiver can look at the arrival time t_l of two or more consecutive correlation peaks. For best averaging, we implemented the algorithm described by the flow chart of figure 5.12. We wait for four consecutive correlation peaks whose period is inside the tolerances $[N, N + N_{gmax}]$ and then estimate the guard interval size by rounding the estimated value to the nearest valid number.

After the estimation of the guard interval value, time tracking algorithm is activated.

The correlation process is very robust to gaussian white noise; in fact, the sum over N_g terms in equation 5.1 averages the noise contribution over at least 64 samples ($T_g = T_s/32$). The correlator output is shown in figure 5.13 for the worst-case of $T_g = T_s/32$, $C/N = 2dB$.

As can be noticed, the peaks are still clearly visible. Only for $C/N = 0dB$ the peaks are no more easily detected by a simple threshold-based algorithm. In this case, however, just increasing the guard interval size allows to obtain additional noise robustness. For example, in figure 5.14 is shown the case $T_g = T_s/16$, $C/N = 0dB$.

The robustness of guard interval acquisition process is limited by the performances
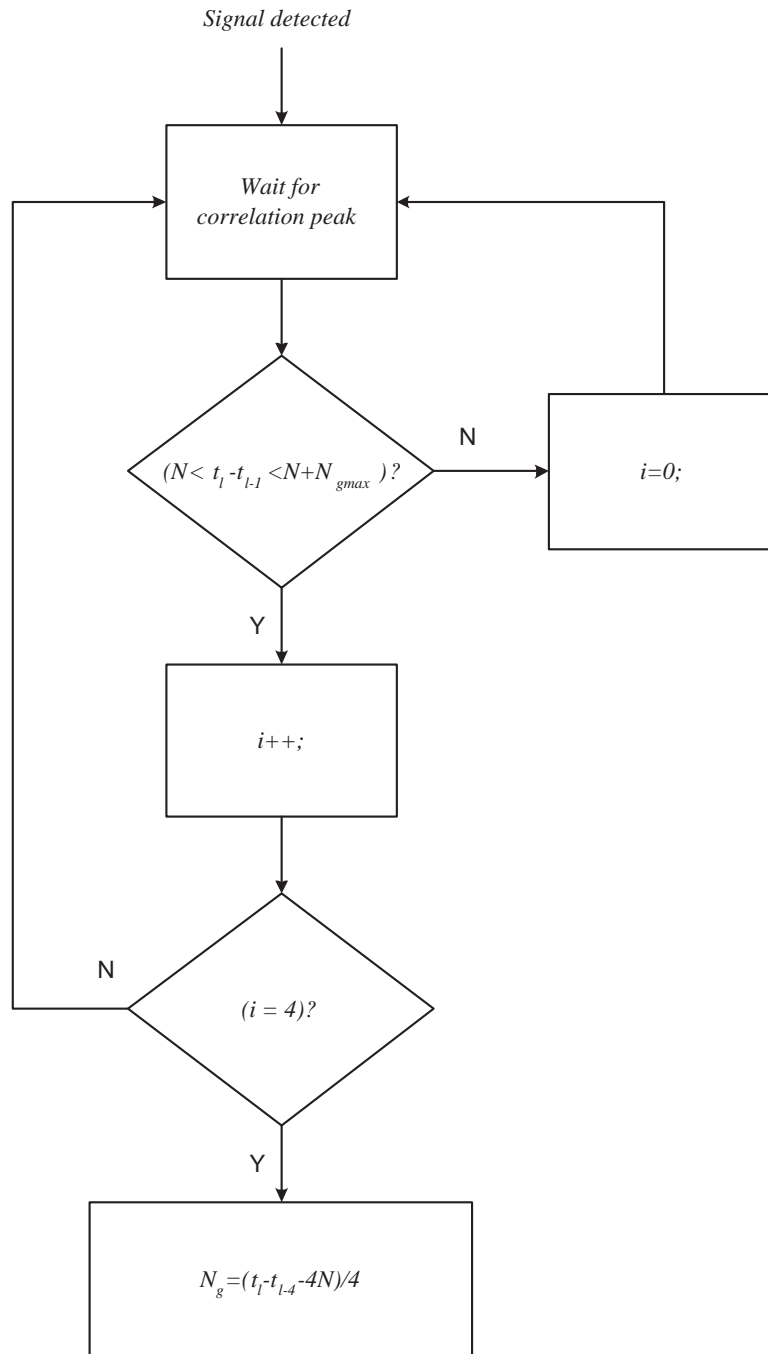
Figure 5.12: Guard interval estimation flow-chart.

of the minimum guard interval size. Considering this point, for the enhanced-mobility COFDM system we discarded the possibility $T_g = T_s/32$, limiting the choices but assuring enhanced reliability for signal acquisition. It must be noted, however, that the choice of the minimum guard interval size does not affect other system parameters; the choice $T_g =$
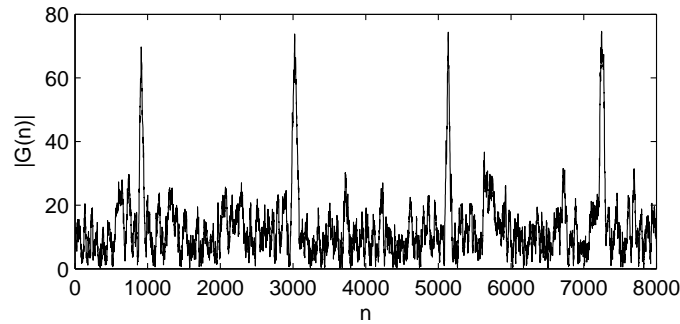
Figure 5.13: Correlation output. $N = 2048, N_g = 64, C/N = 2dB$.
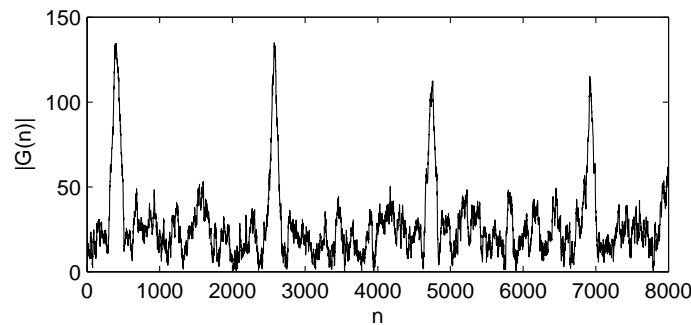
Figure 5.14: Correlation output. $N = 2048, N_g = 128, C/N = 0dB$.

$T_s/32$ offered just a little increase (around 6%) in channel bitrate respect to $T_g = T_s/16$.

Time tracking

The time tracking algorithm must maintain frequency and phase locking of receiver sampling clock. If we denote the transmitter sampling frequency as f_s, the receiver sampling frequency will then be

$$f_s' = f_s(1 + 10^{-6}\varepsilon) \tag{5.3}$$

where ε is expressed in part-per-million (ppm).

Employing high-accuracy Temperature-Compensated Crystal Oscillators (TCXO) or even miniature atomic clock [88] can bring important advantages for time tracking performance. In fact, the ε value is bounded by:

$$\varepsilon \leq \frac{v}{c} + acc_{TX} + acc_{RX}$$

and this bound depends on the sum of a Doppler-related and the two oscillator-related accuracy terms. For $v = 30m/s$, corresponding to mobile speed over $100km/h$, the

Doppler-related term is about $0.1ppm$. Thus, the oscillator accuracies are the dominant terms in the above inequality. TCXO with accuracies up to $1ppm$ can be found and atomic clocks can improve this figure even better.

In order to tolerate consumer-grade oscillators, the time tracking algorithm must be able to acquire and maintain synchronization with values of ε up to $200ppm$.

To estimate ε, we consider the correlation over multiple consecutive OFDM symbols and compare the peak arrival times with the synchronization pulses generated by the flywheel spaced exactly by $N + N_g$ samples.
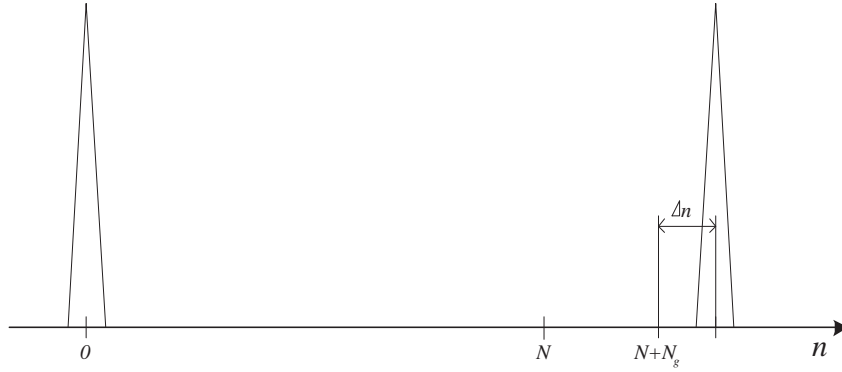
Figure 5.15: Time tracking by correlation peak drift.

As we can observe in figure 5.15, the distance in number of samples of two correlation peaks detected by the receiver is not exactly $N + N_g$, but is affected by an error Δn that can be expressed as:

$$\Delta n = \frac{N + N_g}{10^6} \varepsilon \tag{5.4}$$

Since Δn is lower than unity, it must be accumulated over hundreds or thousands of OFDM symbol to be reliably estimated.

Anyway, the error ε is mostly due to oscillator accuracy. The variations that the frequency error can exhibit are normally very slow if compared to the period of the OFDM symbols, and ε can be considered constant over a period of some seconds.

Under this assumption, the control loop of figure 5.16 has been developed. When initial timing acquisition has been performed and guard interval reliably estimated, the *acquire* control signal is activated and the flywheel is initialized. This ends the acquisition and starts the tracking phase. The loop exploit a *proportional-integral* strategy to modulate the coefficient of the variable interpolator used in the front-end to synthesize the sampling frequency f'_s.
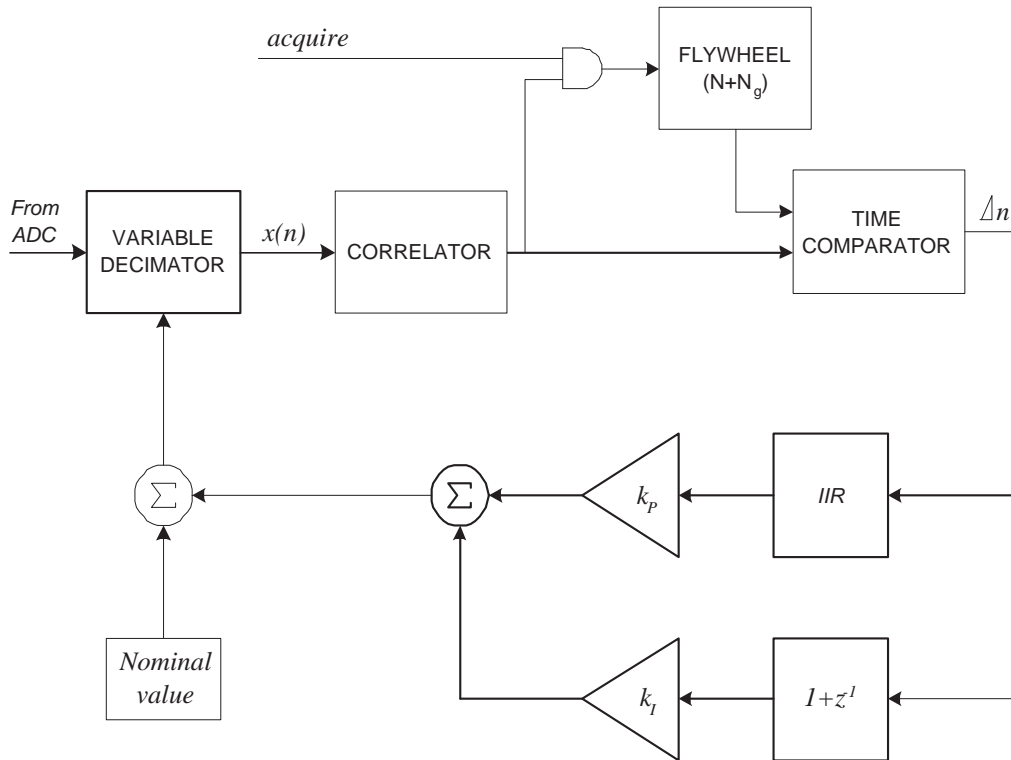
Figure 5.16: Time tracking block diagram.

The proportional term is calculated after a strong low-pass filtering of error Δn, implemented by a first-order IIR filter, to reject most of the noise coming from peak estimator variance.

The algorithm characteristics, notably the convergence speed and the residual error ε_r variance, can be modified working on the parameters k_P, k_I and IIR transfer function. Two different control loop parameters set have been obtained to guarantee fast initial convergence (1st set) and low residual error (2nd set). Table 5.1 shows the coefficients used. As can be noted, the coefficients correspond to power-of-two values, and multiplications are efficiently replaced by bit-shifts.

	set 1	**set 2**
k_P	4	1
k_I	0.0156	0.00195

Table 5.1: Time tracking coefficients, set 1 and 2.

The simulated performance of the two coefficient sets are discussed in the next chapter.

5.2.3   Frequency synchronization

The objective of the AFC in OFDM receivers is to establish subcarrier orthogonality (acquisition) as fast as possible and then maintain orthogonality at all times during reception (tracking). These quite different tasks call for distinct acquisition and tracking algorithms, based on pre- or post-FFT offset estimation. Initially, the frequency error is dominated by a potentially large carrier frequency offset $\Delta f'$. This offset can be expressed as a sum of an integer multiple of the subcarrier spacing and fractional part $\Delta f'_F$.

$$\Delta f' = n_I \Delta f + \Delta f'_F \tag{5.5}$$

As opposed to post-FFT algorithms, pre-FFT acquisition does not suffer from severe Inter-Carrier Interference (ICI), so that the fractional offset $\Delta f'_F$ can be estimated without much self-noise and subsequently be corrected for. After this stage, the orthogonality is re-established and ICI is reduced, so that post-FFT algorithms become viable; the integer offset n_I can now be estimated and corrected. Finally, the receiver supervisor block can switch to post-FFT frequency offset tracking mode where $\Delta f'$ is handled by the tracking loop.

Frequency offset acquisition

To estimate the fractional offset $\Delta f'_F$, let's consider again equation 5.1 with a frequency-shifted received signal

$$r(n) = x(n) e^{j2\pi n \frac{\Delta f'}{N \Delta f}}$$

We obtain:

$$
\begin{aligned}
G(n) &= \sum_{i=0}^{N_g} x(n+i) x^*(n+i+N) e^{-j2\pi \frac{\Delta f'}{\Delta f}} \\
&= e^{-j2\pi \frac{\Delta f'_F}{\Delta f}} \sum_{i=0}^{N_g} x(n+i) x^*(n+i+N)
\end{aligned}
\tag{5.6}
$$

in correspondence of the correlation peak, the sum is done over N_g terms for which $x(n+i) = x(n+i+N)$; hence, the sum gives a real number. The fractional part can be easily extracted considering the phase of $G(n)$ in correspondence to the peak:

$$\Delta f'_F = \Delta f \frac{\angle \left(G(n)|_{n=peak} \right)}{2\pi} \tag{5.7}$$

Once corrected the fractional part of the carrier offset, subcarrier orthogonality is established and FFT can be performed. If we denote as $z_{l,k}$ the Fourier-transformed

samples with frequency index k for OFDM symbol l, the set of frequency indexes $K = [0, 1, ...N]$ can be circularly-rotated by the integer frequency offset n_I. If we consider the continual pilots of each OFDM symbol $z_{l,k}$ with $k \in CP$, we can compute the quantity:

$$W(i) = \sum_{k \in CP} z_{l,k+i} \; z_{l,k+i}^* \tag{5.8}$$

for $i \in [-M, M]$, where M depends on the required frequency offset search range. Since the pilots are inserted with boosted power level, $W(i)$ exhibits the maximum for $i = n_I$.

An indication about the reliability of the estimated n_I can be given by looking at the ratio between the maximum estimator $W(n_I)$ and the second largest candidate $W(n_I')$. If the ratio is above 16/9, the estimated n_I is considered reliable.

Frequency offset tracking

Once accomplished initial frequency offset acquisition, post-FFT methods can be employed to maintain frequency offset tracking. If we consider now:

$$W'(i) = \sum_{k \in CP} z_{l,k+i} \; z_{l-1,k+i}^* \quad i = n_I \tag{5.9}$$

or, assuming n_I already corrected:

$$W' = \sum_{k \in CP} z_{l,k} \; z_{l-1,k}^*. \tag{5.10}$$

Due to the residual frequency error $\Delta f'$, each subcarrier sample $z_{l,k}$ belonging to the continual pilot set $k \in CP$ can be written as:

$$z_{l,k} = \beta H(l,k) e^{j2\pi l \frac{(N+N_g)\Delta f'}{N\Delta f}} \tag{5.11}$$

where β is the boosting factor of the pilots and $H(l,k)$ is the time-variant channel frequency response for subcarrier of index k for OFDM symbol l. Equation 5.10 becomes:

$$W' = \beta^2 e^{j2\pi \frac{(N+N_g)\Delta f'}{N\Delta f}} \sum_{k \in CP} H(l,k) H^*(l-1,k) \tag{5.12}$$

For slowly-varying channels, $H(l,k) \simeq H(l-1,k)$ and then

$$\angle(W') \simeq 2\pi \frac{(N+N_g)\Delta f'}{N\Delta f} \tag{5.13}$$

thus giving an estimate of $\Delta f'$.

This method is more reliable than the guard-interval peak phase extraction, in particular because it cannot be impaired by coherent interferer.

The better control strategy is to switch to post-FFT tracking as soon as frequency offset acquisition is performed.

Implementation issues

The frequency offset is corrected in time domain, by multiplying the baseband complex signal $I + jQ$ with a complex rotating versor generated by a Numerically-Controlled Oscillator (NCO).

For initial pre-FFT fractional frequency offset acquisition, theoretically it would be possible to compute directly

$$\Delta f_F' = \Delta f \; \frac{arctan[Im(G_{peak})/Re(G_{peak})]}{2\pi} \tag{5.14}$$

but this is clearly impractical for RTL design, due to the division and the required computation of the $arctan()$ function. Instead of implementing the closed-form estimator, we chose a successive-approximation approach. The quantity

$$\zeta = \frac{arctan[Im(G_{peak})/Re(G_{peak})]}{2\pi} \tag{5.15}$$

can be approximated as depicted in figure 5.17.
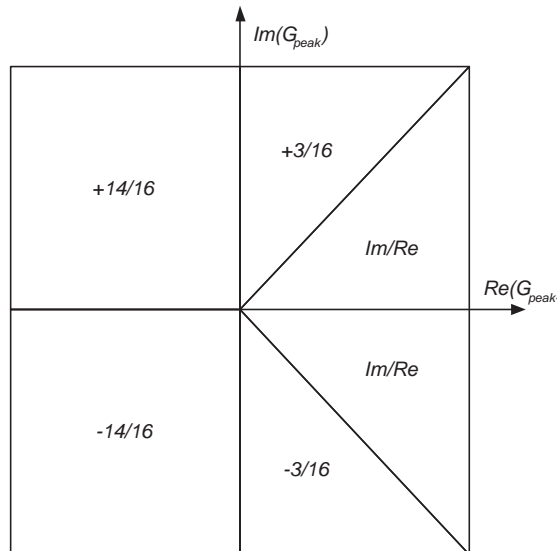
Figure 5.17: Approximated computation of ζ.

The polar plane has been divided in 5 zones, easily detected by looking at the results of the inequalities:

- $Im(G_{peak}) < 0$

- $Re(G_{peak}) < 0$

- $|Im(G_{peak})| < |Re(G_{peak})|$

The four zones that correspond to the upper half of first quadrant, second, third and the lower half of fourth quadrant have been approximated by their central values. For the lower half of first and upper half of fourth quadrant, $2\pi\zeta$ is better approximated by $Im(G_{peak})/Re(G_{peak})$.

The pre-FFT frequency acquisition has been implemented as a closed-loop servo control, conceptually depicted in figure 5.18.
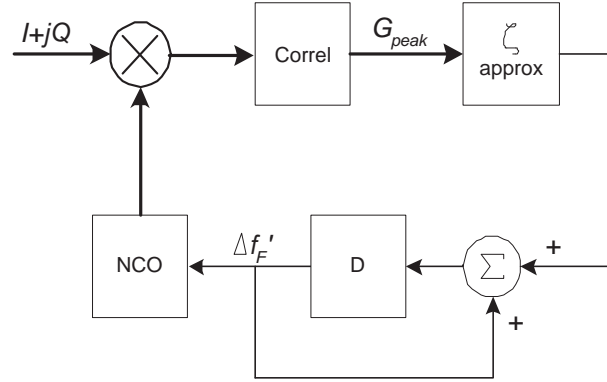
Figure 5.18: Pre-FFT frequency offset servo loop.

To guarantee convergence and reduce noise, a conservative updating policy for the frequency offset has been implemented:

$$\Delta f_F'(l) = \Delta f_F'(l-1) + \rho\zeta\Delta f \tag{5.16}$$

where the updating coefficient ρ is less than unitary.

It can be noted that the algorithm for n_I estimation could be efficiently merged with the subsequent post-FFT frequency offset tracking algorithm. Using equation 5.9 instead of 5.8 leads to equivalent results; even better, for $k \notin CP$ we have that the terms $z(l,k)z^*(l-1,k)$ assume random phases, since data carriers are uncorrelated between consecutive symbols. In this case we can exploit the correlation of continual pilots and not only the boosting factor β to distinguish between pilot and data subcarriers.

5.2.4   Channel estimation

In all OFDM symbols, one pilot is inserted every 12th subcarrier for channel estimation purpose. These are the *scattered pilots* and the set of indexes k for which $z(l, k)$ is a scattered pilot is denoted as SP. Since the value of each transmitted pilot is known by the receiver, it can divide the received value with the *a-priori* known one and thereby obtain an estimate, $H(l, k)$, of the channel at time l for the pilot cell k. However, equalization of the data cells requires a corresponding channel estimate for each of them. These can be obtained by 2-D interpolation in time and frequency between the pilots.

The best possible approach would be to adapt the channel estimation algorithm to take into account the characteristics of the channel. As seen in previous chapter, the 2-D interpolation can be implemented as a cascade of two 1-D filters in time ad frequency domain. Moreover, the time domain filtering can be easily implemented as a linear interpolator. The insertion of a time-domain IIR filter between the two interpolators could be beneficial to reduce the noise contribution when the channel does not change significatively over multiple consecutive OFDM symbols. Once the time response of the channel has been analyzed by inverse FFT and the echo delay spread S has been extracted, the frequency interpolator bandwidth can be adapted to the channel selectivity [42]. Two different sets of frequency-interpolation coefficients have been calculated, corresponding to two different bandwidths.

The block diagram of the channel estimation block is depicted in fig. 5.19.

The finite-state machine supervising the channel estimator process controls the activation of time interpolation, IIR filtering and can vary the set of coefficients for frequency interpolation.

Let now define some metrics to quantify the channel mobility: each scattered pilot $z(l, k)$ of symbol l can be compared to previous pilots $z(l - 4d, k)$, $4d$ symbols before. Let's consider the estimator:

$$V(d) = \sum_{k \in SP} |z(l, k) - z(l - 4d, k)|^2 \tag{5.17}$$

The difference between the scattered pilots at time l and at time $l - 4d$ can be the result of multiple impairments. Assuming accurate time- and frequency-tracking, the estimator $V(d)$ is a measure of the noise, interference and channel mobility. Meanwhile, noise and interference contributions are not function of index d. The contribution induced by channel mobility, on the other side, depends on the time difference $4d$; in fact, as discussed before, the autocorrelation of the channel in the time domain depends on the
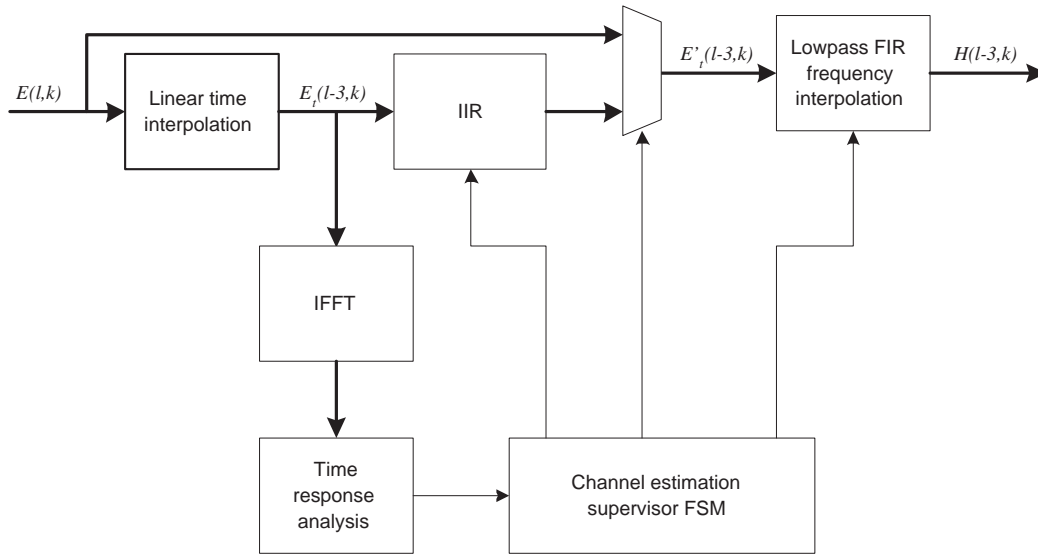
Figure 5.19: Channel estimation block.

time difference and assume its maximum for $\Delta t = 0$.

To reduce memory requirements, the estimator $V(d)$ can be computed on a subset SP' of the whole scattered pilot set SP. The mobility of the channel can be estimated by looking at the ratio $V(4)/V(1)$.

Using the above defined metric, we can distinguish the following cases.

Slowly-varying channel, short echoes ($V(4) < 2V(1)$, $S < N/12$)

This is the case of short-distance fixed or portable applications. The linear time interpolation is activated together with time-domain IIR filtering. $E_t(k)$ is active for every k multiple of 3. Frequency-domain FIR filtering uses the narrow low-pass set of 3x interpolation coefficients.

Slowly-varying channel, long echoes ($V(4) < 2V(1)$, $S > N/12$)

This is the case of long-distance fixed or portable applications. The linear time interpolation is activated together with time-domain IIR filtering. $E_t(k)$ is active for every k multiple of 3. Frequency-domain FIR filtering uses the wide-band set of 3x interpolation coefficients.

Mobile channels, short echoes ($V(4) > 2V(1)$, $S < N/12$)

This is the case of short-distance mobile applications. The time interpolation and filtering are bypassed, to better follow the channel response variations. For a sacrifice of a factor 4 in maximum echo length, a factor 4 in maximum Doppler frequency can therefore be gained. Thus, $E_t(k) = E(k)$ and $E_t(k)$ is active for every $k + r$ multiple of 12, where r takes into account for the scattered pilot position. Frequency-domain FIR filtering uses the narrow low-pass set of x12 interpolation coefficients.

Mobile channels, long echoes ($V(4) > 2V(1)$, $S > N/12$)

This is the case of long-distance mobile applications. The time interpolation must be activated, even if the channel variations could not be closely tracked. The time IIR filtering is bypassed. $E_t(k)$ is active for every k multiple of 3. Frequency-domain FIR filtering uses the wide-band set of x3 interpolation coefficients.

5.2.5   Channel analysis

The channel estimation in the frequency domain can be exploited to refine the FFT window positioning to minimize the ISI coming from excess echo spread. The frequency-domain channel estimation coming from time interpolator is Inverse-FFT transformed to obtain the channel impulse response $H(t)$. Brugger and Hemingway [89] analyzed several strategies that can be exploited to refine the FFT window positioning analyzing the channel impulse response. Among the low-complexity methods presented, no one guarantees good performances for all the cases.

The proposed method uses a mixed-approach. The channel impulse response calculated by the IFFT is first gated by a fixed threshold T to erase spurious contribution deriving by the noise, narrow-band interferer and channel mobility. The echo spread S is calculated as the difference between the maximum and the minimum over-threshold indexes. The center of gravity t_c over the echo spread is also calculated:

$$t_c = \frac{\sum_t H(t)t}{\sum_t H(t)}$$

where the sum is done only on the over-threshold samples. Figure 5.20 shows an example of channel impulse response analysis.

By comparing the echo spread S with the guard interval size T_g, two case are distinguished.
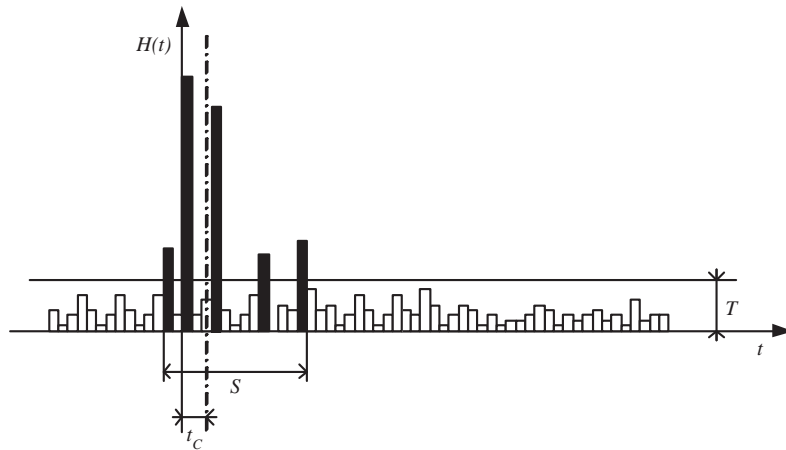
Figure 5.20: Impulse response analysis example.

- **Echo spread smaller than guard interval** $(S < T_g)$: the FFT window can be placed in the middle of the echo spread. No ISI is expected in this case.

- **Echo spread bigger than guard interval** $(S > T_g)$: a variable amount of ISI will be experienced because of the insufficient guard interval size. The center of gravity t_c can thus be used to place the FFT window. Nevertheless, suboptimal window placing can still be possible. Figure 5.21 shows a case in which center of gravity positioning can be enhanced by moving the FFT window to the right, to allow the guard interval to embrace the maximum energy.
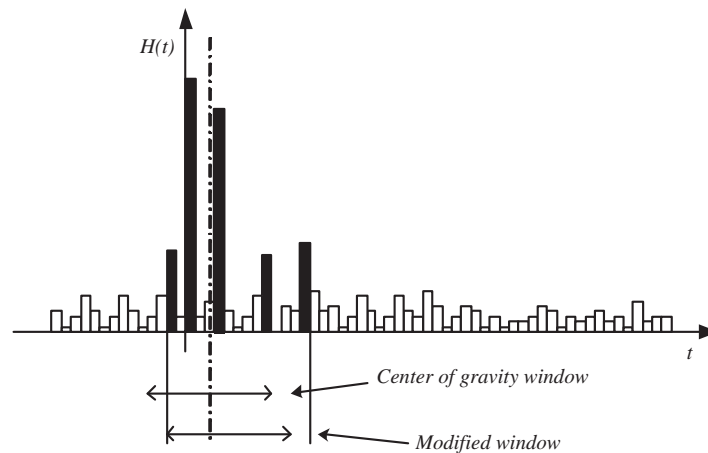
Figure 5.21: Impulse response analysis example.

This method proved to be efficient and guarantees reception even when other widely-

used methods as *first-signal-over-threshold* fails.

A further enhancement can be investigated; beside rectangular-shaped, different windowing functions can improve the performance by mitigating the joint effect of additive noise and inter-carrier interference [90].

5.2.6   Demapper

At the FFT output, the subcarrier samples are sorted into pilot and data samples. As shown before, pilot subcarriers are used to compute channel estimate $H(l, k)$. Data ones undergo flat fading so that each subcarrier $z(l, k)$ can be expressed as

$$z(l, k) = a(l, k)H'(l, k) + n \tag{5.18}$$

where $a(l, k)$ is the data to be equalized, $H'(l, k)$ the channel response and n is uncorrelated additive white noise. Each data sample $a(l, k)$ is taken from a Gray-encoded M-QAM constellation A and carries $ln_2(M)$ data bits of information.

Data equalization

Once obtained an estimated channel frequency response $H(l, k)$, the data subcarriers $z(l, k)$ must be equalized. Conventional equalizers form an estimate $a'(l, k)$ by performing explicit arithmetic division of the form $a'(l, k) = z(l, k)/H(l, k)$ and then performs demapping of the estimate $a'(l, k)$ using the original M-QAM constellation A. Division-free equalization can be performed by calculating $z(l, k)H^*(l, k)$ and then demapping this quantity using the scaled M-QAM constellation $H'(l, k)H'^*(l, k)A$.

The main advantage of this approach is that avoids explicit divisions, anyway this imposes some constraints on the bit numbers for intermediate results. Fechtel and Blaickner [91] indicate 14 bits for $z(l, k)$ quantization and some more bits for intermediate results in the case of Rayleigh channel.

The implemented design employs 18 bits for the intermediate results, thus taking advantage of the embedded multipliers maximum width.

Data demapping

The de-mapping process of the $a'(l, k)$ complex samples can be separated in two separate processes, working on real and imaginary parts in parallel. An appropriate de-mapping procedure (real part) is shown in figure 5.22 for 16-QAM. The two most significative bits (y_0, y_1) determine the quadrant of the full M-QAM constellation. y_0 can be recovered

(first iteration) by examining the real part of the complex sample $a'(l, k)$. As depicted in the left low end of figure 5.22, soft bit s_0 can be easily generated by means of a piecewise linear de-mapping rule. A "strong 0" is thus mapped to $s_0 = +1$, a "strong 1" is mapped to $s_0 = -1$, and a sample lying on the decision boundary is mapped to $s_0 = 0$. Samples lying beyond the limits are saturated to $s_0 = +1$ or $s_0 = -1$. To extract y_2, the same process can be iterated on the reduced constellation:

$$a'_2(l, k) = |a'(l, k)| - S_1 \tag{5.19}$$

where S_1 is the offset corresponding to the center of the first quadrant.
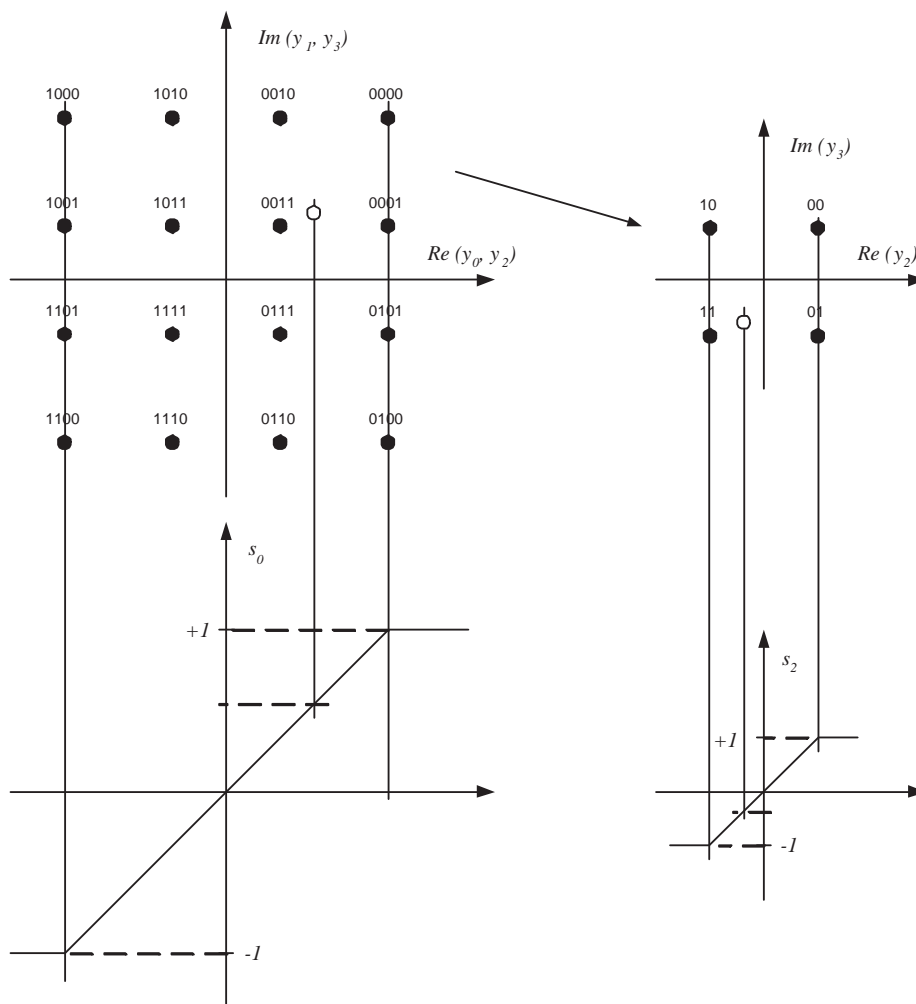
Figure 5.22: Demapping example, 16-QAM, real part.

Soft-metrics calculation

The demapped values obtained as described above must be applied to a logarithmic function to obtain the *soft-metrics* for Viterbi or Turbo decoding. The data are first converted from two-complement to sign-magnitude format. A simple logarithmic function of the magnitude can be achieved by counting the number of leading zeros of the binary word.

The output metrics are 4 bits total, thus 1 sign bit and 3 log-magnitude bits. The output of the log-2 block is normalized by an estimation of the total OFDM symbol power. It is interesting to note how other factors can be taken into account for confidence calculation of each subcarrier [92].

Let's consider the quantity:

$$b(l, k) = |z(l, k) - z(l - 4, k)|^2 \quad \text{with} \quad k \in SP \tag{5.20}$$

that express the difference of the received scattered pilot and the previous received one for the same subcarrier. This estimator is the result of noise, narrow-band interferers and channel mobility. The noise term is usually uniformly distributed between the whole set of modulated subcarriers, since it is mainly due to RF first amplification stages. The presence of a narrow-band interferer would corrupt the received value and result in high $b(l, k)$ values for subcarriers corresponding to the indexes k affected by this impairment. Channel mobility comes into play only if the mobility is so high that $z(l, k) \simeq z(l - 4, k)$ does not hold anymore.

The terms $b(l, k)$ can be time- and frequency-interpolated to obtain the estimator $B(l, k)$ for every k. This positive real-valued estimator can be used to reduce the confidence the corresponding subcarrier, and can provide important performance gains since it allows to effectively erase the contributions of co-channel interferer.

The logarithmic sign-magnitude soft metric is finally applied to a saturation block that maintain the signal in the range between 0 and 7 and allows the representation of the log-magnitude on 3 bits only.

The complete logarithmic processing is depicted in figure 5.23.

5.2.7 Diversity selection

Diversity can provide great performance enhancements especially for multipath propagation scenarios, where several subcarriers are affected by deep fades in the frequency domain. The signals received by two antenna adequately spaced ($l >> \lambda$) exhibit un-
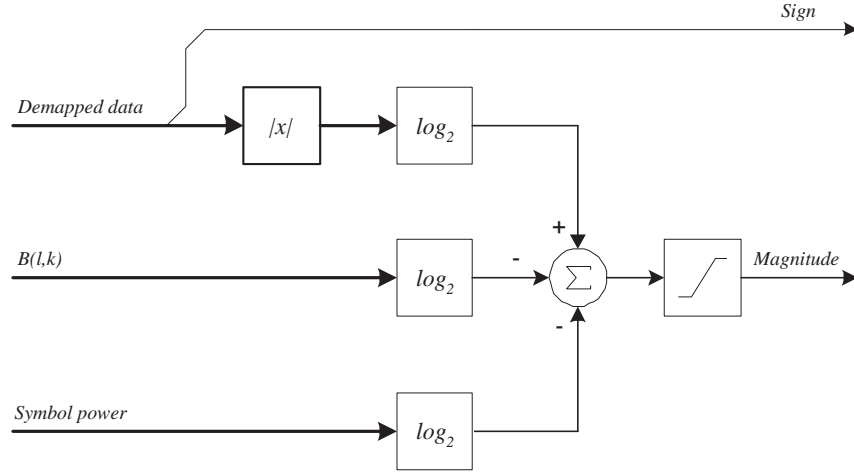
Figure 5.23: Soft-metrics generation

correlated frequency fades and then the combination of the subcarriers of the two signals greatly enhances the system performance.

Two combining methods have been studied. The first one is derived by the two-branch Maximal-Ratio Receive Combining (MRRC). The second one is a low-complexity adaptation that can be identified as Maximum-Confidence Selection (MCS) method.

Simulations have been performed to evaluate the performance gains that these method can offer, in particular for COST207 mobile channels models.

MRRC diversity

The MRRC scheme has been identified as an optimum combining scheme for Gaussian distributed noise [60]. If we write the received baseband signals as:

$$r_0 = h_0 s_0 + n_0$$
$$r_1 = h_1 s_0 + n_1 \tag{5.21}$$

where n_0 and n_1 are complex Gaussian distributed, and represent noise and interference contributions. The maximum likelihood decision rule can be applied on the signal:

$$\tilde{s}_0 = h_0^* r_0 + h_1^* r_1 \tag{5.22}$$

where h_0^* and h_1^* are the complex-conjugate of the channel frequency responses. As can be seen, this method can be integrated in the proposed demapper only accepting some compromises; in particular, the data coming from the two channel equalizers must be summed before undergoing logarithmic conversion. This can be done assuming that the

normalizations in the logarithmic domain were of the same entity for the two front-ends. This hypothesis can hold well for $B(l,k)$, and special attention must be paid to AGC strategy in order to assure similar OFDM symbol power between the two demodulators. A conceptual block diagram is shown in figure 5.24.
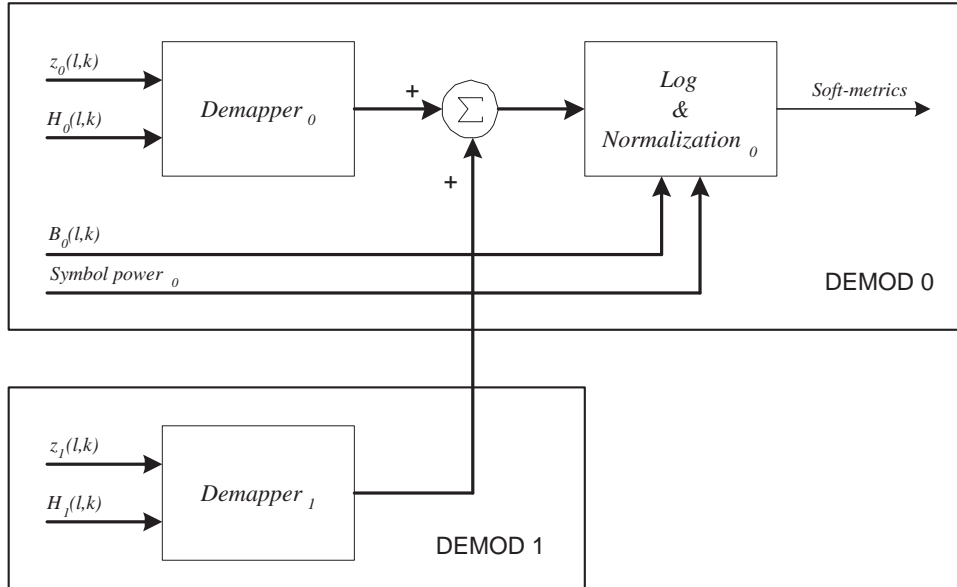
Figure 5.24: MRRC diversity conceptual block diagram.

MCS diversity

Another possibility is constituted by selecting for each subcarrier the soft-metric that has the higher confidence between the two. This process can be carried out on the 4-bit quantized and normalized quantities in the logarithmic domain. Simulations shows that sub-optimal performance improvements can be expected employing this strategy, but the assumptions of similar OFDM symbol power normalization terms is no more necessary. Moreover, only 4 bits instead of 18 have to be exchanged between the two receivers. The conceptual block diagram of the MCS diversity scheme is shown in figure 5.25.

   The hardware platform has been developed to allow the deployment of two-antenna diversity systems; in this case, two demodulator modules have to be mounted in the apposite locations and a data bus that directly links the two boards has been included.
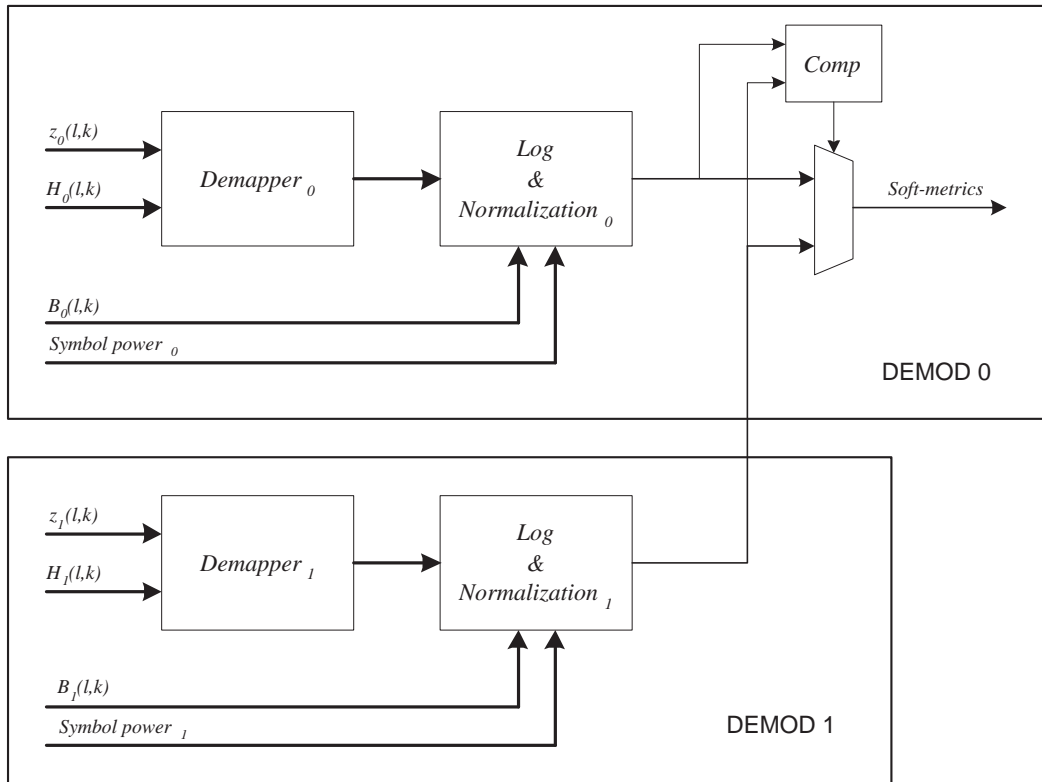
Figure 5.25: MCS diversity conceptual block diagram.

5.3 Considerations on time interleaver

The insertion of the time interleaver for the enhanced-mobility COFDM system allows the achievement of very good performance in presence of deep shadow fading events. Simulations show that fading events up to one third of time interleaver depth can be recovered. Since the time interleaver maximum depth is about 16000 OFDM symbols (QPSK), data blanking up to about 5000 OFDM has to be supported.

To obtain these performances, the receiver front-end must be able to cope with signal loss of this entity – in particular, it must maintain timing and frequency synchronization. This section identifies and analyzes the requirements of time and frequency algorithms that are necessary to fully exploit time interleaver theoretical performances.

5.3.1 Time synchronization

The time tracking algorithm is the most critical part that has to be addressed to fully exploit the time interleaving potential. The residual time synchronization error ε_r generates a drift between the flywheel-generated OFDM symbol start times and the actual missed

OFDM symbol start times. Let's recall equation 5.4; the peak correct position shifts of Δn samples over a single OFDM symbol:

$$\Delta n = \frac{N + N_g}{10^6}\varepsilon_r$$

and this error will be accumulated over the fading event duration. When the signal is detected again, the correlation peaks are retrieved and their position will be drifted respect to the position foreseen by the synchronization flywheel. Being the fading event length up to 5000 OFDM symbols, the amount of total drift (in number of samples) is:

$$\Delta n_t = 5 \cdot 10^3 \frac{N + N_g}{10^6}\varepsilon_r \simeq 10\varepsilon_r$$

Thus, the amount of total drift, expressed in number of samples, is one order of magnitude greater than the residual timing synchronization error ε_r, expressed in *ppm*.

The time synchronization algorithm normally discards peaks whose arrival times are out of a predefined *tolerance* to avoid sparse errors and improve the tracking performances. This tolerance has been set to 16 samples, and this imposes a severe constraint on residual sampling frequency error ε_r. Moreover, when the time tracking algorithm tries to re-lock on the incoming signal, the tracking algorithm would exhibit large transient ε_r to re-absorb the large peak drift, with the risk that a successive fading event could cause excessive peak drift and thus cause loss of lock of the receiver.

For this reason, the time synchronization Finite-State-Machine (FSM) that supervises the tracking process can issue an *acquire* command to the flywheel without performing initial acquisition and guard interval estimation processes. The flow-chart that describe the FSM behavior is depicted in figure 5.26.

In particular, let's highlight some important aspects of the control strategy.

- Peaks whose arrival time is outside the preselected *tolerance* are discarded and are equivalent to missing peaks.

- The *faults* indicator counts the number of faulty peaks (missing or outside the tolerance). Valid peaks don't directly reset this counter.

- When more than 20 faulty peaks are detected, the flywheel will be re-initialized by the first valid peak.

- When the number of faulty peaks is over the maximum recoverable number of OFDM symbols, the synchronization is lost and timing acquisition and guard interval detection should be performed again.
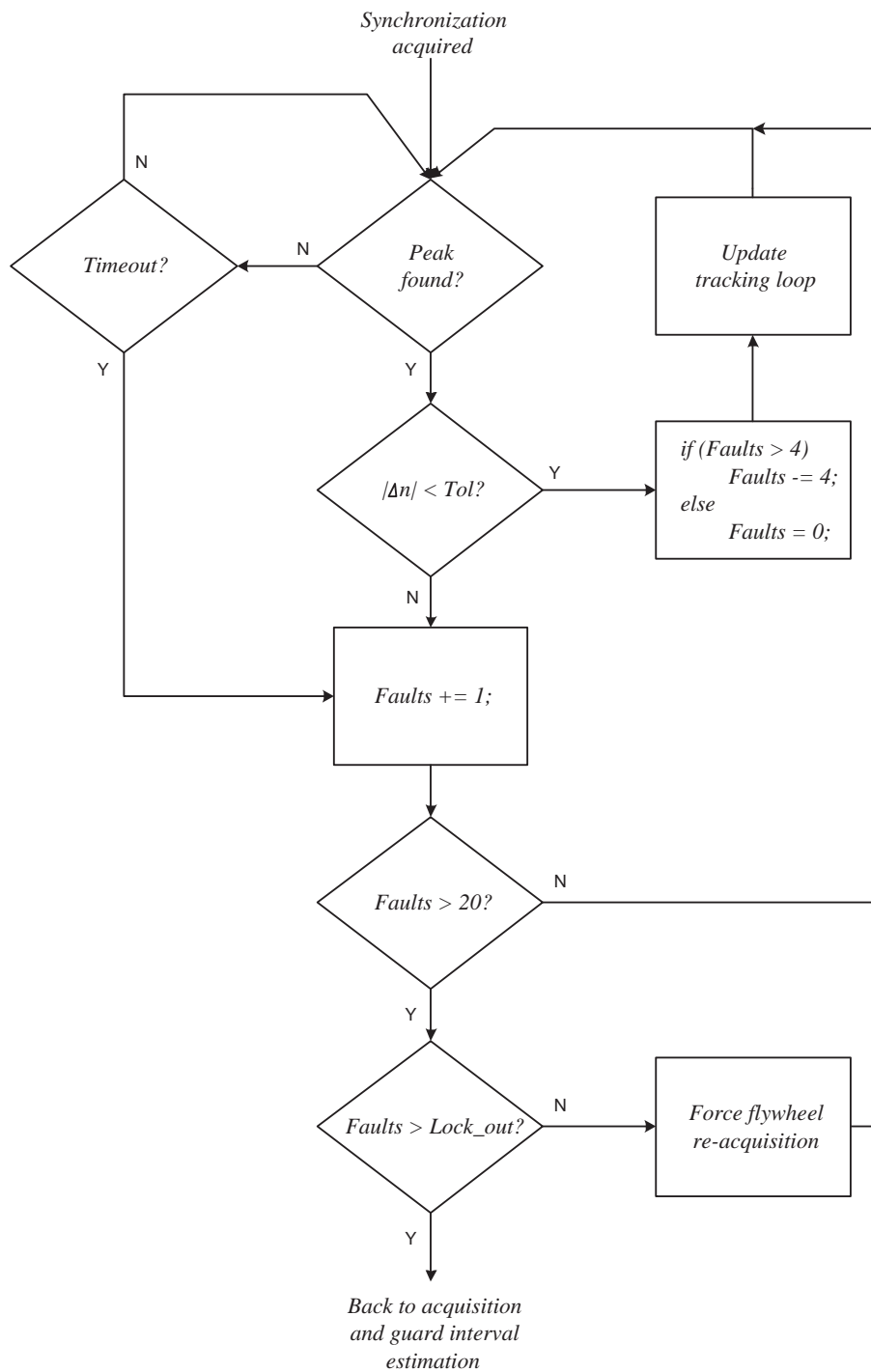
Figure 5.26: Time tracking FSM flow-chart.

• A flag is provided to signal the absence of valid correlation peaks and a probable fading condition; this indicator, associated with post-FFT ones based on TPS de-

coding (see later), can be used to determine the strategy for other receiver tasks (eg: channel estimation time filtering will be performed with $\alpha = 1$).

5.3.2 Frequency synchronization

The frequency synchronization task does not suffer the problems of drifting as the time synchronization one. The residual frequency error $\Delta f'$ does not accumulate over time and when the fading event is over and the signal is recovered, about the same amount of residual frequency error can be expected. However, the frequency tracking algorithm must not update the frequency offset accumulator during signal fades.

An adequate reliability indicator to gate the frequency updating algorithm is the *TPS reliability* flag. For each OFDM symbol, the 17 TPS subcarriers are differentially demodulated and the 17 hard-decision bits are added together to obtain the TPS bit. The quantity:

$$d(l) = \sum_{k \in TPS} \begin{cases} 0 & \text{if } Re[z(l,k)z^*(l-1,k)] \geq 0 \\ 1 & \text{if } Re[z(l,k)z^*(l-1,k)] < 0 \end{cases}$$

is analyzed and the *TPS bit* and *TPS reliability* indicator are generated as shown in figure 5.27.
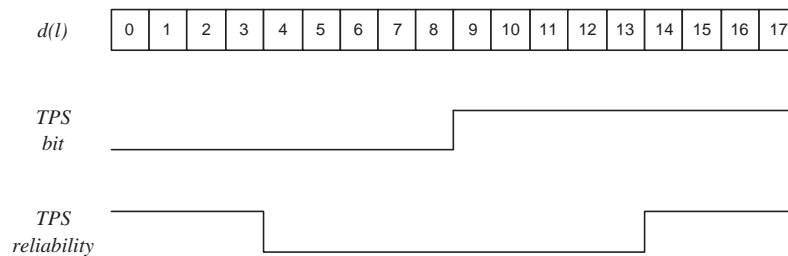
Figure 5.27: TPS demodulation and TPS reliability flag.

The differential TPS decoding does not require a valid channel estimation; thus, this indicator offers great robustness to channel frequency selectivity and mobility, as confirmed by the performed simulations.

The TPS reliability flag can be efficiently used to gate the post-FFT based frequency tracking algorithm previously proposed. Simulations demonstrate that the frequency error can be correctly frozen until the signal was found again.

5.4   System design

5.4.1   Processing cores

Once used only for glue logic, FPGAs have progressed to a point where system-on-chip (SoC) designs can be built on a single device. The number of gates and features has increased dramatically to compete with capabilities that have traditionally been offered through ASIC devices only. As FPGA devices progressed both in terms of resources and performance, the latest FPGAs have come to provide "platform" solutions that are easily customizable for system connectivity, DSP, and/or data processing applications.

The enhanced-mobility COFDM system has been implemented in hardware, exploiting the processing power and reconfigurability of Xilinx Virtex2/Virtex2Pro FPGAs. Among the features that greatly contributed to the design of the modulator and demodulator cores, the most prominent was the availability of fast dedicated multiplier blocks.

The main features of Virtex2/Virtex2Pro families can be summarized as follow:

- Fast on-the-field reconfigurability;

- More than 400MHz maximum internal clock speed;

- Fast internal static memories with configurable data size;

- Dedicated 18 bit x 18 bit multiplier blocks;

- Internal Digital Clock Managers (DCM);

- Wide choice of I/O standards;

- Integrated PowerPC core (Virtex2Pro only);

- Integrated gigabit serial interconnection cores (Virtex2Pro only).

5.4.2   Analog interfaces

The digital-to-analog converter (DAC) quality plays an important role for an OFDM modulator. It must be noted that, unlike single-carrier systems, OFDM modems are very sensitive to amplitude and phase distortions of the analog chain. While the problem is particularly relevant for RF power amplifier design, it must be addressed for the other analog parts as well.

In the recent past, direct GHz-band analog I/Q modulators have appeared on the market with performances that fulfill the OFDM requirements of our systems.

In this case, two digital-to-analog converters are required to obtain I and Q signals for direct analog modulation. Mismatches of the two converters and of the analog chain up to the I/Q modulator can greatly limit the system performance. In practice, there are a lot of sources of I/Q imbalance but they can all be reduced to three sources that can be used to model them all.

Perhaps the best known source of imbalance is the phase deviation from the ideal 90-degrees between the I and Q local oscillator signals. This skews the IQ plane and can be modelled by letting the I signal to leak into the Q branch [83]. This can be seen in single carrier systems as a skewing of the constellation points. This phase mismatch is typically constant over the channel but varies from one channel to another, making it difficult to compensate with fixed correction schemes.

Amplitude mismatch between the branches can be either constant or frequency dependent within the channel depending on the source of the error.

The third source of imbalance is much more serious because it treats the upper and lower sidebands differently and is impossible to detect with the known time domain methods. This imbalance typically comes from the baseband filters when there is a mismatch of the cutoff frequencies between the two branches.

The main parameters for DAC selection were:

- Maximum sampling frequency - for a given channel bandwidth and thus for the chosen baseband sampling frequency, this number determines the maximum allowed oversampling factor. Oversampling and filtering in the digital domain allow relaxing the constraints for analog I/Q anti-aliasing filters and thus minimizing the contribution of the third above-mentioned source of I/Q imbalance.

- Resolution and S/(N+THD) - the OFDM signal exhibits high dynamic range. High resolution and good linearity is required for analog interfaces. 10 or more bits are required for baseband DAC, and good performances in terms of spurious-free dynamic range and signal-to-noise ratio.

- Channel balance - since I and Q requires two separate DACs, it is of primary importance the gain and offset matching of the two channels. Manual trimming is often required to guarantee imbalances of less than 0.1dB.

Taking into considerations these requirements, a possible choice for the modulator DAC is the 14-bit DAC2904 from Burr-Brown. Operating with high update rates of up to 125MSPS, the DAC2904 offers spurious-free dynamic range of 78dB, and enables the generation of very-high output frequencies suitable for Direct IF applications. The DAC2904

has been optimized for communications applications in which separate I and Q data are processed while maintaining tight-gain and offset matching.

For demodulation, the choice has been to implement second-IF direct sampling. Sampling rate conversion down to nominal sampling frequency and I/Q recovery are performed in the digital domain.

In this case, a single-channel analog-to-digital converter is needed. Oversampling is again desirable to relax the constraints of analog anti-aliasing filters. Since the proposed system should successfully overcome fast shadowing and signal power fluctuations, a high resolution converter must be chosen to cope with imperfect AGC control. Again, adjacent-channel power can leak from channel selection filters and since the power ratio between selected and adjacent channels can be significant, additional bits are required to avoid saturations in the demodulator front-end.

For this reason, a 14 bits ADC must be selected. A possible candidate could be Analog Device's ADS5422Y, that offers good performances with moderate power consumption.

5.5 Implementation figures

The modulator has been synthesized and fits in a single Virtex2 device (XC2V2000). The resource utilization of the modulation core is summarized in table 5.2.

Primitive	Used	Total	Percentage
Slice Flip-Flops	4463	21504	21%
4-input LUTs	4785	21504	22%
Occupied slices	4427	10752	41%
BlockRAMs	16	56	28%
MULT18X18S	18	56	32%
GCLKs	2	16	13%
DCMs	1	8	13%

Table 5.2: Resource utilization, modulation core.

The demodulator was implemented using two Virtex2Pro devices (XC2VP30): the first one include the front-end processing, FFT transformation, channel estimation and data demapping; the second one is dedicated to time-deinterleaving and Forward-Error

Correction (FEC). The simplified demodulator block diagram is depicted in figure 5.28. The system partitioning can be observed.

The RTL design is still under development; the first successful tests with deep time interleaving demonstrated that the interleaver allows to overcome the short but deep signal fading that can be encountered in real world situations due to interposition of small obstacles and trees. Some additional work is required to refine the receiver performances.

The resource utilization of the demodulation cores is summarized in table 5.3 and 5.4. These figures refer to Viterbi concatenated error-correction scheme. The first FPGA figures can be reduced by data bit width optimizations but still refers to partially incomplete design.

Primitive	Used	Total	Percentage
Slice Flip-Flops	7321	27392	26%
4-input LUTs	8505	27392	31%
Occupied slices	6845	13696	49%
BlockRAMs	58	136	42%
MULT18X18s	40	136	29%
GCLKs	3	16	18%
DCMs	1	8	13%

Table 5.3: Resource utilization, demodulation core, FPGA 1.

Primitive	Used	Total	Percentage
Slice Flip-Flops	16749	27392	61%
4-input LUTs	20152	27392	73%
Occupied slices	10439	13696	76%
BlockRAMs	46	136	34%
MULT18X18s	35	136	26%
GCLKs	4	16	25%
DCMs	2	8	25%

Table 5.4: Resource utilization, demodulation core, FPGA 2.
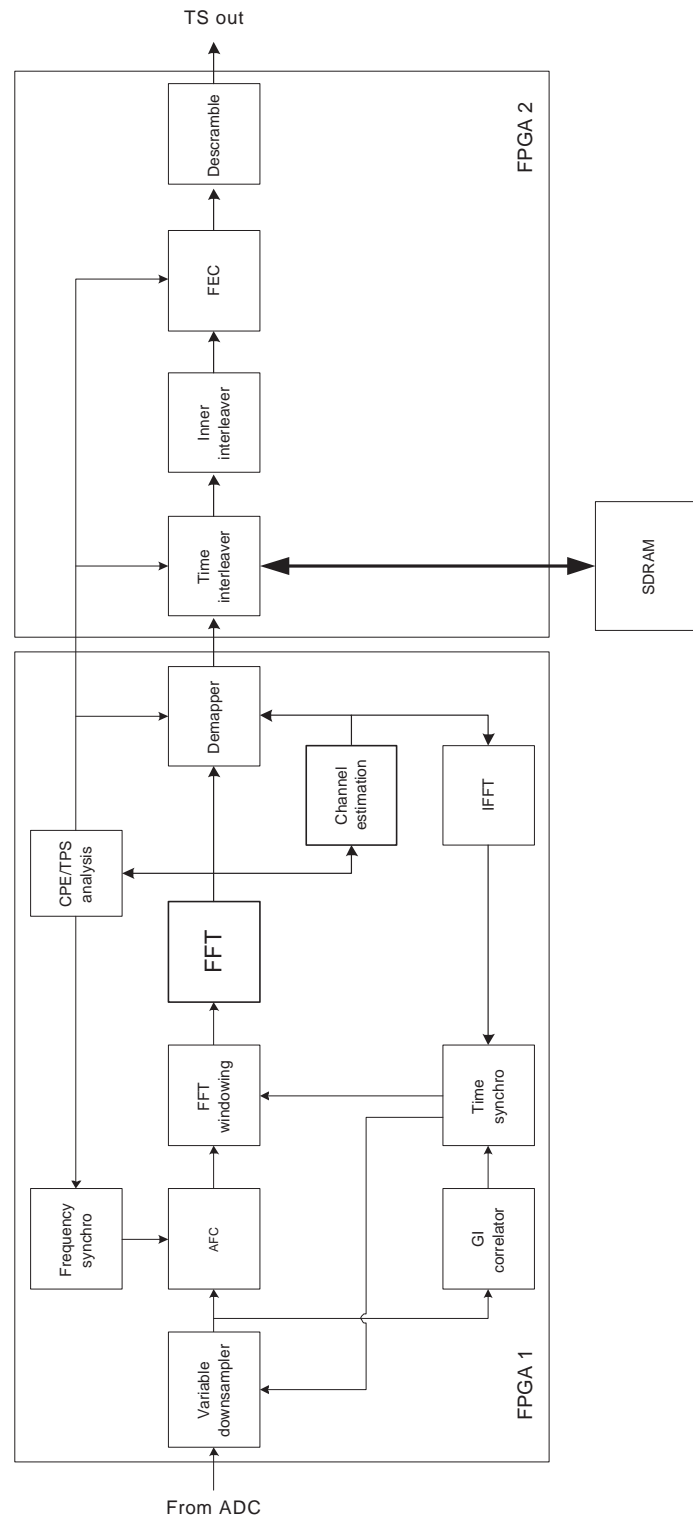
Figure 5.28: Receiver global block diagram.

5.6 Chapter summary

A prototype system has been designed to test the proposed solutions and perform field trials. In this chapter, the main receiver algorithms have been studied and the performances have been analyzed. Moreover, some optimizations have been presented to reduce the hardware complexity. In particular, an AGC algorithm with adaptive convergence speed and digital post-correction have been proposed, where the post-correction function has been efficiently approximated using only bit shifts and adders. Time synchronization employs two different set of coefficients to guarantee fast convergence and residual errors below 1ppm. The frequency acquisition algorithm has been implemented as a closed-loop control where the *arctan()* function has been replaced by a two-step approximation scheme. Channel estimation takes advantage of time filtering to improve the performances in presence of slowly-moving channels with only a small amount of additional logic. The proposed channel analysis algorithm guarantee consistent results without incurring in the drawbacks often encountered in existing receivers. A low-complexity diversity selection scheme that combine good performances and reduced data exchange between the two receivers has been presented.

The introduction of deep time interleaving poses some practical problems especially related to time and frequency synchronization algorithms, that must be addressed to fully exploit the protection to single events of failure that this technique can offer. Some reliability estimators and a special time acquisition strategy has been developed to guarantee robust reception.

Regarding the verification system, a prototype receiver has been developed and the main design choices related to processing cores and analog interfaces have been discussed. Xilinx Virtex2/Virtex2Pro FPGA families have been selected for their processing power, device density and reduced power consumption. As analog interfaces, 14-bits analog-to-digital and digital-to-analog converters have been selected.

Some preliminary result of the FPGA-based implemented system demonstrated that the time interleaver is able to successfully overcome short but deep fading events due to small obstacles interposition between transmitter and receiver without residual data errors.

Chapter 6

Simulation results

6.1   Chapter introduction

In this chapter the main simulation results are presented. Among the investigated aspects, the front-end tasks of time acquisition and guard interval estimation are analyzed for static and mobile channels. Frequency acquisition and tracking performances are analyzed in terms of C/N ratio for AWGN channel. Channel estimation time filtering is analyzed as a function of the value of parameter α for AWGN and mobile channels. The performances of time interleaving and two-antennas diversity are shown in the following subsections. Turbo codes performances are then summarized. Finally, the complete system is simulated in two typical field cases to determine the overall performances.

6.2   Timing estimator and Guard Interval recovery

Several simulation runs have been performed to define the capacity of the timing estimator block to acquire and maintain synchronization.

Two different environments have been implemented in the C/C++ simulator, in order to separately evaluate the performances of the acquisition and of the tracking algorithms.

6.2.1   Timing acquisition performances

To evaluate the acquisition performances, only AWGN and Rayleigh channel models have been used. Mobile channel models can not be employed because the fluctuations of OFDM symbol power generate misleading simulations results.

Since the enhanced-mobility COFDM is a system based on continuous-transmission, the receiver is not asked to acquire synchronization immediately on the first received OFDM symbol. Even if the first correlation peaks are highly corrupted by noise, the receiver can be able to lock on subsequent peaks less destructively affected. Anyway, to quantify the acquisition capabilities, *successful acquisition percentage* has been employed - this number giving the ratio of successful timing acquisition occurred before timeout. The timeout is equivalent to about 100 OFDM symbols.

Figure 6.1 shows the acquisition performances in terms of percentage of successful acquisitions for an AWGN channel. It must be noted that for timing acquisition, the correlator must be set for the minimum guard interval size, thus the correlator sum is done over 64 (2048/32) terms. Theoretically, just the width of the correlator peak should change as a function of the real employed guard interval size. In practice, the control strategy can take advantage of a larger correlation peak to avoid false positives and greatly

enhance the acquisition reliability. Anyway, the parameters employed by the algorithm and control strategy developed have been tweaked for a best compromise between the four possibilities. The best case is for $GI = 1/8$, where the error-free point reaches $-3.5dB$. The performance of the case $GI = 1/4$ is surprisingly worse than the latter one. After investigation, it has been found that sometimes the correlation goes below threshold during the large correlation peak, thus generating multiple detected pulses. Employing the shortest guard interval size of $GI = 1/32$, error-free acquisition is not guaranteed for C/N below $1dB$.
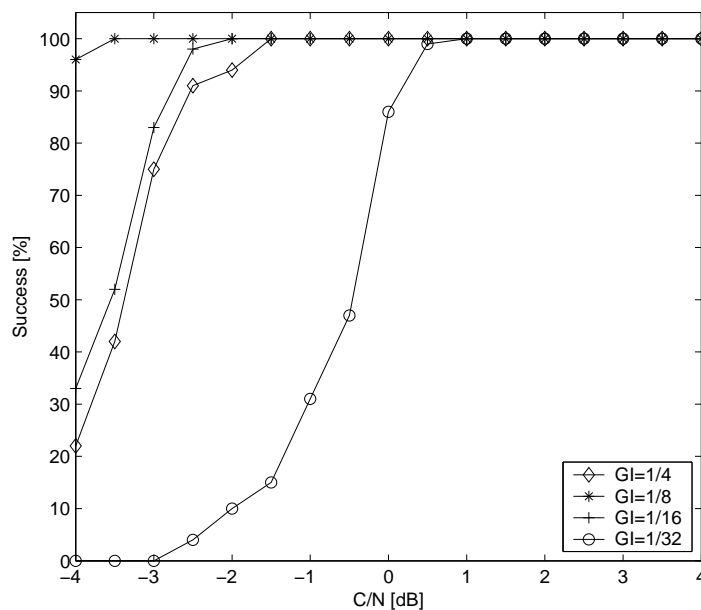
Figure 6.1: Successful timing and guard interval acquisition percentage, AWGN channel.

Figure 6.2 shows the acquisition performances in terms of successful attempts percentage for a Rayleigh channel. Beside a predictable general decrease of the performances, it must be noted that the case $GI = 1/32$ is greatly impaired, because the Rayleigh channel caused a sensible spread of the peak energy, and it can be hardly detected. These simulations justify the choice of avoiding $GI = 1/32$ for the proposed system.

6.2.2 Time tracking performances

The time tracking control loop has been simulated using Matlab/Simulink. The evolution of the estimated error ε', with $\varepsilon = 100ppm$ and employing the first set of parameters, is shown in figure 6.3.

The residual error $\varepsilon_r = \varepsilon - \varepsilon'$ drops below $10ppm$ after 550 OFDM symbols, thus
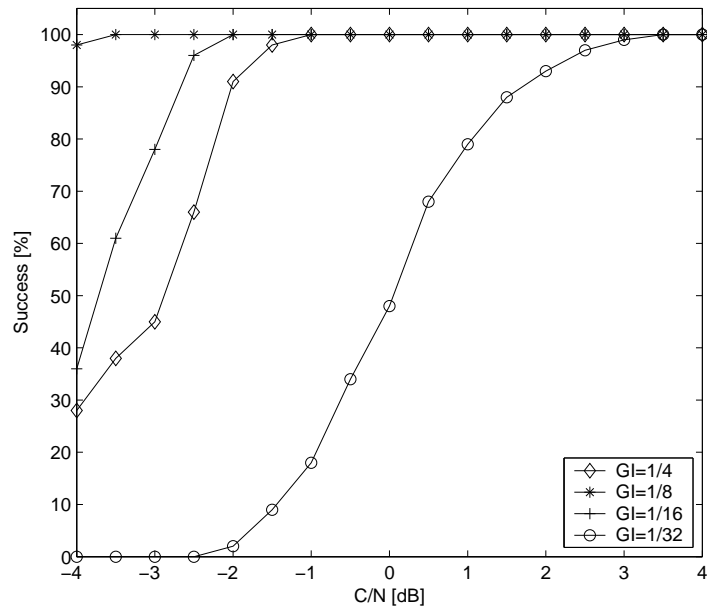
Figure 6.2: Successful timing and guard interval acquisition percentage, Rayleigh channel.
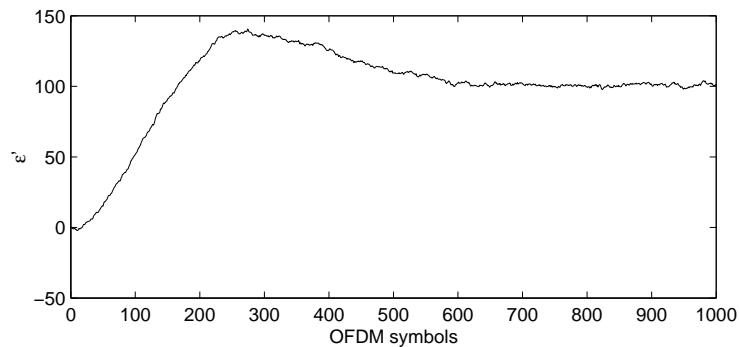
Figure 6.3: Estimated error ε', first set of parameters.

leading to a locking time of about $100ms$ for a $8MHz$ system. The residual error variance is related to the variance of the peak extraction algorithm; local residual errors up to $5ppm$ can be expected with this set of coefficients.

With the second set of coefficients, the proposed control strategy exhibits residual errors ε_r of about $1ppm$.

6.3 Frequency estimation and tracking

6.3.1 Frequency estimation

The performances of initial fractional frequency acquisition algorithm, based on correlation peaks angle, have been simulated employing a Rayleigh channel model with $C/N = 3dB$. The evolution of the standard deviations of the residual frequency error $\Delta f'$ as function of guard interval size is summarized in table 6.1.

Guard interval	stddev ($\Delta f'$)
1/4	7 Hz
1/8	11 Hz
1/16	23 Hz
1/32	52 Hz

Table 6.1: Rayleigh channel, $C/N = 3dB$.

Since the FFT orthogonality is guaranteed for $\Delta f' << \Delta f$ and $\Delta f = 4464Hz$ with the above figures, we can conclude that the accuracy of the estimator is sufficient to guarantee FFT orthogonality for all the guard interval sizes.

6.3.2 Frequency tracking

The Common Phase Error standard deviation is not dependent on the guard interval used and is less sensitive to narrow-band interferer than correlation-based methods. Table 6.2 shows the standard deviation of the CPE estimator for an AWGN and a Rayleigh channel, expressed in Hz, for $\Delta f = 4464Hz$.

C/N [dB]	stddev(CPE) - AWGN	stddev(CPE) - Rayleigh
3.0	386 Hz	398 Hz
6.0	260 Hz	282 Hz

Table 6.2: CPE standard deviation, AWGN and Rayleigh channels .

The performances depends mostly by the noise level and not by the channel frequency response, how can be noted observing that AWGN and Rayleigh figures don't differs significatively. However, the estimator is affected by the channel mobility, since this is a

differential estimator. It must be noted that the above figures refers to the standard deviation of the CPE estimator, not to the standard deviation of the AFC tracking algorithm itself. The performances of the AFC tracking method based on CPE estimator, with updating coefficient $\alpha_{CPE} = 1/16$, are shown in table 6.3.

C/N [dB]	stddev($\Delta f'$) - AWGN	stddev($\Delta f'$) - Rayleigh
3.0	23 Hz	25 Hz
6.0	17 Hz	18 Hz

Table 6.3: $\Delta f'$ standard deviation, AWGN and Rayleigh channels.

From the above figures, it can be evicted that AFC tracking algorithm based on CPE estimator with relatively fast updating policy already provides residual frequency errors below 1% of intercarrier spacing, even for the worst analyzed case.

6.4   Channel estimation time filtering

Figure 6.4 shows the performances in terms of after-Viterbi Bit Error Ratio (BER) of the IIR time filter in AWGN condition, QPSK modulation, code rate $R = 1/2$. For each combination of C/N and time filtering parameter, 5 simulation runs of 1000 OFDM symbols have been performed. The maximum and the minimum values between the 5 results have been discarded and the lasting 3 values have been averaged.

It must be noted that in these conditions, the simulator estimated channel response is completely static; the AFC and time tracking algorithms are disabled and thus the channel response do not exhibit phase shift or phase rotations between consecutive OFDM symbols. Thus, is it obvious that longer time filtering granted for better performances due to the improved filtering of the noise that affects the pilots used for channel estimation. The factors α used in the simulations correspond to easy implementation figures, where multiplications are replaced by shift-add operations. The set of α factors used in figure 6.4 correspond to shifts of 2, 4, 6 and 8 bits, respectively.

The gain in terms of required C/N to obtain the quasi-error free condition ($BER = 2 \cdot 10^{-4}$) is summarized in table 6.4. As can be noted, the performance improves up to the point where the channel estimation can be considered no more affected by noise. This limit is very close to the condition of $\alpha = 0.004$.
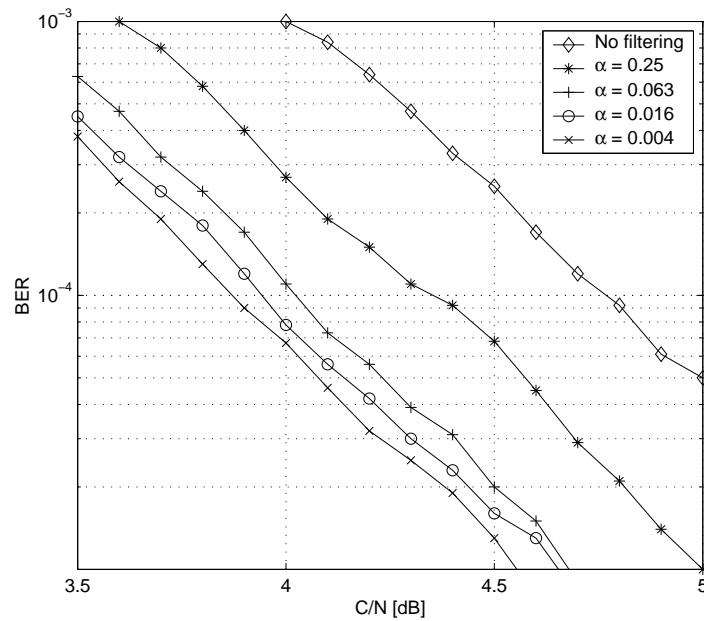
Figure 6.4: After-Viterbi BER as a function of channel estimator time filtering α coeffcient, AWGN, QPSK, R=1/2.

α	required C/N	C/N difference
no filter	4.6dB	-
0.25	4.1dB	-0.5dB
0.063	3.9dB	-0.7dB
0.016	3.8dB	-0.8dB
0.004	3.7dB	-0.9dB

Table 6.4: AWGN channel, QPSK R=1/2.

Unfortunately, when the channel mobility is taken into account, long time filtering is no more suitable. Figure 6.5 shows the performances for COST 207 *Typical Urban* channel profile, with mobile speed of $80km/h$. Even if multiple simulation runs have been done, the results are still affected by some errors due to the irregular nature of the channel model employed; as can be noted, the graphs does not exhibit a smooth evolution. This does not allow us to quantify precisely the gain in term of C/N for the QEF point; anyway, it can be noted that $\alpha = 0.25$ improves the performances by $0.7dB$, and $\alpha = 0.063$ further increase the gain to $1.1dB$. However, employing time filtering in the channel estimation introduces an error floor dependent on the combination of filter bandwidth and channel coherence time. These error floors are clearly visible for $\alpha = 0.063$ and $\alpha = 0.016$ and

are caused by insufficient filtering bandwidth; in the case of $\alpha = 0.016$, the error floor is around $1 \cdot 10^{-4}$ and the overall performances are clearly degraded for all the C/N of interest. The slow time response of the IIR filter (strong low-pass behaviour) impairs the tracking of the channel response evolution.
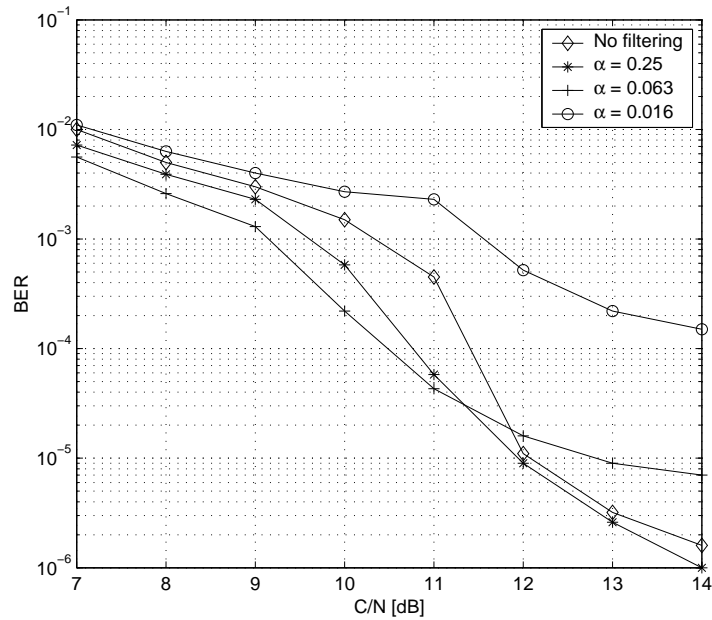
Figure 6.5: After-Viterbi BER, COST207-TU, QPSK, R=1/2.

Field trials showed that the estimated channel response exhibit a certain amount of time variance even for static channels, mainly due to AFC and time tracking algorithms. In these conditions, values of $\alpha = 0.016$ and $\alpha = 0.004$ cannot be used and thus has been discarded.

6.5   Time Interleaving

The performance improvements coming from the insertion of the time interleaver has
been evaluated in several different scenarios. Four different cases are here presented,
that embraces deep shadowing effects caused by small obstacles, mild shadowing coming
from trees interposition and two cases of highly mobile and frequency-selective channels.
The first two figures refer to the sparse shadowing models *SPARSE 2* and *SPARSE 4*.
The third and fourth tests have been performed employing *COST207 - Rural Area* and
COST207 - Typical Urban channel models. For each combination of channel model, time
interleaving depth and C/N value, 5 simulation runs of 1000 OFDM symbols have been
performed. The maximum and the minimum values between the 5 results have been
discarded and the lasting 3 values have been averaged. It must be noted, however, that
the after-Viterbi BER cannot be compared over the quasi-error-free point $(2 \cdot 10^{-4})$, since
the errors are not random distributed. For this reason, in the following BER graphs the
points highlighted with a small circle denote simulations that does not exhibit erroneous
packet at the output of Reed-Solomon decoder, while points highlighted with a cross
generated erroneous transport stream packets at the output of the RS decoder.

6.5.1   Sparse shadow model 2

The received power is depicted in figure 6.6. This sparse shadow model exhibit a short
but strong attenuation peak around symbol number 500. The maximum attenuation is
around $26dB$.

Figure 6.7 shows the performances of the system without time interleaving, with 96
symbols interleaving and with 192 symbols interleaving.

In this condition, the system without time interleaving must guarantee a power margin
of the same amount of the strongest attenuation peak to ensure reception without errors.
Following these considerations, and recalling that the modulation scheme used (QPSK,
R=1/2) requires C/N=5dB for an AWGN channel, we can note that the system without
time interleaver requires $C/N = 30dB$, or equivalently $25dB$ of power margin to guaran-
tee error-free transmission. Just employing the shortest time interleaving (96 symbols)
reduces this margin to $7dB$, while using a longer time interleaver it can be reduced down
to $3dB$. Further increasing the time interleaver depth would give only modest additional
benefits.

Another interesting result can be extrapolated by the above figure; by observing the
BER evolution of the system with time interleaving depth 96 around $C/N = 12dB$, we can
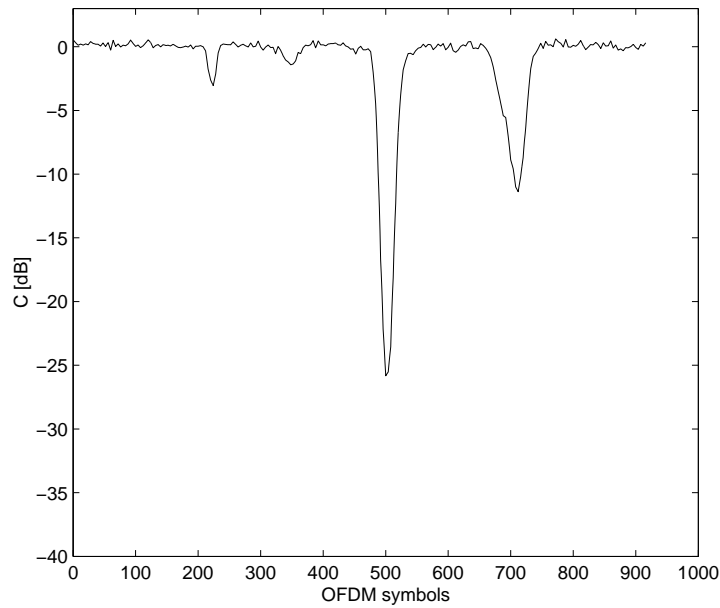
Figure 6.6: Sparse shadow model 2 - evolution over time.
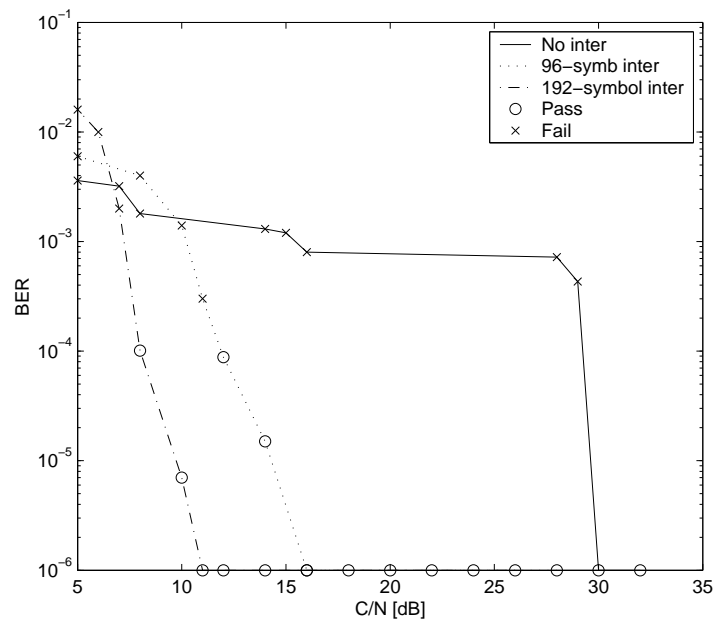
Figure 6.7: After-Viterbi BER, Sparse shadow model 2 with time interleaving.

note that this C/N point correspond to a deep fade of about 30 OFDM symbols; during this period, the received power is below the noise floor and the data are completely lost. We can conclude that the time interleaver is capable to recover fades of up to 1/3 the time interleaver depth in the most robust Viterbi-based modulation scheme QPSK, R=1/2.

6.5.2 Sparse shadow model 4

The received power is depicted in figure 6.8. This sparse shadow model exhibit multiple short attenuation peaks, with the strongest value around $13dB$.
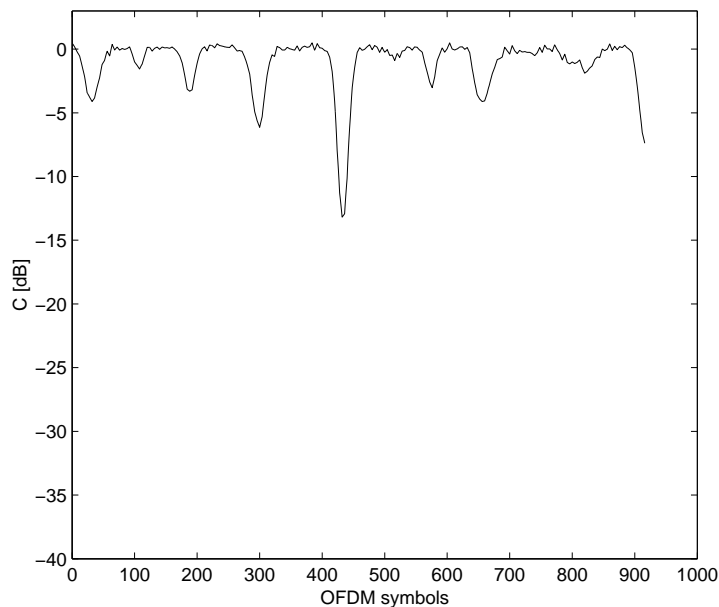
Figure 6.8: Sparse shadow model 4 - evolution over time with time interleaving.

In this case, the power margin reduction is clearly lower; anyway, the presence of multiple peaks is interesting to stress the spreading capability of the time interleaver. Figure 6.9 shows the performances of the system without time interleaving, with 96 symbols interleaving and with 192 symbols interleaving.

We can note that the system without time interleaver requires a power margin of $12dB$ to successfully overcome the strong attenuation peak. Just employing the shortest time interleaving (96 symbols) enhances this figure to $3dB$, while using a longer time interleaver the power margin can be reduced down to $2dB$.

6.5.3 COST207 - Rural Area

The COST207 Rural Area model represents a fast-moving, low-selective mobile channel. For the channel response evolution over time, refer to the already presented figure 3.13. The performances with no interleaving and with interleaver depths of 96, 192 and 384 symbols are shown in figure 6.10

The performance enhancement is about 10dB for the 96-symbols and 192-symbols interleavers, and employing the 384-symbols interleaver depth, the required C/N for error-
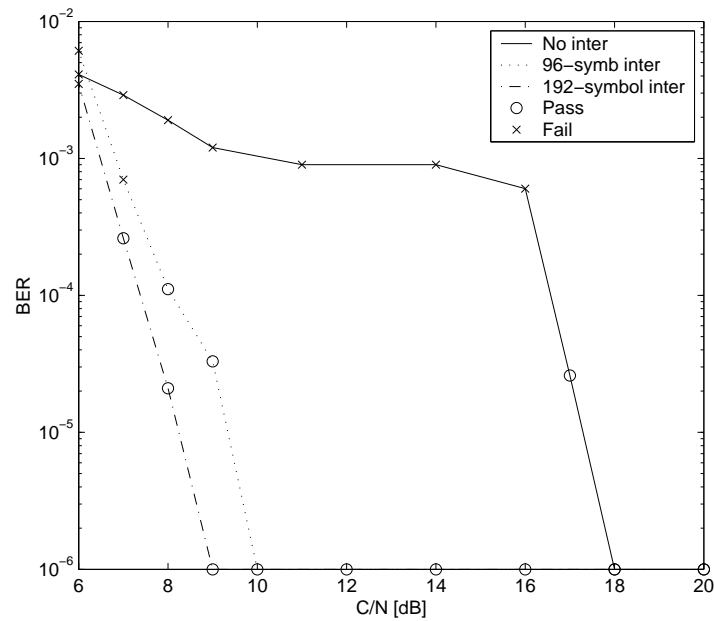
Figure 6.9: After-Viterbi BER, Sparse shadow model 4 with time interleaving.
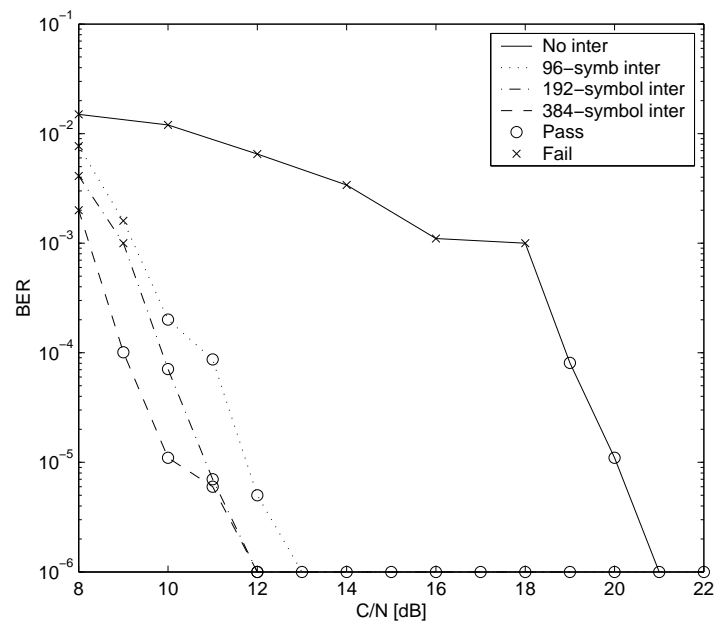
Figure 6.10: After-Viterbi BER, COST207 Rural Area with time interleaving.

free reception can be lowered to $9dB$, corresponding to a $11dB$ improvement over the system without time interleaving. Further increasing the interleaver depth does not offer sensible performance improvements. The high performance gain due to time interleaver

insertion comes from the characteristics of the channel model, that exhibit important fades over the entire frequency span, mainly around symbol number 300, that are effectively recovered by the time interleaver.

6.5.4 COST207 - Typical Urban

The COST207 Typical Urban model represents an example of a fast-moving, highly selective mobile channel. For the channel response evolution over time, refer to figure 3.14. The performances with no interleaving and with interleaver depths of 96, 192 and 384 symbols are shown in figure 6.11
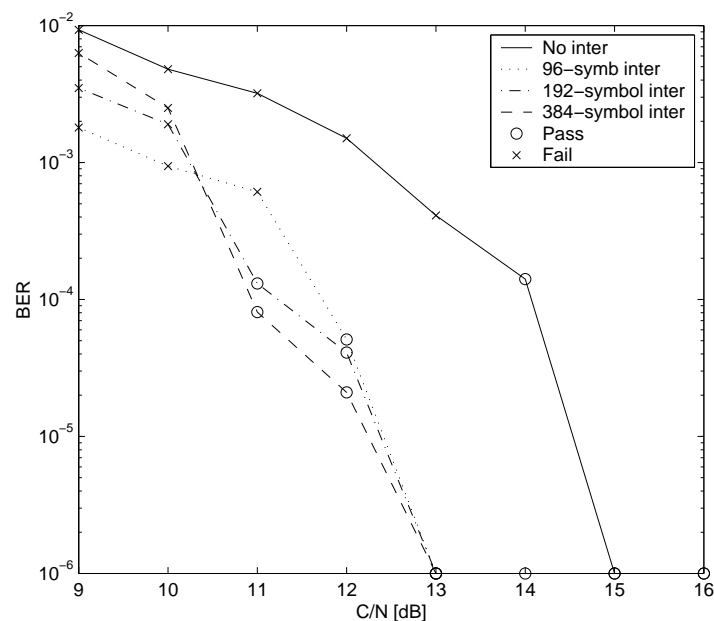
Figure 6.11: After-Viterbi BER, COST207 Typical Urban with time interleaving.

The performance enhancement is about 2dB for the 96-symbols and 3dB for the 192-symbols time interleaver. Further increasing the interleaver depth does not offer great performance improvements; in fact, increasing the interleaver size to 384 symbols does not improve the above figures significatively. This is due to the structure of the time interleaver, that optimally spreads sparsely-located deep fading.

6.6   Two-antenna diversity

The performances of a two-antenna diversity receiver based on Maximum-Confidence Selection (MCS) and Maximal-Ratio Receive Combining (MRRC) have been evaluated using the mobile channel models. In particular, *COST207 - Typical Urban* and *COST207 - Hilly Terrain* models have been used. For each combination of channel model, diversity scheme and C/N value, 5 simulation runs of 1000 OFDM symbols have been performed. The maximum and the minimum values between the 5 results have been discarded and the lasting 3 values have been averaged.

6.6.1   COST 207 - Typical Urban

Figure 6.12 shows the evolution of the after-Viterbi BER with no diversity, MCS and MRRC two-antenna diversity methods, employing *COST207 - Typical Urban* channel model.
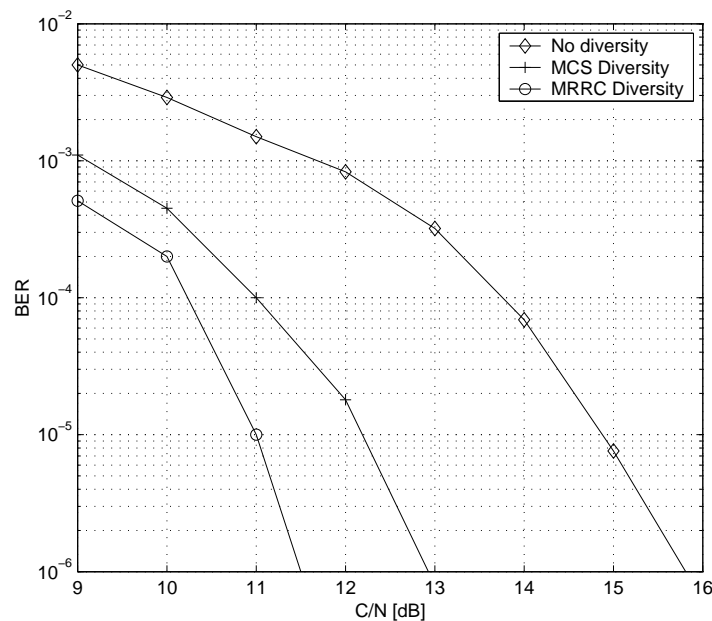
Figure 6.12: After-Viterbi BER, COST207 Typical Urban with diversity.

From the above figure, the performance improvement in term of C/N difference is 2.8dB employing the MCS method and 3.3dB employing MRRC diversity.

6.6.2 COST 207 - Hilly Terrain

For *COST207 - Hilly Terrain* model, figure 6.13 shows the evolution of the after-Viterbi BER with no diversity, MCS and MRRC two-antenna diversity methods.
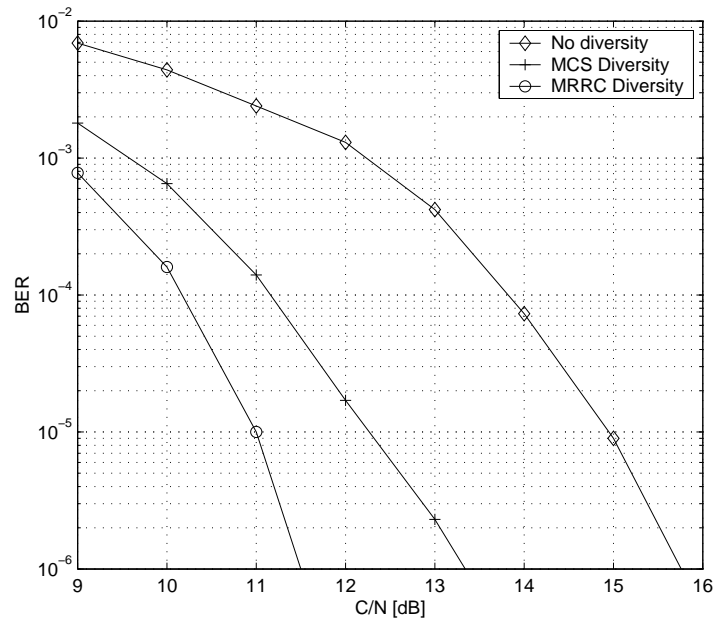
Figure 6.13: After-Viterbi BER, COST207 Hilly Terrain with diversity.

From the above figure, the performance improvement in term of C/N difference is 2.6dB employing the MCS method and 3.5dB employing MRRC diversity.

6.7 Turbo Codes

The performances of PCCC turbo codes have been extensively studied by Lattuada [79]. In this subsection only a brief summary of the achieved results is presented.

In figure 6.14 and 6.15 the performance in terms of Eb/No of PCCC inner coder are shown for Ricean and Rayleigh channel, respectively.
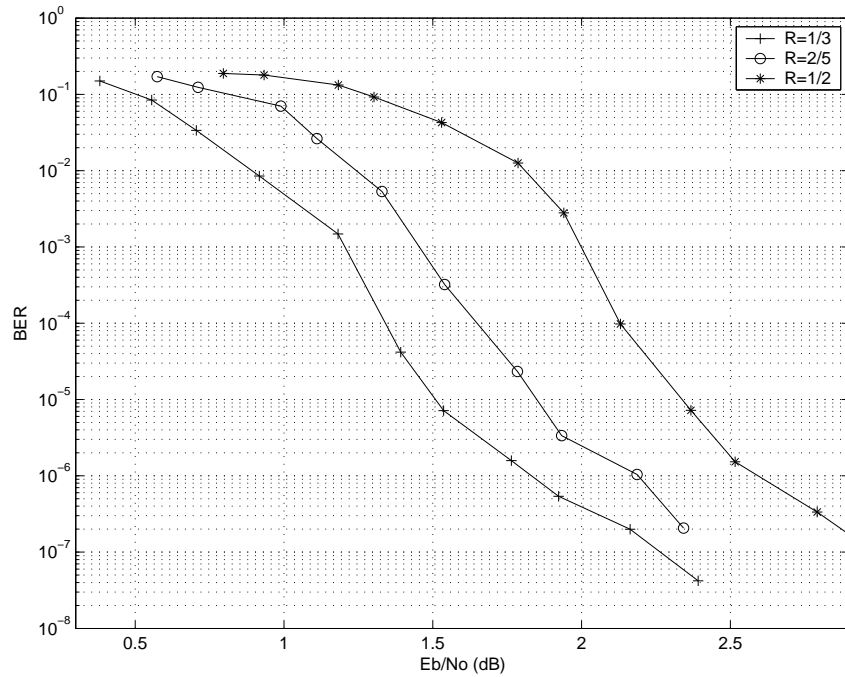
Figure 6.14: After-PCCC BER, Ricean channel.

The gains in these conditions are respectively 1.85dB and 2dB compared to DVB-T convolutional coding scheme.

In figure 6.16 the performance in terms of Eb/No of the complete concatenated scheme PCCC+RS, inner code rate $R = 1/3$, are shown for COST207 channel models.
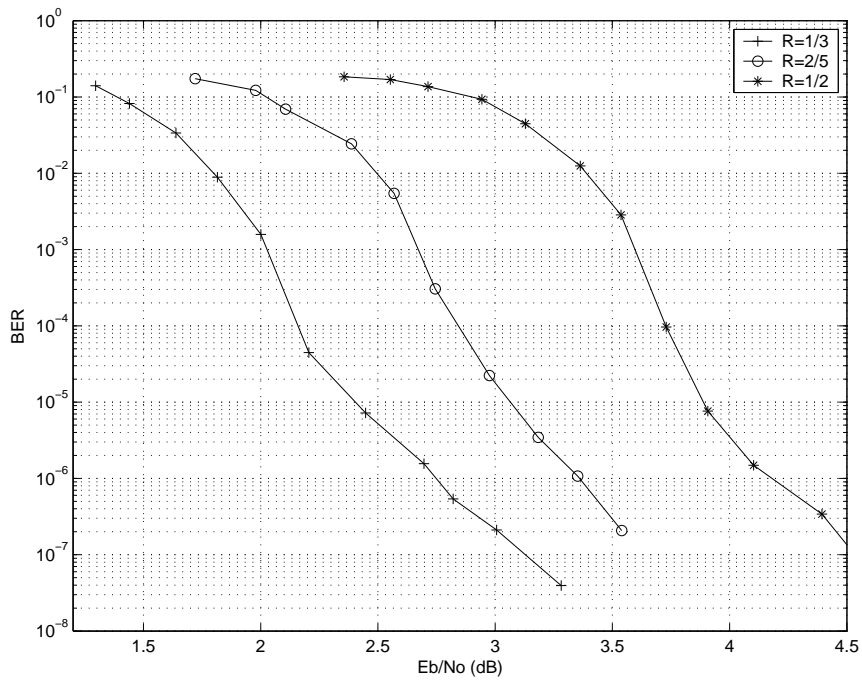
Figure 6.15: After-PCCC BER, Rayleigh channel.
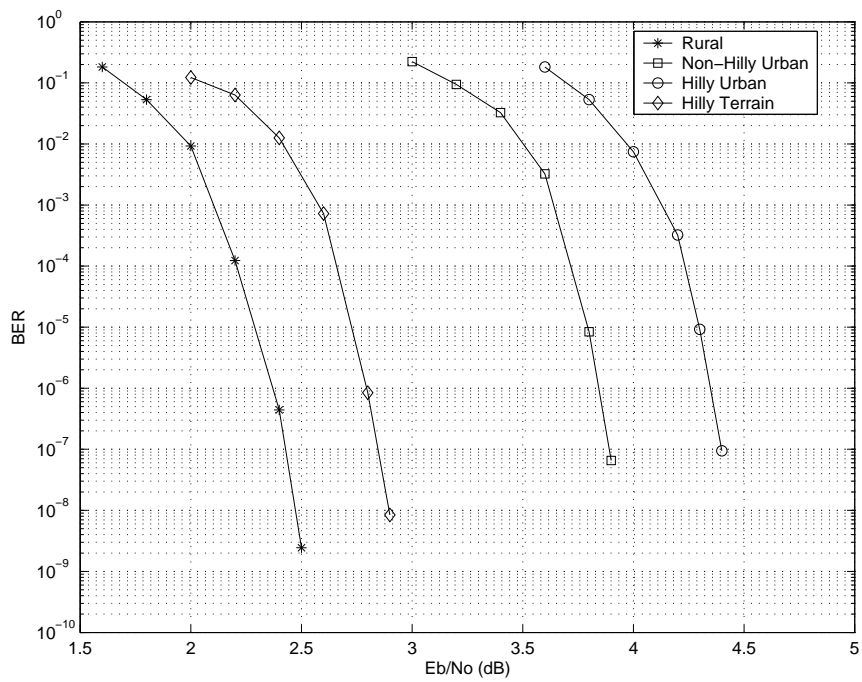
Figure 6.16: System performances, COST207 channel models, PCCC $R = 1/3 +$ RS.

6.8   Application examples

After having analyzed the performances of the different receiver tasks, two simulations of the global system have been performed. All the receiver blocks are enabled; in particular, the time and frequency tracking algorithms are activated, channel estimation is performed based on the adaptive scheme described in the previous chapter. The interpolation and filtering strategy selected by the receiver FSM is indicated.

6.8.1   Case 1 - Multimedia relay

Application characteristics

The first simulation represents the case a multimedia relay link. The main requirement of such application is the robustness, especially to sparse shadow fading events, while the latency is not an issue. The bandwidth is equal to $8MHz$, the mobile speed is $30km/h$. The channel model is the *SPARSE4* shadow fading.

System parameter choice

As error correction scheme, the $R = 1/2$ PCCC turbo code concatenated scheme has been chosen and the time interleaver depth is set to 6144 symbols, corresponding to a latency of about 1.4 seconds. QPSK constellation is selected for maximum robustness, and the guard interval is set to 1/16. The useful bitrate is then equal to $5.5Mbps$.

Simulation results

The receiver exploits full time and frequency interpolation and time filtering in the channel estimation process with $\alpha = 0.063$ due to the limited mobility. Simulations are performed on a 10 second time frame and 5 simulation runs are averaged for each C/N value. As can be seen from figure 6.17, the error-free point is improved from the original value of $17.0dB$ down to about $5.5dB$, thus approaching the performances of the original system in the AWGN scenario. The performance gain can be mainly ascribed to the combination of deep time interleaving and powerful turbo codes, but it must be noted that time and frequency synchronization tasks are able to follow the channel evolution without accounting for additional signal degradation.
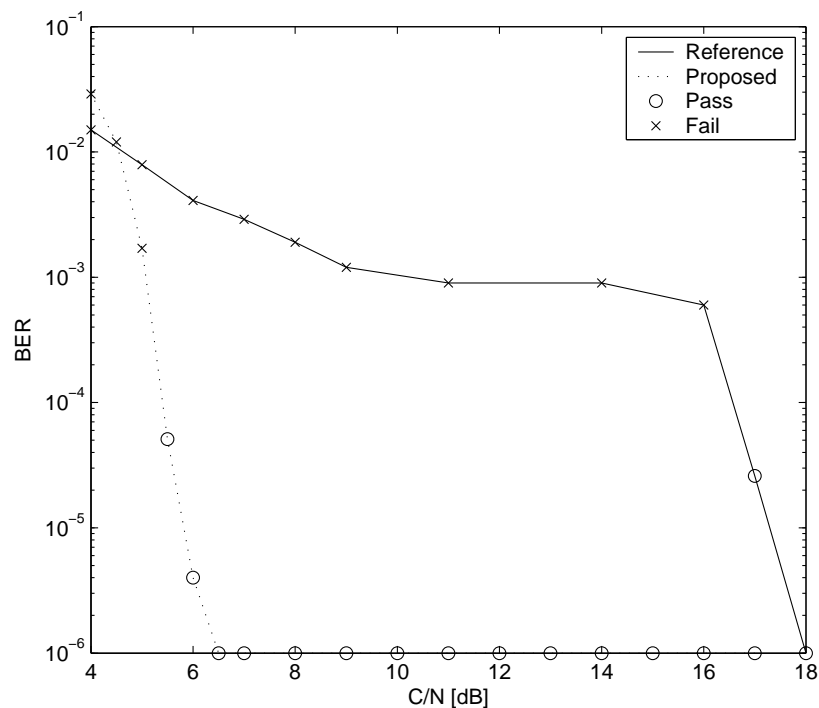
Figure 6.17: Global system performances, case 1.

6.8.2 Case 2 - High mobility with diversity

Application characteristics

The second simulation represents the case of a highly mobile and difficult multipath scenario, where two-antenna receiver diversity can be exploited over a $20MHz$ bandwidth. The main requirements of this application example are robustness and reduced latency. The mobile speed is set to $120km/h$. The channel model is the *COST207 - Typical Urban* shadow fading.

System parameter choice

The error correction scheme is based on more robust $R = 1/3$ PCCC turbo code, the time interleaver depth is set to 192 symbols, corresponding to a latency of about 17 milliseconds. The insertion of a minimal time interleaving is beneficial to the global performances without incurring in excessive latency. The QPSK constellation is selected for maximum robustness, and the guard interval is set to 1/8. The MCS combining strategy is selected to exploit diversity with reduced hardware complexity. The useful bitrate is equal to $9.0Mbps$.

Simulation results

The receiver exploits full time and frequency interpolation, but time filtering is disabled. Simulations are performed on a 10 second time frame and 5 simulation runs are averaged for each C/N value. As can be seen from figure 6.18, the error-free point is improved from the $14.0dB$ value of the one-antenna reference system down to about $7.5dB$. The performance gain can be mainly ascribed to the combination of time interleaving, powerful turbo code and diversity combining.
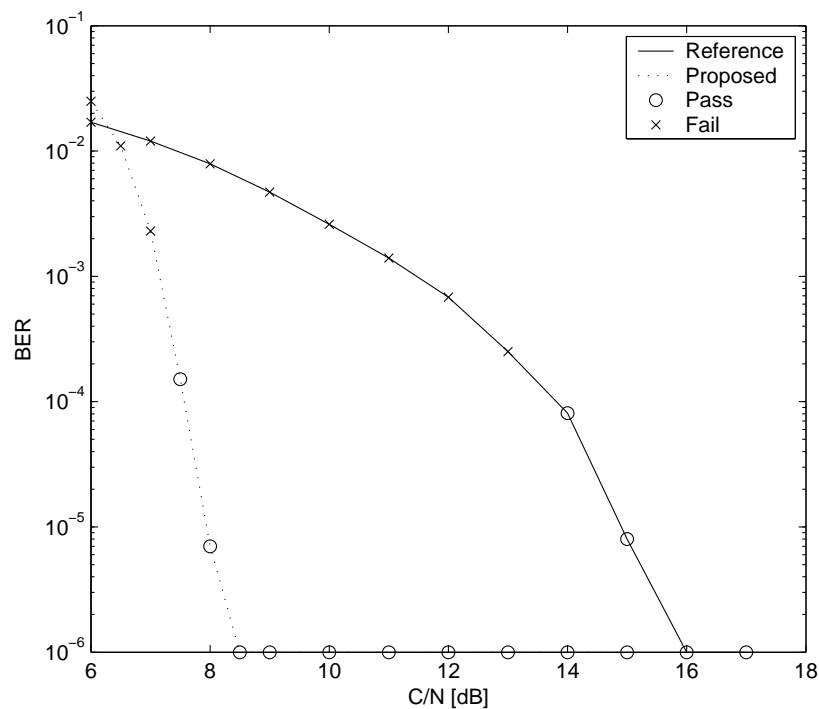
Figure 6.18: Global system performances, case 2.

Again, it is interesting to note how the performance of the complete system is the result of several different protection methods; diversity combining proved to be very effective for mobile multipath scenarios, time interleaving averages the capacity of the channel over the time interleaver depth thus avoiding the punctual failures of the original system and turbo codes account for additional error correction capabilities. Finally, time and frequency synchronization algorithms proved to be able to acquire and maintain lock even for mobile multipath and shadow fading channels.

6.9 Chapter summary

In this chapter the main simulation results have been presented.

The performances of time acquisition and tracking algorithm have been studied to evaluate in particular the capacity to overcome long signal fading while maintaining OFDM symbol synchronization. The proposed algorithm, employing two different set of coefficients, successfully demonstrated fast convergence and residual error around $1ppm$. The correlation detection is able to maintain lock and perform time tracking with C/N down to $-2dB$ employing a 1/16 guard interval.

The AFC performances have been studied to find the minimum C/N that guarantee correct initial frequency offset estimation. The tests demonstrated that the acquisition algorithm is robust enough to estimate the fractional and integer part of the frequency offset for $C/N = 3dB$.

An adaptive channel estimation algorithm has been proposed that guarantee good performances for all the combinations of mobility and echo spread. In particular, time filtering can be employed for low-mobility channels and performance improvements of $0.7dB$ can be expected employing the more robust modulation scheme.

The insertion of deep time interleaving gives clear advantages especially for channels impaired by sparse shadow fading. Two simulation runs employing the proposed sparse shadow fading model have been performed and the results demonstrate that the additional power margin that must be used to overcome sparse deep fading events can be dramatically reduced. This means that single failure points can be avoided by employing adequate time interleaving with little or no additional power margin. Moreover, time interleaving offers significant gain even for COST207 channel models, where the C/N improvement is equal to $11dB$ for *Rural Area* and $3dB$ for *Typical Urban* channel models.

The performances of the two receiver diversity techniques exploiting a two-antenna setup have been evaluated with two COST207 channel models, the *Typical Urban* and the *Hilly Terrain* ones. The MCS method already guarantees gains of $2.7dB$, while MRRC technique offers $3.4dB$ improvement if compared to a single-antenna receiver.

A further possible enhancement comes from the modifications of the forward error correction scheme with the use of PCCC turbo codes as inner coder in a concatenated error correction scheme. The performance improvement is significant, and exploiting the additional code rate 1/3 the gain over the DVB-T convolutional scheme is $2dB$.

Finally, two simulations of the complete proposed system are presented. They represent two typical applications: multimedia relay and high mobility with two-antenna diversity. The simulations demonstrated how the proposed features can improve significantly

the overall performances, lowering the minimum required C/N value for both analyzed cases down to $5.5dB$ and $7.5dB$, respectively, thus underlining also the robustness of the time and frequency synchronization algorithms.

Chapter 7

TDM OFDM system

7.1   Chapter introduction

In this chapter the requirements of an OFDM system tailored to short- and medium-range multimedia wireless applications are analyzed. The limited range makes Time-Division-Multiplexing a viable option to share the RF channel resource between multiple terminals without incurring in excessive latency. The main parameters of such a TDM OFDM system have been studied and the 802.16a standard represents a good starting point for the definition of a specialized system. The main parameters of the physical layer have been analyzed and some application examples have been studied. Moreover, for a reduced-mobility scenario, a mechanism of adaptive pre-distortion is presented that improves the performances for multipath environment and does not require modifies of existing receivers.

7.2   Application requirements

There are several applications for which short- to medium-distance multimedia links are required. In this case, OFDM parameters as inter-carrier frequency and number of active carriers must be defined considering the application characteristics; in particular, reduced transmission ranges directly translates into reduced echo spread, and shorter guard intervals can be used. At the same time, shorter OFDM symbol durations can be employed. Channel bandwidths up to 24MHz have to be addressed.

For these applications, very different propagation scenarios can be encountered.

Indoor applications experience strong multipath, due to the reception of multiple high-energy echoes. Anyway, in this case reduced mobility and line-of-sight environment can be expected. An appropriate channel model is the Ricean one, with reduced delay tap and low K factor. Examples of this kind of applications include studio television production employing wireless camera, indoor sports events, video surveillance, etc.

Outdoor applications require strong robustness for highly-mobile environments and larger echo spread tolerance. In this case, Rayleigh and COST207 are appropriate channel models. Moreover, to simulate outdoor events, shadow fading can be added. Applications examples are outdoor television production: bicycle races as Tour de France, Marathons, etc.

For the above-mentioned applications, there is a strong interest to share the RF channel between multiple terminals and eventually to have a reduced-bitrate return channel broadcasted to all the terminals. For television production of indoor and outdoor events, the return channel can convey the "live" video feedback to each wireless camera along

with configuration data and even auxiliary audio channels for director-cameraman dialog. The uplink total data rate can be dynamically shared between the cameras as a function of the desired video quality. For video surveillance, again the channel can be efficiently shared between multiple wireless video cameras and the return channel can be employed to control, for example, camera orientation and zoom. The reduced distance range and the consequent short OFDM symbol period makes Time-Division-Multiplexing (TDM) feasible. In fact, the inevitable latency due to the buffering required to pack the continuous multimedia stream into allocated transmission time slot can be limited to some tens of millisecond.

7.3 TDM OFDM system parameters

By the combination of maximum tolerable echo spread and sampling frequency, the main OFDM parameters can be determined. The radio bandwidth dictates directly the choice of the sampling frequency of an OFDM system. For these applications, f_s can be expected to vary between 5 and 30MHz. The maximum tolerable echo spread, increased by a security factor, gives the duration of the maximum guard interval. Protection to echo spread up to $1km$ is required, so T_g up to $3\mu s$ must be supported. For efficiency reasons, a maximum guard interval of $T_g = 1/4\ T_s$ is considered. This gives a minimum useful symbol period of 12 μs. Thus, the symbol length in number of samples is

$$N = T_s f_s$$

and with the above numbers, $N \leq 360$ samples. Hence, a system employing $N = 512$ carriers with guard interval up to 1/4 would fulfill the requirements.

To share the same RF channel between uplink and downlink, Time-Division Duplexing (TDD) can be used. To implement this mechanism, "turnaround" times TTG and RTG should be inserted between uplink (UL) and downlink (DL) transmissions to account for power amplifiers and antenna switching times. The period between the starting times of two downlink transmissions is called *frame*. To share the channel between multiple terminals, Time-Division Multiplexing (TDM) can be employed. A guard time T_2 between consecutive uplink subframes should be inserted to account for different propagation times and avoid collisions at the receiver of the base station. This interval is usually shorter than TTG and RTG. Figure 7.1 shows the frame structure of the TDM OFDM system.

A TDM OFDM system incurs in some inefficiencies due to the need to re-synchronize the receiver at the beginning of each TDM burst; two or more reference symbols are transmitted at the beginning of each TDM burst for frequency and timing acquisition. These
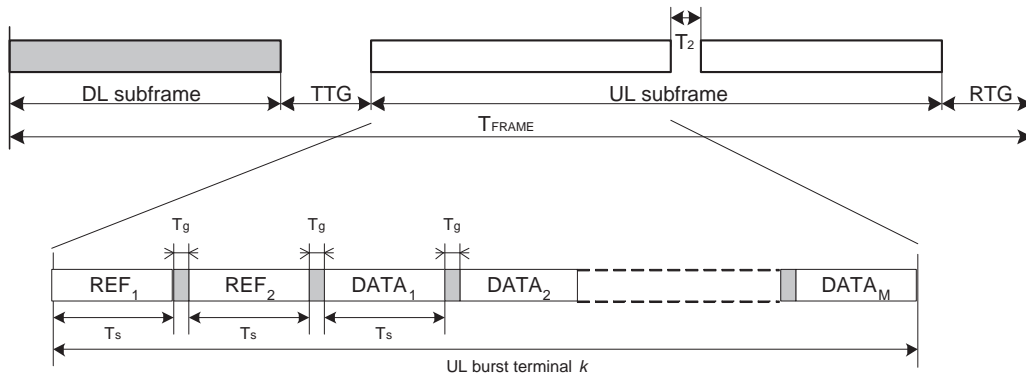
Figure 7.1: Frame structure.

two symbols don't carry a data payload, thus they constitutes a loss in the bandwidth efficiency of the overall system. To partially overcome this problem, the number M of subsequent OFDM symbols inside each transmission subframe should be high enough to bring the efficiency term

$$\epsilon = \frac{M}{M + 2}$$

as close to 1 as possible. Since $M \to \infty$ gives $\epsilon \to 1$, then the subframes should be as long as possible.

On the other side, the total system data latency is lower-bounded by the frame length; it depends on the number of terminals sharing the RF channel and on individual subframes lengths.

7.4   The 802.16a Wireless-MAN OFDM physical layer

Among the four different physical layers presented in the 802.16a amendment, the Wireless-MAN OFDM one is the most interesting for our applications. The parameters of this modulation scheme are recalled in table 7.4.

As can be noted, the total number of subcarriers $N = 256$ imposes some constraints to the maximum tolerable echo spread. For $BW = 24MHz$, the sampling frequency is $28MHz$ and the maximum guard interval length is equal to $2.8\mu s$ that is slightly lower than the required value.

The Point-to-Multipoint (PMP) frame structure will be employed, since mesh network capability is not required by the addressed applications. The frame length is encoded in the synchronization field and can be equal to 131, 258 and 508 OFDM symbols for PMP

Parameter	Required value
Total number of subcarriers (N)	256
Active subcarriers	200
Baseband excess bandwidth (f_s/BW)	8/7 or 7/6
Guard interval (T_g/T_s)	1/4, 1/8, 1/16, 1/32
Data subcarriers	192
Lower frequency guard carriers	28: from -128 to -101
Higher frequency guard carriers	27: from 101 to 127
Fixed locations pilot indexes	-84,-60,-36,-12,12,36,60,84

Table 7.1: Main parameters of WirelessMAN - OFDM PHY.

networks. As a general rule, the longer frame duration (508) will be employed as long as the corresponding latency can be accepted.

The sub-channelization capability of the uplink is not required. The system will always modulate all 192 data subcarriers. The shorter guard interval (1/32) should be avoided to improve the robustness in noisy environment. The ratio f_s/BW can be imposed equal to 8/7, thus limiting out-of-band emissions.

Some *a-priori* choices can be made, but other system parameters need to be determined. For each applications, the starting hypothesis are:

- *Channel bandwidth (BW)* – this figure depends on the available RF bandwidth allocated for the application. For outdoor TV production events, the radio channels are normally pre-allocated and the bandwidth varies between 8 and $24MHz$; indoor productions can employ lower RF power and exploit license-exempt frequencies with channel bandwidth up to $24MHz$; video surveillance can exploit channels with reduced bandwidth down to $4MHz$.

- *Base-terminal distance (r)* – the base station to terminal maximal distance can be as high as $1km$ for outdoor applications, but most of the applications will experience distances lower than $100m$. This figure is directly related with expected echo spread and dictates the required multipath protection.

- *Maximum system latency (T_l)* – the system latency is determined by the maximum time interval between two consecutive transmission of each terminal. During this time, multimedia data has to be buffered and this constitutes an additional latency in the encoding-decoding chain that must be accounted for.

The OFDM PHY system parameters are calculated as follows.

Sampling frequency f_s: the system sampling frequency f_s derives directly from the channel bandwidth BW:

$$f_s = \frac{8}{7}BW$$

Guard interval $GI = T_g/T_s$: given the distance r and the sampling frequency f_s, the guard interval can be determined as the minimum value between the allowed guard interval (1/4, 1/8 and 1/16) that satisfies:

$$T_g/T_s > \frac{f_s r}{Nc}$$

Frame duration T_F: the frame duration should be selected as the higher value m between the PMP permitted frame durations of 131, 258 and 508 OFDM symbols that satisfies:

$$m < \frac{T_l}{T_s + T_g}$$

but the standard can be advantageously extended to support longer frame durations.

These are the parameters that must be identified from the beginning; other parameters as the code rate, the forward-error correction scheme and the modulation order can be adapted during system operation to achieve the maximum total bitrate while the requested robustness is guaranteed. Three application examples follow this brief discussion.

7.5 Application examples

7.5.1 Outdoor television production

For outdoor television production as for example *Tour de France* and the marathon during Olympic Games 2004, motorcycle cameras follow the athletes and the signals are relayed to the reception site through one or more helicopters. These application requirements are summarized in table 7.2.

Bandwidth	BW	12 MHz
Distance	r	< 1 km
Maximum latency	T_l	< 20 ms

Table 7.2: Application requirements.

From these figures, the system parameters of table 7.3 have been determined.

Sampling frequency	f_s	13.71 MHz
Guard Interval	GI	1/4
Frame duration	T_F	11.86 ms (508 T_s)

Table 7.3: Main application parameters.

7.5.2   Indoor television production

Indoor television production are typically studio productions employing a mix of wired and wireless cameras, but even sport events inside stadium can be classified as indoor productions. Often the largest bandwidth can be exploited for these events, but latency requirements are the main concern. These application requirements are summarized in table 7.4.

Bandwidth	BW	20 MHz
Distance	r	< 200 m
Maximum latency	T_l	< 10 ms

Table 7.4: Application requirements.

From these figures, the system parameters of table 7.5 have been determined.

Sampling frequency	f_s	22.86 MHz
Guard Interval	GI	1/8
Frame duration	T_F	6.4 ms (508 T_s)

Table 7.5: Main application parameters.

7.5.3   Video surveillance

Video surveillance applications can fully exploit the capacity to share the radio channel between multiple terminals. In this case, channel bandwidth as low as 4 MHz can be expected. Latency is not the main concern. These application requirements are summarized in table 7.6.

From these figures, the system parameters of table 7.7 have been determined.

Bandwidth	BW	4 MHz
Distance	r	< 100 m
Maximum latency	T_l	< 50 ms

Table 7.6: Application requirements.

Sampling frequency	f_s	4.57 MHz
Guard Interval	GI	1/16
Frame duration	T_F	30.23 ms (508 T_s)

Table 7.7: Main application parameters.

7.6   Adaptive pre-equalization

Employing Time-Division Duplexing (TDD) to share the RF channel between uplink and downlink has some advantages. Among those, the reciprocity of the radio channel can be exploited for slowly-varying channel responses. This implies that both base station and terminals can know the channel frequency response that their emissions will experience. This can be particularly interesting to enhance the performances of one of the two links. Since the more power-constrained one is the uplink, the terminal could exploit its channel response knowledge to adapt its emission.

Most of the adaptive modulation schemes presented in the literature have the disadvantage of requiring a fair amount of processing both in the transmitter and in the receiver. We aimed to find a method to enhance the performances with little or no processing at the receiver.

In this scope, linear frequency pre-equalization represents an optimal choice. This technique, introduced by Keller and Hanzo [81] was shown to be very sensitive to time variations and power clipping at the transmitter. A fixed bit-rate channel inversion-based OFDM system has been presented by Al-Susa and Ormondroyd [82], who analyzed the behaviour of three channel pre-equalization: *total channel inversion, subcarrier blocking* and *controlled channel inversion* methods have been evaluated.

These methods relies on the possibility of having a good estimation of the channel response in the frequency domain. It must be noted, however, that the estimation will be affected by different extent by gaussian noise and the weakest subcarriers can not be reliably estimated.

The OFDM symbols can be multiplied in the frequency domain by a function $G(k)$ of

the previously estimated channel response. The expected improved performances come from the boosting of the weak subcarriers, balanced with the attenuation of the strongest one.

Ideally, the function $G(k)$ could be chosen equal to

$$G(k) = \frac{1}{H(k)}$$

to obtain a completely flat frequency response at the receiver. This correspond to the *total channel inversion* method, but the nulls of the estimated channel response $H(k)$ require infinite boost of the corresponding subcarrier. Moreover, if we denote as P the total transmitted power without pre-distortion, the resulting total transmitted power P' with pre-distortion activated will be

$$P' = P\frac{\sum_k G^2(k)}{K}$$

where K is the number of modulated subcarriers.

We propose employing the function

$$G'(k) = \begin{cases} l & \sqrt{\frac{1}{H(k)}} > l \\ \sqrt{\frac{1}{H(k)}} & \sqrt{\frac{1}{H(k)}} \leq l \end{cases} \tag{7.1}$$

with limiting term $l = 1.3$. The optimum parameter l has been determined by simulations with Ricean and Rayleigh channel models. This technique could be called *controlled channel modulus partial inversion* and has the advantage of not requiring the knowledge of the channel estimate phase. Channel estimation and correction is still performed at the receiver. This method improves the already known *controlled channel inversion* especially for strong multipath scenario. The limiting term choice is justified by the simulations presented in the following chapters. The function $G'(k)$ has to be normalized to obtain $G(k)$:

$$G(k) = G'(k)\sqrt{\frac{K}{\sum_k G'^2(k)}} \tag{7.2}$$

Figure 7.2 shows the function G(k) calculated for the Ricean channel model, with limit $l = 2.0$. No clipping is applied in this case.

Simulations will show that the proposed pre-distortion method enhances the performances for strong multipath channel models, without requiring additional processing at the receiver. This is particularly interesting because this method can enhance the performances of TDM OFDM systems without modifying existing receivers.
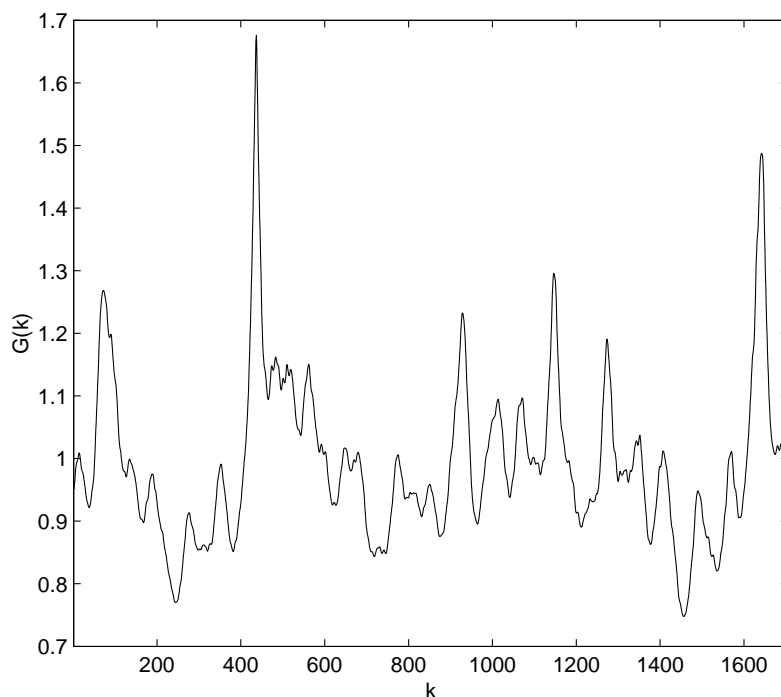
Figure 7.2: Pre-distortion function, Ricean channel, $l = 2.0$.

7.6.1   Rayleigh channel model

The adaptive pre-equalization method has been simulated using the Rayleigh channel model of the DVB-T standard. For each combination of C/N and limit factor l, 5 simulation runs of 1000 OFDM symbols have been performed. The maximum and the minimum values between the 5 results have been discarded and the lasting 3 values have been averaged. The BER evolution around the QEF point is shown in figure 7.3. Table 7.8 summarizes the C/N improvements as a function of the limit l employed.

test	required C/N	C/N difference
no pre-dist	8.2dB	-
limit = 2.0	7.8dB	-0.4dB
limit = 1.7	7.6dB	-0.6dB
limit = 1.5	7.2dB	-1.0dB
limit = 1.3	7.0dB	-1.2dB
limit = 1.1	7.4dB	-0.8dB

Table 7.8: Adaptive pre-equalization, Rayleigh channel.
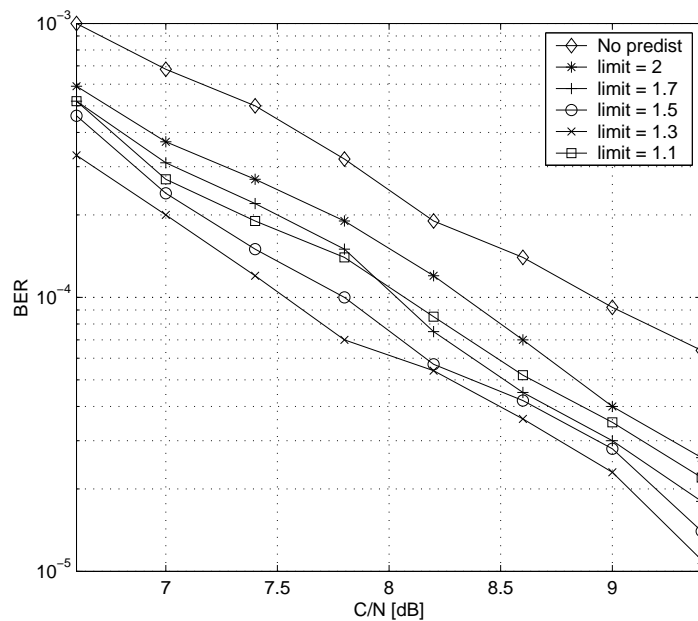
Figure 7.3: After-Viterbi BER, Rayleigh channel with adaptive pre-equalization.

The channel inversion can allocate a big amount of the total power to overcome the deep fading in the frequency domain, thus limiting the function $G(k)$ can be beneficial. As can be noted by the performed simulation runs, the best performances are obtained for $l = 1.3$. Employing this value, performance gains of 1.2dB are obtained.

7.6.2 Ricean channel model

The tests of figure 7.4 on Ricean channel show that only little improvements can be achieved for this type of channel.

In this case, the simulations show comparable results with only little dependency by the limiting factor. This can be justified because the Ricean channel already exhibit performances closer to AWGN ones than the Rayleigh channel analyzed before.

It must be noted that $l = 1.7$ results in no clipping at all of the inverted channel response, thus simulations with $l = 2.0$ have been omitted.

Table 7.9 summarizes the C/N results as a function of the *limit* employed.

By comparing the results of table 7.8 and 7.9, the choice $l = 1.3$ showed to offer the best performances for Rayleigh channel and suboptimal performance for Ricean channel.
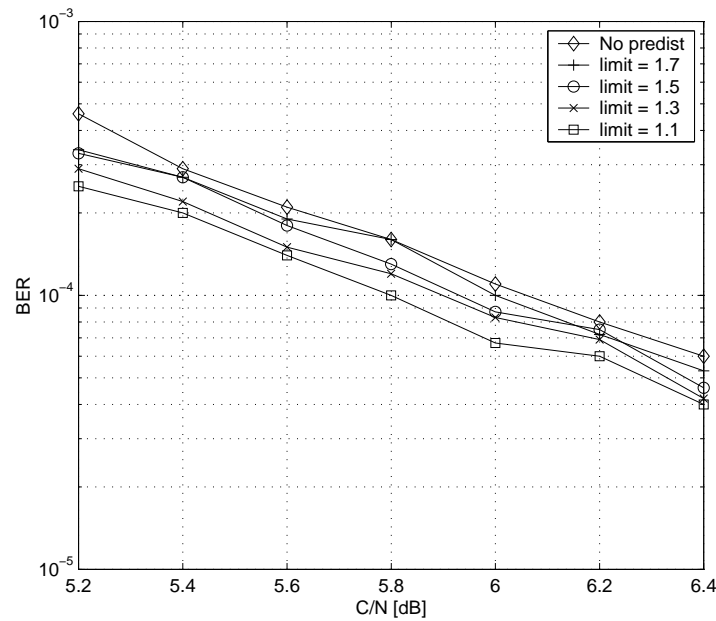
Figure 7.4: After-Viterbi BER, Ricean channel with adaptive pre-equalization.

test	required C/N	C/N difference
no pre-dist	5.6dB	-
limit = 1.7	5.6dB	0dB
limit = 1.5	5.5dB	-0.1dB
limit = 1.3	5.5dB	-0.1dB
limit = 1.1	5.4dB	-0.2dB

Table 7.9: Adaptive pre-equalization, Ricean channel.

7.7   Chapter summary

For low- to medium-distance applications, a TDM OFDM system has been proposed to efficiently share the RF channel between multiple terminals and to implement a return channel for monitoring and terminal control. The 802.16 standard has been identified as a good starting point for deploying a TDM OFDM network for NLOS scenario exploiting the Wireless-MAN OFDM Physical layer of the 802.16a amendment. The main parameters of such a system have been discussed and some application examples have been addressed. Furthermore, a low-complexity pre-distortion method has been presented and the performances have been evaluated employing Ricean and Rayleigh static channel models. Improvements up to $1.2dB$ can be expected for low-mobility environments.

Chapter 8

Conclusions

8.1   Chapter introduction

This chapter concludes the presentation of the work by resuming the problems addressed and the achieved results. Directions for further studies are also indicated.

8.2   Proposed solutions

In the last years, great interest have raised for wireless digital systems aimed to convey multimedia data at rates above 10Mbps. In particular, television productions are requiring digital modulation schemes capable of guarantee error-free links over difficult terrestrial propagation channels. Moreover, very recently the interest for other promising applications with similar requirements is growing. The existing and widely used DVB-T modulation scheme, while offering good performances for fixed and portable scenarios, does not fulfill all the requirements of the above-mentioned applications. In particular, the channel bandwidth can extend up to 24MHz, the link distance ranges from a hundred of meter to some tens of kilometers, mobility being the major issue or not. Usually point-to-point unidirectional links are required, but especially for the larger bandwidth scenarios, radio channels could be effectively shared between multiple transmitters; moreover, a return channel can be implemented for terminals control and can be exploited to provide a low-bitrate multimedia return link.

A software simulator has been written to test the performances of the proposed modulation schemes and receiver architectures. To guarantee the fastest execution times, the simulator has been implemented in C/C++. Object-oriented programming has been used to avoid explicit block initializations and to hide privata data. Nevertheless, an interface has been developed to exchange data with Matlab and exploit its powerful data presentation capabilities.

Several channel models have been implemented. Among those, Ricean and Rayleigh multipath channel models, as described in annex B of the DVB-T standard, and COST207 mobile models. From field trials in Athens, during the Olympic Games 2004, a particular shadow fading behaviour has been observed. For this reason, beside the well-known log-normal shadow fading model, a novel shadow fading model able to reproduce the observed channel behaviour has been provided.

Two different systems have been proposed to optimally cover the whole range of different applications.

The first one is targeted to unidirectional long and medium range applications and has been called **enhanced-mobility COFDM system**. It extends the DVB-T modulation

scheme introducing variable bandwidth, deep time interleaving and turbo codes. The modulation parameters of such a system have been fully specified and the transmission parameter signalling format has been modified to include additional information while retaining basic compatibility over existing systems that employ the 2K mode of DVB-T standard.

The main receiver processing tasks for the implementation of the enhanced-mobility COFDM system have been analyzed and simulation results have been presented.

In particular, an AGC algorithm with adaptive convergence speed and digital post-correction have been proposed, where the post-correction function has been efficiently approximated using only bit shifts and adders.

The performances of time acquisition and tracking algorithm have been studied to evaluate in particular the capacity to overcome long signal fading while maintaining OFDM symbol synchronization. The proposed time tracking algorithm, employing two different set of coefficients, successfully demonstrated both fast convergence and residual error below 1ppm. The correlation detection is able to maintain lock and perform time tracking with C/N down to -2dB employing a 1/16 guard interval.

The AFC performances have been studied to find the minimum C/N that guarantee correct initial frequency offset estimation. The tests demonstrated that the acquisition algorithm is robust enough to estimate the fractional and integer part of the frequency offset for C/N = 3dB. The frequency acquisition algorithm has been implemented as a closed-loop control where the *arctan()* function has been replaced by a two-step approximation scheme.

An adaptive channel estimation algorithm has been proposed that guarantee good performances for all the combinations of mobility and echo spread. In particular, time filtering is employed for low-mobility channels and performance improvements of about 0.7dB can be expected.

The insertion of deep time interleaving offers great advantages especially for channels suffering sparse shadow fading. Two simulation runs employing the proposed sparse shadow fading model have been performed and the results demonstrated that the required power margin can be dramatically reduced. Moreover, time interleaving showed significant gain even for COST207 channel models, where the C/N gain reaches 11dB for Rural Area and 3dB for Typical Urban models. Thus, most of single failure events of the original system can be avoided by employing adequate time interleaving and reduced power margin.

A further possible enhancement comes from the modifications of the forward error

correction scheme with the use of turbo codes as inner coder in a concatenated error correction scheme. Exploiting the additional code rate 1/3, the performance gain over the DVB-T convolutional scheme is about 2dB.

The proposed channel analysis algorithm guarantees good performances in all the multipath scenarios, without incurring in the drawbacks usually encountered employing the simpler strategy usually found in commercial receivers.

Two different methods to exploit two-branch receiver diversity have been studied. The well-known MRRC method, although offering optimal performances, is not easily implemented in the hardware design because of the structure of the demapper and the large amount of data that it requires to be exchanged. A method based on Maximal-Confidence Selection (MCS) showed good performance and does not incur in the above-mentioned drawbacks.

Two simulations have been performed to validate the system global performances in two typical field applications. In the *multimedia relay* case, the bandwidth is equal to $8MHz$ and the channel is a slowly-moving sparse shadow fading model. Deep time interleaving is used and the latency is raised to about 1.4 seconds. The combination of time interleaver and PCCC turbo codes gives a $11.5dB$ advantage over the original DVB-T system. In the second case, called *high mobility with diversity* the bandwidth is wider ($20MHz$) and the channel is a faster *COST207 - Typical Urban* model. Minimum time interleaving is used to limit the latency to about 17 milliseconds. The combination of time interleaver, powerful $R = 1/3$ PCCC turbo codes and MCS two-antenna diversity gives a $6.5dB$ advantage over the single-antenna DVB-T system.

Finally, the **enhanced-mobility COFDM system has been implemented** on a FPGA-based hardware. The floating-point high-level routines developed inside the C/C++ simulator framework have been rewritten in fixed-point low-level VHDL code. Several optimizations have been presented to reduce the hardware complexity.

For low and medium range applications, the requirements and characteristics of a system based on a TDM OFDM scheme has been analyzed. The time-division duplexing allows to efficiently share the RF channel between multiple terminals and to implement a return channel for monitoring and camera control. The 802.16 standard have been identified as a good framework to deploy a TDM OFDM network for NLOS scenario exploiting in particular the Wireless-MAN OFDM Physical layer of the 802.16a amendment. Moreover, since for TDM systems both base station and terminals experience the same frequency channel response thanks to the reciprocity of the RF channel, the estimated

channel response can be used to implement adaptive modulation schemes for subsequent transmission over the same channel. Aiming at low complexity schemes, an adaptive pre-equalization in the frequency domain has been proposed to mitigate the effects of strongly-selective multipath fading. The main advantage of this method is that it doesn't require any additional processing or knowledge at the receiver side; this method can thus be employed without further system modifications. Simulations showed significant performance improvements of about 1.2dB for Rayleigh channel and 0.2dB for Ricean channel.

8.3 Improvements over existing solutions

The digital wireless systems based on DVB-T modulation that are currently being used for television productions don't guarantee error-free links for the mobile applications we would like to address. Moreover, the bandwidth is limited to 8MHz, when allocated channels can range up to 24MHz.

The first proposed system modifies the DVB-T standard and overcomes the bandwidth limitation while providing protection toward single point of failures, encountered especially in mobile applications and caused by multipath and shadow fading. The enlarged RF bandwidth can be trade with link robustness employing turbo codes with rate 1/3. The receiver structure has been studied along with synchronization algorithms aimed to guarantee the desired performance even for very low C/N ratios. Simulations show great performance gains in typical application scenarios, with sensible power margin reduction. The first field tests of the implemented prototype system confirm the robustness of the proposed OFDM modulation scheme and receiver architecture.

8.4 Future work

The prototype of the enhanced-mobility system already demonstrates the ability to cope with difficult terrestrial channel. Nevertheless, some receiver blocks has still to be finalized and the overall design must be optimized in term of data path width to achieve the best compromise between performances and complexity. The complexity reduction will allow to limit the power consumption and to employ smaller and cheaper FPGAs for the final design.

New applications are emerging for this kind of system. For example, there is strong demand for modulation schemes able to guarantee high bitrate and extremely robust links between airplanes and ground stations. Further investigations should be carried to

validate the proposed system and reception architecture in this scenario. The mobility speed can approach MACH 1 and some modifications will be required to withstand the increased Doppler spread.

Robust reception strategies for the second proposed system, aimed to short to medium range applications and exploiting Time Division Multiplexing, must be investigated by extensive simulations. The capacity to share the radio resource between multiple terminals while providing a backward channel requires a specific high frequency design with duplexing capability. The physical system has to be developed and is foreseen for the end of year 2005.

This system could represents a major advantage especially for indoor applications like studio production or video surveillance.

Bibliography

[1] ETSI: *"Radio Broadcasting Systems; Digital Audio Broadcasting (DAB) to mobile, portable and fixed receivers"*, ETSI EN 300 401 V1.3.3 (2001-05)

[2] ETSI: *"Digital Video Broadcasting (DVB); Framing structure, channel coding and modulation for 11/12 GHz satellite services"*, EN 300 421 V1.1.2 (1997-08)

[3] ETSI: *"Digital Video Broadcasting (DVB); Framing structure, channel coding and modulation for cable systems"*, EN 300 429 V1.2.1 (1998-04)

[4] ETSI: *"Digital Video Broadcasting (DVB); Framing structure, channel coding and modulation for digital terrestrial television"*, ETSI EN 300 744 V1.4.1 (2001-01)

[5] G. Faria: *"The Digital Video Broadcasting System"*, ITIS France, 2000

[6] IEEE: *"Part 11: Wireless LAN Medium Access Control (MAC) and Physical Layer (PHY) specifications: High-speed Physical Layer in the 5 GHZ Band"*, IEEE Std 802.11a - 1999 (Supplement to IEEE Std 802.11-1999)

[7] S. O'Leary, D. Priestly, N. McSparron: *"Mobile broadcasting of DVB-T signals"*, IEEE transactions on broadcasting, Vol. 44, No. 3, September 1998.

[8] IEEE: *"Part 16: Air Interface for Fixed Broadband Wireless Access Systems"*, IEEE Std 802.16 - 2001

[9] IEEE: *"Part 16: Air Interface for Fixed Broadband Wireless Access Systems Amendment 2: Medium Access Control Modifications and Additional Physical Layer Specifications for 211 GHz"*, IEEE Std 802.16a - 2003 (Amendment to IEEE Std 802.16 - 2001)

[10] U. Reimers: *"DVB-T: the COFDM-based system for terrestrial television"*, Electronics and Communication engineering journal, pp.28-32, Feb 1997.

[11] S. B. Weinstein, P. M. Ebert: *"Data transmission by Frequency-Division Multiplexing using the Discrete Fourier Transform"*, IEEE Transactions on Communication Technology, Vol. 19, No. 5, pp. 628-634, October 1971.

[12] R. Poole: *"The echo performance of DVB-T receivers"*, EBU technical review September 2001.

[13] V. Benedetto, G. D'Aria, L. Scarabosio: *"Performance of COFDM systems with waveform shaping"*, IEEE International Conference on Communications, ICC '97, vol. 3, pp. 1241-1245, 1997.

[14] J. L. Massey: *"Shift-Register Synthesis and BCH Decoding"*, IEEE Transactions on information theory, IT-15, pp. 122-127, January 1979.

[15] E. R. Berlekamp: *"The Technology of Error Correcting Codes"*, Proceedings of the IEEE, Vol. 68, No. 5, pp. 564-593, May 1980.

[16] L. H. Charles Lee: *"Convolutional coding: fundamentals and applications"*, Artech House, London, 1997.

[17] C. Berrou A. Glavieux and P. Thitimajshima: *"Near Shannon Limit error-correcting coding and decoding: Turbo Codes"* ICC'93, Conf. Rec. pp.1064-1070, Geneva, May 1993.

[18] P.A Beerel, P.A. Chugg, K.M: *"A low latency SISO with application to broadband turbo decoding"* Selected Areas in Communications, IEEE Journal on , Volume: 19 Issue: 5 , May 2001 pp.: 860 -870.

[19] S.-Y. Chung, T. Richardson, and R. Urbanke: *"Analysis of sum-product decoding of low-density parity-check codes using Gaussian approximation"* IEEE Trans. Inform. Theory, vol. 47, pp. 657-670, Feb. 2001.

[20] S. ten Brink: *"Convergence of iterative decoding"* Electron. Lett., vol. 35, no. 13, pp. 806-808, May 24th, 1999.

[21] S. Benedetto, D. Divsalar, G. Montorsi, and F. Pollara: *"Serial concatenation of interleaved codes: Performance analysis, design, and iterative decoding"* IEEE Trans. Inform. Theory, vol. 44, pp. 909-926, May 1998.

[22] C. Berrou, C. Duillard and M. Jezequel: *"Multiple parallel concatenation of circular recursive convolutional (CRSC) codes"*, Ann. Telecomm. Tome 54, N3-4, pp. 166-172, March-April 1999.

[23] C. Berrou, C. Duillard and S. Kerouedan: *"The advantages of Non-Binary Turbo Codes"* Information Theory Workshop, 2001. Proceedings. 2001 IEEE, 2001 Page(s): 61 -63.

[24] DVB: *"Interaction channel for satellite distribution systems"* ETSI EN 301 790, V1.2.2, pp. 21-24, Dec 2000.

[25] J.J. van de Beek, M. Sandell, P.O. Börjesson: *"On synchronization in OFDM systems using the cyclic prefix"*, Proceedings of the RVK'96, pp.663-667 , Lulea, Sweden, June 1996.

[26] T.M. Schmidl, D.C. Cox: *"Robust Frequency and Timing Synchronization for OFDM"*, IEEE Transactions on communications, vol. 45, pp. 1613-1622, Dec. 1997.

[27] H. Minn, V.K. Bhargava: *"A simple and efficient timing offset estimation for OFDM systems"*, IEEE Vehicular Technology Conference Proceedings, vol.1, pp. 51-55, May 2000.

[28] M. Gertou, G. Karachalios, D. Triantis, K. Papantoni and P. I. Dallas: *"Synchronization Approach for OFDM based Fixed Broadband Wireless Access Systems"*, IST Communications Mobile Summit 2001, Barcelona, Spain, 9-12 Sept. 2001.

[29] E.G. Larsson, G. Liu, J. Li, G.B. Giannakis: *"Joint symbol timing and channel estimation for OFDM based WLANs"*, IEEE Communications Letters, vol. 5, no. 8, pp.325-327, August 2001.

[30] H. Sari, G. Karam, I. Jeanclaude: *"Transmission techniques for digital terrestrial TV broadcasting"*, IEEE Communications magazine, pp.100-109, Feb. 1995.

[31] W. Warner, C. Leung: *"OFDM/FM frame synchronization for mobile radio data communication"*, IEEE Transactions on vehicular technology, vol. 42, pp. 302-313, August 1993.

[32] T. de Couasnon, R. Monnier, J. Rault: *"OFDM for digital TV broadcasting"*, Signal processing, vol. 39, pp. 1-32, 1994.

[33] M. Sandell, J.J. van de Beek, P. Börjesson: *"Timing and frequency synchronisation in OFDM systems using the cyclic prefix"*, Proceedings of international symposium on synchronization, pp. 16-19, Dec. 1995.

[34] P. Moose: *"A technique for orthogonal frequency diviion multiplexing frequency offset correction"*, IEEE Transactions on Communications, vol. 42, pp. 2908-2914, Oct. 1994.

[35] F. Claßen, H. Meyr: *"Synchronisation algorithms for an OFDM system for mobile communications"*, Codierung für quelle, Kanal and Übertragung, no. 130, pp. 105-113, 1994.

[36] F. Daffara, O. Adami: *"A new frequency detector for orthogonal multicarrier transmission techniques"*, IEEE Proceedings of vehicular technology conference, pp. 804-809, July 1995.

[37] M. Russell, G. Stüber: *"Interchannel interference analysis of OFDM in a mobile environment"*, IEEE International Vehicular Technology Conference, vol.2, pp.820-824, 1995.

[38] J.G. Proakis: *"Digital communications"*, Prentice-Hall, 3rd edition, 1995.

[39] F. Tufvesson, T. Maseng: *"Pilot assisted channel estimation for OFDM in mobile cellular systems"*, Vehicular Technology Conference, vol. 3 , pp. 1639-1643, May 1997.

[40] R. van Nee, R. Prasad: *"OFDM for wireless multimedia communications"*, Artech House Publishers, 2000.

[41] P. Höher: *"TCM on frequency-selective land-mobile fading channels"*, Proceedings of the Tirrenia International Workshop on Digital Communications, Tirrenia, Italy, Sept. 1991.

[42] F. Sanzi, J. Speidel: *"An adpative two-dimensional channel estimator for wireless OFDM with application to mobile DVB-T"*, IEEE Transactions on broadcasting, vol. 46, no. 2, pp. 128-133, June 2000.

[43] A.A. Hutter, R. Hasholzner, J.S. Hammerschmidt: *"Channel Estimation for Mobile OFDM system"*, IEEE Vehicular Technology Conference, vol. 1 , pp.305-309, Sept. 1999.

[44] O. Edfors, M. Sandell, J.J. van de Beek, S.K. Wilson, P.O. Börjesson: *"OFDM channel estimation by Singular Value Decomposition"*, IEEE Vehicular Technology Conference, pp.923-927, May 1996.

[45] J.J. van de Beek, O. Edfors, M. Sandell, S. Wilson, P. Börjesson: *"On channel estimation in OFDM systems"*, IEEE Proceedings of Vehicular Tehnology Conference, vol. 2, pp. 815-819, July 1995.

[46] C.S. Yeh; Y. Lin; Y. Wu: *OFDM system channel estimation using time-domain training sequence for mobile reception of digital terrestrial broadcasting*, IEEE Transactions on Broadcasting, Vol. 46 , Issue 3 , pp. 215-220, September 2000.

[47] A. Duel-Hallen, S. Hu, H. Hallen: *"Long range prediction of fading signals"*, IEEE Signal processing magazine, vol. 17 , pp. 62-75, May 2000.

[48] F. Tufvesson, M. Faulkner, T. Maseng: *"Pre-compensation for Rayleigh fading channels in time division duplex OFDM systems"*, IEEE Proceedings of 6th international workshop on intelligent signal processing and communications systems, pp. 57-63, Nov. 1998.

[49] F. Tufvesson: *"Design of wireless communication systems - Issues on synchronization, channel estimation and multi-carrier systems"*, Department of Applied Electronics, Lund University, Sweden, 2000.

[50] E. Al-Susa, R. Ormondroyd: *"A predictor-based decision feedback channel estimation method for COFDM with high resiliance to rapid time-variations"*, IEEE Proceedings of Vehicular Tehnology Conference, vol. 1, pp. 273-278, Sept. 1999.

[51] A. Petropulu, Z. Ruifeng, R. Lin: *"Blind OFDM channel estimation through simple linear precoding"*, IEEE Transactions on Wireless Communications, Vol. 3, Issue 2, pp. 647-655, March 2004.

[52] R. W. Heath, G. B. Giannakis: *"Exploiting input cyclostationarity for blind channel identification in OFDM systems"*, IEEE Trans. Signal Processing, vol. 47, pp. 846856, March 1999.

[53] B. Muquet, M. de Courville, P. Duhamel, and V. Buenac: *"A subspace based blind and semi-blind channel identification method for OFDM systems"*, Proceedings on IEEE Workshop Signal Processing Advances Wireless Communications, pp. 170173, May 1999.

[54] X. Cai, A. N. Akansu: *"A subspace method for blind channel identification in OFDM systems"*, Proceedings on ICC, vol. 2, pp. 929933, March 2000.

[55] H. Wang, Y. Lin, B. Chen: *"Data-Efficient Blind OFDM Channel Estimation Using Receiver Diversity"*, IEEE Transactions on signal processing, Vol. 51, No. 10, October 2003.

[56] G. J. Foschini, M. J. Gans: *"On limits of wireless communication in a fading environment when using multiple antennas"*, Wireless Personal Communications, Vol. 6, No. 3, March 1998

[57] Y. Li, J.H. Winters, N.R. Sollenberger: "Signal detection for MIMO OFDM wireless communications", Communications, 2001. ICC 2001. IEEE International Conference on, Volume: 10 , 2001

[58] A.N. Mody, G.L. Stber: "Synchronization for MIMO OFDM systems", Global Telecommunications Conference, 2001. GLOBECOM '01. IEEE, 2001

[59] S.Diggavi, N. Al-Dhahir, A. Stamoulis: "Intercarrier Interference in MIMO OFDM", Communications, 2002. ICC 2002. IEEE International Conference on, Volume: 1, 2002

[60] S. M. Alamouti: "A simple transmit diversity technique for wireless communications", Communications, IEEE journal on select areas in, Vol. 16, No. 8, October 1998

[61] A. Chevreuil, L. Vandendorpe: "MIMO MMSE-DFE: a general framework", Statistical Signal and Array Processing, 1998. Proceedings, Ninth IEEE SP Workshop on, 1998

[62] Kung, S.Y.; Yunnan Wu; Xinying Zhang: "Bezout equalization for STBC-MIMO systems", Acoustics, Speech, and Signal Processing, 2002 IEEE International Conference on, Volume: 3, 2002

[63] R.S. Blum, Y. Li, J.H. Winters, Q. Yang: "Improved Space-Time Coding for MIMO-OFDM Wireless Communications", Communications, IEEE Transactions on, Volume: 49 Issue: 11, November 2001

[64] J. Hayes: *"Adaptive feedback communications"*, IEEE Communication Technology, Vol. 16, pp. 29-34, February 1968.

[65] W. Webb, R. Steele: *"Variable rate QAM for mobile radio"*, IEEE Transactions on Communications, Vol. 43, pp. 2223-2230, july 1995.

[66] J. Torrance, L. Hanzo: *"Upper bound performance of adaptive modulation in a slow Rayleigh fading channel"*, Electronics Letters, Vol. 32, pp. 718-719, April 1996.

[67] S. Otsuki, S. Sampei, N. Morinaga: *"Square QAM adaptive modulation/TDMA/TDD systems using modulation level estimation with Walh function"*, Electronics Letters, Vol. 31, pp. 169-171, February 1995.

[68] R.O. LaMaire, M. Zorzi: *"Effect of correlation in diversity systems with Rayleigh fading, shadowing, and power capture"*, IEEE Journal on Selected Areas in Communications, vol. 14 , no. 3, pp. 449 - 460, April 1996

[69] M.M. Zoonozi, P. Dassanayake: *"Shadow fading in mobile radio channel"*, Seventh IEEE International Symposium on Personal, Indoor and Mobile Radio Communications, PIMRC'96, Vol.2, pp. 291-295, October 1996.

[70] D. Giancristofaro: *"Correlation model for shadow fading in mobile radio channels"*, Electronics Letters, vol. 32, no. 11, pp. 958-959, May 1996.

[71] A.J. Coulson, A.G. Williamson, R.G. Vaughan: *"A statistical basis for lognormal shadowing effects in multipath fading channels"*, IEEE Transactions on communications, vol. 46, no. 4, pp. 494-502, April 1998.

[72] M. Zorzi: *"Power control and diversity in mobile radio cellular systems in the presence of Ricean fading and log-normal shadowing"*, IEEE Transactions on vehicular technology, vol. 45, no. 2, pp. 373-382, May 1996.

[73] J.D. Parsons: *"The mobile radio propagation channel"*, Pentech Press, London, 1992.

[74] R. Steele: *"Mobile Radio Communications"*, New York, IEEE Press, 1992.

[75] G.S. Bae, H.K. Son: *"A study of the 2.3GHz bands propagation characteristic measured in Korea"*, IEEE Antennas and Propagation Society International Symposium, vol. 2, pp. 995-998, 2003.

[76] Peter B. Kenington: *"High Linearity RF Amplifier Design"*, Artech House Publishers, 2000.

[77] A.A. Hutter: *"Design of OFDM systems for frequency-selective and time-variant channels"*, Broadband Communications. 2002 International Zurich Seminar on Access, Transmission, Networking- pp. 39-1 – 39-6

[78] S. Anikhindi, G. Cradock, R. Makowitz, C. Patzelt: *"A commercial DVB-T demodulator chipset"*, IEE International Broadcasting Convention, Conf. publication no.447, pp. 528-533, September 1997

[79] M. Lattuada: *"Efficient error correction solutions for wireless digital video"*, EPFL PhD dissertation, Institut de traitement des signaux, 2004.

[80] F. Said, H. Aghvami: *"Linear two dimensional pilot assisted channel estimation for OFDM systems"*, 6th IEE Conference on Telecommunications(Conf. Publ. No. 451), pp. 32-36, 1998

[81] T. Keller, L. Hanzo: *"Sub-band adaptive pre-equalised OFDM Transmission"*, Proceedings of VTC'99, pp. 334-338, 1999.

[82] E. Al-Susa, R. Ormondroyd: *"An improved channel inversion based adaptive OFDM system in the presence of channel errors and rapid time variations"*, IEEE International Vehicular Technology Conference, pp. 1114-1119, 2000.

[83] J.K. Cavers, M.W. Liao: *"Adaptive compensation for imbalance and offset losses in direct conversion transceivers"*, IEEE Transactions on Vehicular Technology, vol. 42, pp. 581-588, Nov. 1993.

[84] L. Erup, F.M. Gardner, R.A. Harris: *"Interpolation in digital modems – Part II: Implementation and Performance"* IEEE Transactions on communications, vol. 41, pp. 998-1008, June 1993.

[85] A.M. Eltawil, B. Daneshrad: *"Interpolation based Direct Digital Frequency systhesis for Wireless Communications"* Wireless Communications and Networking Conference, vol. 1, pp. 17-21, March 2002.

[86] J.J. van de Beek, M. Sandell, M. Isaksson, P.O. Börjesson: *"Low-Complex Frame Synchronization in OFDM Systems"*, Fourth IEEE International Conference on Universal Personal Communications, pp. 982-986, November 1995

[87] T. Keller, L. Hanzo: *"OFDM synchronisation techniques for wireless local area networks"*, IEEE PIMRC'96, pp. 963-967, Oct. 1996.

[88] S. Knappe, P. Schwindt, V. Shah, L. Hollberg, J. Kitching, L. Liew and J. Moreland: *"Microfabricated atomic frequency references"*, Proceedings of the IEEE International Frequency Control Symposium, August 2004, Montreal, Canada.

[89] R. Brugger, D. Hemingway: *"OFDM receivers - impact on coverage of inter-symbol interference and FFT window positioning"*, EBU Technical Review, July 2003.

[90] H.M. Weinfurtner: *"Optimum Nyquist Windowing in OFDM Receivers"*, IEEE Transactions on Communications, Vol. 49, No. 3, pp. 417-420, March 2001.

[91] S.A.Fechtel, A.Blaickner: *"Efficient FFT and equalizer implementation for OFDM receivers"*, IEEE Transactions on Consumer Electronics, vol. 45, no. 4, pp. 1104-1107, november 1999.

[92] W.C. Lee, H.M. Park, J.S. Park: *"Viterbi Decoding Method Using Channel State Information in COFDM Systems"*, IEEE Transactions on Consumer Electronics, Vol. 45 , Issue 3 , pp. 533-537, August 1999

[93] M. Lattuada, R. Posega, M. Mattavelli, D. Mlynek: *"Improving DVB-T Forward Error Correction By Concatenated Turbo Code Scheme"*, Packet Video 2003, 28-29 April, Nantes, 2003

Renzo POSEGA   25 September 1974
Ch. de la Tour Grise, 28   not engaged
1007 Lausanne
Switzerland

Tel.   021 6245170
Mobile: 078 7914739
E-mail: rposega@yahoo.it

Nationality: Italian
Swiss working papers: B

Objective: Project Manager in a hardware-related project

Studies:

- ✓ Scientific maturity diploma,   60/60   Trieste, Italy, 1993;
- ✓ Electrical Engineering diploma,   110/110 *cum laudæ*   Trieste, Italy, 1999;
- ✓ Electrical Engineering PhD, entitled "*Advanced OFDM Systems for Terrestrial Multimedia Links*"   Lausanne, Switzerland, 2005.

Job experience:

- ✓ Stage at Telit (formerly: Telital) in the scope of electrical engineering diploma entitled: "*Study of a RAKE receiver for the IS95 standard*" – 6 months during years 1998/1999.
- ✓ Military Service as Navy Officier during 1999/2000 (14 months).
- ✓ R&D engineer for Livetools Technology during the PhD period, in particular:
- ✓ Development of DTNG systems, and implementation of the COFDM receiver in FPGA (VHDL) during year 2004.

Languages:

- ✓ Italian – mother language
- ✓ English – fluent
- ✓ French – fluent

Technical skills:

- ✓ Video coding
- ✓ Digital modulations
- ✓ Digital signal processing (hardware/software)
- ✓ Embedded system design
- ✓ Verilog and VHDL hardware synthesis languages
- ✓ C/C++ language
- ✓ Schematic and PCB design (Protel)

Personal interests:

- ✓ DIY in high-end audio equipment (amplifiers, DAC, signal processors)
- ✓ Sports: ski, swimming, bicycle